

Rapid Prototyping of Thermoplastic Microfluidic Devices for Medium Volume Production by Combining Hot Embossing and Milling

by

Daniel Konstantinou

A thesis submitted in conformity with the requirements
for the degree of Masters of Applied Science

Graduate Department of Mechanical and Industrial Engineering
University of Toronto

© Copyright 2015 by Daniel Konstantinou

Rapid Prototyping of Thermoplastic Microfluidic Devices for Medium Volume Production by Combining Hot Embossing and Milling

Daniel Konstantinou

Masters of Applied Science

Graduate Department of Mechanical and Industrial Engineering
University of Toronto

2015

Abstract

Microfluidics technology promises to advance many current areas of research including point-of-care diagnostics and cell-based assays. However, there is a need to address current challenges associated with the iterative design and fabrication process of microfluidic systems in thermoplastics that are amenable to mass production downstream. The objective of this study was to develop an optimized fabrication approach that will enable medium volume production of microfluidic devices made in thermoplastics PMMA and COP. The aim is to use the approach as an intermediate step between rapid prototyping in PDMS and high-volume production in plastics. An optimized approach will enable rapid testing of designs and reduce the time and cost of microfluidic chip development. Results showed that epoxy molds can be made consistently and can be applied to hot embossing of thermoplastic materials, which when combined with micromilling can rapidly produce prototyped thermoplastic microfluidic devices at a medium volume production scale.

Acknowledgements

Firstly, I would like to thank my advisor, Professor Edmond Young, for allowing me to join his Laboratory of Integrative Biology and Microengineered Technologies. I am truly thankful for having him as an advisor and proposing a thesis project that has provided me with a wealth of knowledge and experience that I will carry with me for the rest of my life. I would also like to thank Professor Edmond Young for his continued support and guidance from the beginning to the end and every day in between. Thank you to my committee members, Professor Axel Guenther and Professor Hani Naguib for taking time out of their busy schedules to review my work and provide excellent commentary to help further improve the quality of my thesis.

As part of my specific graduate research focus, I was afforded the opportunity to work closely with Bio-Rad Laboratories through an internship opportunity. The purpose of this internship was to work with Bio-Rad Laboratories towards the common goal of developing a streamlined microfluidic device fabrication process in thermoplastic materials for rapid prototyping purposes at a medium-volume production scale. I would like to thank the members of Bio-Rad Laboratories that have been involved in this project, specifically Nenad Kircanski, Amir Sadri and Tal Rosenzweig. Their input and guidance have been sincerely appreciated; the time that Amir spent with me was invaluable.

I would also like to thank my fellow lab members Dr. Alwin Wan, Dr. Deepika Devadas, Ashkan Shirazi, Thomas Moore, Tobe Madu and Mouhita Humayun. Their input, banter and friendship made every day a wonderful experience.

Finally, I would like to dedicate this thesis to my parents, Chris and Vicky Konstantinou, and my sister, Monica Konstantinou. I am eternally grateful for their love and unwavering support. They have been there for me throughout my entire life and sacrifice so much to see me happy. I owe everything to them and I love them to the moon and back.

Table of Contents

Abstract	ii
Acknowledgements	iii
List of Tables.....	viii
List of Figures	ix
Chapter 1.....	1
1.1 Motivation	1
1.2 Project Description	4
Chapter 2.....	10
2.1 Choosing Device Material.....	10
2.1.1 PDMS.....	10
2.1.2 PS.....	11
2.1.3 PMMA	11
2.1.4 COP	12
2.1.5 Comparison of Different Materials for Microfluidic Device Fabrication	13
2.2 Photolithography and Soft Lithography.....	15
2.2.1 Photolithography – Silicon Master Fabrication	15
2.2.2 Soft Lithography	17
2.3 Microfabrication of Plastics	19
2.3.1 Epoxy Mold Making	19
2.3.2 Hot Embossing.....	20
2.3.3 Milling.....	22
2.3.4 Bonding.....	23

2.4 Remaining Challenges	25
Chapter 3.....	27
3.1 Introduction.....	27
3.2 Materials and Methods.....	29
3.2.1 Photolithography Masks	29
3.2.2 SU-8 Negative Photoresist.....	31
3.2.3 Silicon Wafers	31
3.2.4 Pyrex Wafers	34
3.2.5 Mask Aligner System.....	36
3.3 Optimization of Spin Speed for Precise Feature Heights.....	37
3.4 Alignment of Multi-Height Features during UV Exposure.....	41
3.4.1 OAI Mask Aligner System Model 30	41
3.4.2 EVG Mask Aligner	43
3.4.2.1 Silicon wafer	43
3.4.2.2 Pyrex Wafer	45
3.5 Feature Side Wall Draft Angle	47
3.5.1 Silicon Wafer Substrate	47
3.5.2 Pyrex Wafer Substrate through Backside Lithography	50
Chapter 4.....	54
4.1 Introduction.....	54
4.2 Materials and Methods.....	57
4.2.1 PDMS Negative-Relief Feature Mold Fabrication.....	57
4.2.2 Epoxy Fabrication Protocol	59
4.2.3 Elimination of Bubbles from Bulk Epoxy Material	62
4.2.4 Epoxy Mold Fabrication Jig	64

4.2.5	Micromilling 3D Features	67
4.3	Results	69
Chapter 5.....		74
5.1	Introduction.....	74
5.2	Hot Embossing Machines.....	76
5.2.1	Carver Press.....	76
5.2.2	EVG 520HE.....	78
5.3	Hot Embossing Protocol	82
5.3.1	Carver+PMMA+Epoxy	82
5.3.2	Carver+COP+Epoxy	84
5.3.3	EVG+PMMA+Epoxy	86
5.3.4	EVG+COP+Epoxy	88
5.3.5	Epoxy Surface Coating with Releasing Agent.....	90
5.4	Feature Transfer Fidelity	92
5.4.1	Carver+PMMA+Epoxy	92
5.4.2	Carver+COP+Epoxy	94
5.4.3	EVG+PMMA+Epoxy	96
5.4.4	EVG+COP+Epoxy	97
5.4.5	Statistical Analysis	98
5.5	Epoxy Mold Deformation.....	99
5.6	Comparison Between Epoxy and Silicon Masters	102
5.6.1	Silicon Master Hot Embossing	102
5.6.2	Epoxy Mold Hot Embossing	107
5.6.2.1	Start-up Optimization & Epoxy Mold Robustness.....	107
5.6.2.2	Multiple Epoxy Molds from Single Silicon Master.....	109

5.6.2.3	Preservation of Optimized Silicon Master	110
5.7	Throughput capabilities	112
Chapter 6.....		117
6.1	Introduction.....	117
6.2	Materials and Methods.....	118
6.2.1	SolidWorks 3D CAD Design.....	118
6.2.2	SprutCAM	119
6.2.3	Tormach PCNC & G-Code	121
6.3	Alignment of Embossed Features with Milling Coordinates	123
6.3.1	Embossed Alignment Marks.....	123
6.3.2	Precise Alignment of Embossed Features with Milling Coordinates	125
6.3.3	Tolerance Built into Original Design.....	127
6.4	Results	129
6.5	Milling Throughput Capabilities.....	131
Chapter 7.....		136
7.1	Conclusion.....	136
7.2	Summary.....	139
7.3	Future work	141
References		142

List of Tables

Table 2-1 SU-8 characteristic processing times (in minutes) for different variants and film thicknesses [57].....	16
Table 2-2 Solubility parameters for selected thermoplastic polymers and organic solvents [78].....	25
Table 5-1 Parameters tested for hot embossing characterization of PMMA with the use of the Carver Press.....	83
Table 5-2 Parameters tested for hot embossing characterization of COP with the use of the Carver Press.....	85
Table 5-3 Parameters tested for hot embossing characterization of PMMA with the use of the EVG 520HE	87
Table 5-4 Parameters tested for hot embossing characterization of COP with the use of the EVG 520HE	89
Table 5-5 Measurements made of two separate epoxy mold grids after multiple hot embosses.....	102
Table 5-6 Measurements made on the silicon wafer, PDMS negative-relief feature mold and positive-relief epoxy mold at four separate locations on the microfluidic design	112
Table 5-7 Times associated with the beginning and ending of each hot emboss performed throughout the week-long throughput test, as well as the time per each hot emboss.	115
Table 6-1 Times associated with the beginning and ending of each hot emboss and milling procedure performed throughout the week-long throughput test, as well as the time per each hot emboss and milling procedure.	134
Table 6-2 Number of devices produced each day that successfully passed the quality assurance check.....	135

List of Figures

Figure 1.1: Commercially available microfluidic devices produced by (A) Ibidi Diagnostics. (n.d.). Retrieved July 21, 2015, from http://ibidi.com , (B) Microfluidic ChipShop GmbH. (n.d.). Retrieved July 21, 2015, from http://microfluidicchipshop.com , (C) Fluidigm. (n.d.). Retrieved July 21, 2015, from https://www.fluidigm.com , and (D) Xona Microfluidics. (n.d.). Retrieved July 21, 2015, from http://xonamicrofluidics.com	4
Figure 1.2: Flowchart of microfluidic device fabrication process, showing what is produced at each stage. The process involves (A) the fabrication of an SU-8 master mold, (B) fabrication of a negative-relief feature PDMS mold, (C) fabrication of a positive-relief feature epoxy mold, (D) hot embossing a thermoplastic material with the fabricated epoxy mold, (E) milling a perimeter around the embossed features, and (F) bonding a cover to the embossed thermoplastic material.	6
Figure 2.1: Process of making microfluidic devices with PDMS [12]......	18
Figure 2.2: Polystyrene microfabrication process. (A) Fabrication of a PDMS slab of uniform thickness to replicate the SU-8 master. (B) Casting of the epoxy in a PDMS cavity composed of the replicate of the SU-8 mold and a PDMS ring. (C) Cured epoxy mold. (D) Flattening of the PS sample to a desired thickness by use of metal shims. (E) Hot embossing of the PS sheet for through-hole fabrication (remove CA and COP for non-through-hole approach). (F) Thermal bonding of two PS sample pieces. (G) Fabrication recipes for different hydraulic press procedures. Pressure is nominal value calculated on the basis of mold surface area of 50-75mm. Force-temperature functions used for through-hole embossing are shown as an example. Temperature curve consists of heating, dwell, and cooling phases. In the dwell phase, force may be successively ramped over time. During cooling, the final applied force during dwell was maintained to prevent sink marks in the embossed part[4].	21
Figure 2.3: (A) A schematic showing the basic components of a CNC mill, which can use computer-aided design (CAD) models to produce finished devices. The mill consists of a worktable (to provide motion in the XY-plane), a cutting tool (to remove material from the workpiece), and a spindle (to hold the cutting tool, spin the cutting tool, and provide motion along the Z-axis). (B) A photograph showing a CNC micromill during operation. (C) A photograph of a micromilled thermoplastic device that contains a variety of feature geometries and sizes [31].	23
Figure 3.1: 3 photolithography masks that were used to fabricate the 3-layer SU-8 master mold.....	33
Figure 3.2: A comparison between SU-8 fabrication processes involving a silicon wafer substrate and a Pyrex wafer substrate. (a) shows the first layer of SU-8 being spun onto the substrate material and (B) shows the first layer being selectively exposed to UV light, where the silicon wafer substrate is being exposed through frontside lithography and the pyrex wafer substrate is being exposed through backside lithography. (C) shows a second layer of SU-8 being spun on top of the first layer of SU-8 and (D) shows the second layer of SU-8 being selectively exposed to UV light	

through frontside lithography for the silicon wafer substrate and through backside lithography for the Pyrex wafer substrate. (E) shows the developed silicon and Pyrex wafer master molds.....	35
Figure 3.3: Graphed data of SU-8 layer thicknesses achieved under different spincoating rates (RPM). Plotted data points were separated by recorded clean room humidity and theoretical MicroChem values were also plotted for comparison.....	40
Figure 3.4: Precise alignment of microfluidic device features during UV exposure. The images show the alignment achieved between SU-8 layer 1 and SU-8 layer 3, with respective feature heights of 100 and 300 micrometers.....	47
Figure 3.5: Illustration showing the concept of positive and negative draft angles in comparison to the line normal to the surface of the substrate material.....	48
Figure 3.6: Cross-sectional PDMS image of microfluidic feature exposed with an energy value of (A) 420 mJ/cm ² , (B) 1000 mJ/cm ² and (C) 5000 mJ/cm ²	50
Figure 3.7: Comparison of draft angles of SU-8 features that were exposed through backside lithography at (A) 250 mJ/cm ² with a draft angle of ~+9° (B) 275 mJ/cm ² with a draft angle of ~+3.6°.....	51
Figure 3.8: Plotted data of draft angles achieved through backside lithography with a Pyrex wafer substrate under varying UV energy exposures. Error bars represent standard deviations, with n=3 for 100 μm feature heights and n=6 for the 300 μm feature height.....	53
Figure 4.1: Epoxy mold fabrication process with (A) PDMS being poured overtop the SU-8 features in order to create a negative-relief feature PDMS mold, (B) aluminum-filled epoxy being poured overtop the PDMS negative-relief feature mold and subsequently being cured and having its back surface milled to create a uniformly thick epoxy and (C) the epoxy mold being released from the PDMS mold.....	61
Figure 4.2: Image taken of a fabricated epoxy mold with positive-relief microfluidic features	62
Figure 4.3: 50 mL conical tubes filled with mixed epoxy being centrifuged in an upside-down orientation in order to isolate all bubbles that are trapped within the bulk of the epoxy to the bottom end of the conical tube.	62
Figure 4.4: Image showing congregated bubbles revealed after mixed epoxy had been centrifuged. The bubbles are at the opening of the conical tube because the 50 mL conical tube was centrifuged in a right side up orientation for ease of imaging purposes.....	64
Figure 4.5: Images taken throughout the epoxy mold fabrication process including (A) epoxy mold fabrication jig by itself, (B) aluminum-filled epoxy poured onto the PDMS mold located at the center of the epoxy mold fabrication jig, (C) milled epoxy backside of epoxy mold after curing process had completed and (D) released epoxy mold sitting flat on a cutting table.....	67

Figure 4.6: Endmill cutting directly into an epoxy mold feature.....	69
Figure 4.7: Images of taken of epoxy mold features including (A) epoxy mold feature before centrifugation step was introduced, (B) epoxy mold feature after centrifugation step was introduced, (C) epoxy mold feature before milling step was introduced, (D) epoxy mold feature after milling step was introduced and (E) image of epoxy mold created with the use of epoxy mold fabrication jig.	73
Figure 5.1: Image of Carver Press hot embossing machine taken from Carver Inc. website with permission.	76
Figure 5.2: Image of EVG 520 HE taken from EV Group website with permission.	78
Figure 5.3: Hot embossing being performed on a thermoplastic material with the use of an epoxy mold. All items labelled and presented in the order that they are found during the hot embossing process. After an application of force and temperature, the thermoplastic material is released from the hot embossing machine with a transfer of microfluidic features from the epoxy mold.....	81
Figure 5.4: Images taken of epoxy mold surface before and after the application of the Weicon Mould Releasing Agent.	91
Figure 5.5: The 4 locations where cross-sectional measurements were taken for the characterization of the hot embossing process using thermoplastics PMMA and COP with the use of the Carver Press and EVG 520 HE hot embossing machines.	92
Figure 5.6: Theoretical cross-sectional shape of epoxy mold and embossed thermoplastic PMMA for the purpose of describing how the Discrepancy Index was calculated.	93
Figure 5.7: Cross-sectional normalized discrepancy graphs of the 4 locations on the microfluidic device where characterization was performed for PMMA using the Carver Press. Sample size of n=3 for all conditions. The maximum Discrepancy Index axis value is 0.25 for Location 1, Location 2, Location 3 and Location 4.....	94
Figure 5.8: Cross-sectional normalized discrepancy graphs of the 4 locations on the microfluidic device where characterization was performed for COP using the Carver Press. Sample size of n=3 for all conditions. The maximum Discrepancy Index axis value is 0.50 for Location 1 and 0.10 for Location 2, Location 3 and Location 4.....	95
Figure 5.9: Cross-sectional normalized discrepancy graphs of the 4 locations on the microfluidic device where characterization was performed for PMMA using the EVG 520HE. Sample size of n=3 for all conditions. The maximum Discrepancy Index axis value is 0.50 for Location 1 and 0.12 for Location 2, Location 3 and Location 4.	97
Figure 5.10: Cross-sectional normalized discrepancy graphs of the 4 locations on the microfluidic device where characterization was performed for COP using the EVG 520HE. Sample size of n=3 for all conditions. The maximum Discrepancy Index axis value is 0.70 for Location 1 and 0.10 for Location 2, Location 3 and Location 4.	98

Figure 5.11: Hypothesized result of epoxy mold surface grid after hot embossing was performed at a high compressive force.....	100
Figure 5.12: Grid pattern milled directly into epoxy mold surface	101
Figure 5.13: Hot embossing being performed on a thermoplastic material with the use of a silicon wafer with SU-8 features. All items labelled and presented in the order that they are found during the hot embossing process. After an application of force and temperature, the thermoplastic material is released from the hot embossing machine with a transfer of microfluidic features from the silicon wafer master mold.....	103
Figure 5.14: SU-8 features being removed from the silicon wafer substrate and becoming embedded in the thermoplastic material during demolding.....	104
Figure 5.15: Amplification in the number of hot embossing molds that can be created from the use of a single silicon wafer master mold.	110
Figure 5.16: Cross-sectional measurements of a microfluidic feature being made on an SU-8 feature from a silicon master mold, a PDMS negative-relief feature mold produced from the same silicon master mold and an epoxy positive-relief feature mold produced from the same PDMS mold.	111
Figure 6.1: Front and back side of microfluidic design produced in SolidWorks.....	119
Figure 6.2: Device perimeter being milled after microfluidic features had been embossed directly into the thermoplastic material.....	122
Figure 6.3: Image of alignment marks on the surface of the hot embossing epoxy mold.	124
Figure 6.4: Concept of the hot embossed thermoplastic material being transferred to the milled sacrificial layer. The negative-relief embossed alignment marks fit directly onto the positive-relief milled alignment marks in a complementary fashion.....	126
Figure 6.5: Knowledge of the alignment mark coordinates with respect to the milled sacrificial layer origin, and also with respect to the microfluidic features, provided the information necessary to calculate of appropriate zeroing location for milling of backside features.	127
Figure 6.6: Extended nozzle region of the microfluidic design allowed for a buffer when milling was performed in order to assure that the precise cross-sectional dimensions were achieved post-milling.	129
Figure 6.7: Images taken of a finished device that was fabricated through hot embossing of microfluidic features and milling of the device perimeter and additional backside features.	130

Chapter 1

Introduction

1.1 Motivation

Microfluidic technology is a continually increasing area of biotechnology research and innovation. The field has a wide range of applicability and can extend from genomics research to fuel cell studies to the characterization and analysis of cell-cell interactions. Microfluidic technology has much promise in its potential to help progress many current areas of research including, but not limited to, point-of-care diagnostics and personalized medicine. There are certain aspects of microfluidics, which will be discussed shortly, that make it unique in dealing with various biological studies.

Microfluidics runs on the concept that small micro-sized channels, which are sealed and pumped with fluid, will behave in a predictable manner and allow for a higher degree of control and manipulation by the researcher. A mathematical understanding of fluid dynamics can be applied to these micro-scale systems [1] and this allows for a profoundly powerful interface between engineering design and biological analysis. Designs can be constructed in such a way that physiological conditions are emulated through the flow of the fluid in the micro-channels. If a researcher were to be interested in angiogenesis, they could design their microfluidic device in such a way that the *in vivo* conditions will be

more accurately emulated *in vitro* [2] and thus be equipped with a greater degree of understanding of the pathology.

Microfluidic technology has an inherent advantage over current systems used for a multitude of biological studies. As previously stated, microfluidics has the robust capabilities of being able to take on a large number of geometries, which are only limited by the method of fabrication. These different geometries allow researchers to more accurately emulate physiological conditions, compared to the status quo.

In regards to drug discovery, microfluidics offers an avenue to more accurately assess the efficacy of a particular substance and help to lower time associated with research and development. There is also the added benefit of reducing the volume of expensive reagents, which provides a further lowering of costs. Ethical issues associated with animal testing can also be considered when looking into microfluidic technology as an alternative or additional avenue for analysis [3].

There are many benefits associated with the use of microfluidics. However, there are technical challenges that need to be addressed in order to achieve adoption and scalability for microfluidic technology. For example, engineers must have an understanding of the materials most suitable for the particular application and what advantages/disadvantages these materials provide. There are also challenges associated with deciding on any given fabrication method. Fabrication of microfluidic technology can be accomplished through several different avenues, each with its own benefits and limitations.

Biotechnology companies would like to incorporate microfluidics into their research and development departments in order to move forward with commercialization of this useful technology. Currently, there are a number of microfluidic devices that are commercially available. Figure 1.1 introduces some of these companies that are producing microfluidic devices including Microfluidic ChipShop GmbH, Ibidi Diagnostics, Fluidigm and Xona Microfluidics. One company in particular is Bio-Rad Laboratories, Inc. who has shown great interest in the incorporation of microfluidics into their research and development department. However, there is a need to address challenges associated with the iterative design and fabrication process of microfluidic systems. Iterative design of biotechnology is a laborious process that can cost a company a tremendous amount of time and money. There is a strong need for rapid prototyping of microfluidic devices using materials that are amenable to mass production downstream.

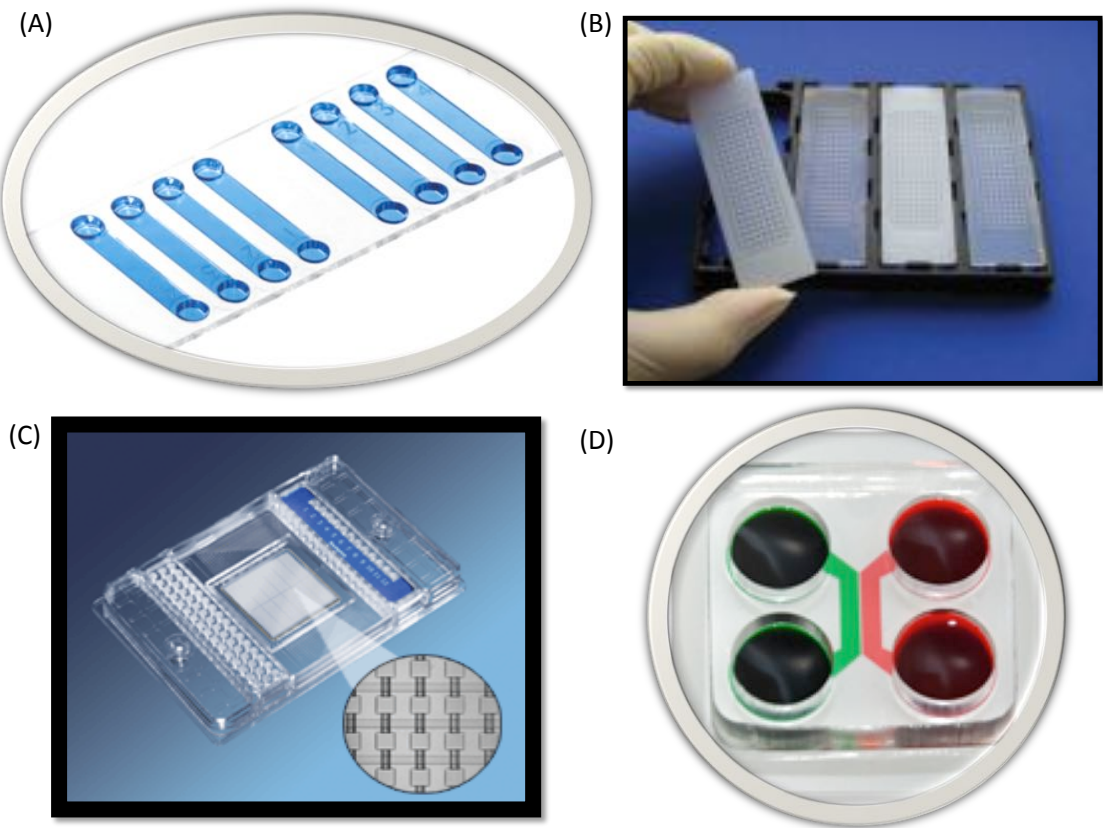


Figure 1.1: Commercially available microfluidic devices produced by (A) Ibidi Diagnostics. (n.d.). Retrieved July 21, 2015, from <http://ibidi.com>, (B) Microfluidic ChipShop GmbH. (n.d.). Retrieved July 21, 2015, from <http://microfluidicchipshop.com>, (C) Fluidigm. (n.d.). Retrieved July 21, 2015, from <https://www.fluidigm.com>, and (D) Xona Microfluidics. (n.d.). Retrieved July 21, 2015, from <http://xonamicrofluidics.com>.

1.2 Project Description

The objective of my research is to develop an optimized fabrication approach that will enable medium volume production of microfluidic devices (i.e., dozens of chips per week) made in various thermoplastics. Thermoplastics are the material of choice when dealing with high-volume production, as it allows for fabrication techniques such as injection molding to be employed. Creating an avenue for rapid prototyping in thermoplastics allows the iterative design process of research and development to more

accurately emulate the conditions that will be seen in the final product. The aim is to use the optimized fabrication process for medium-volume production as an intermediate step between rapid prototyping in polydimethylsiloxane (PDMS) and high-volume production in plastics. An optimized approach will enable rapid testing of designs and reduce the time and cost of microfluidic chip development.

A low-cost, streamlined fabrication process previously developed for polystyrene (PS) [4] has been extended and applied to poly(methylmethacrylate) (PMMA) and cyclic-olefin polymer (COP). Briefly, the process described in Figure 1.2 involves:

1. Fabrication of a silicon-based master mold of 3D positive-relief features by photolithography
2. Micromolding of a negative PDMS mold from the master
3. Fabrication of a positive-relief aluminum-filled epoxy mold from the PDMS mold
4. Hot embossing of microchannel features from epoxy mold onto PMMA or COP thermoplastic
5. Micromilling of the outer edge of the microfluidic device to release the microfluidic chip from the embossed plastic bulk sheet
6. Solvent bonding of multiple plastic layers to create sealed, leak-free devices (not within the scope of this thesis).

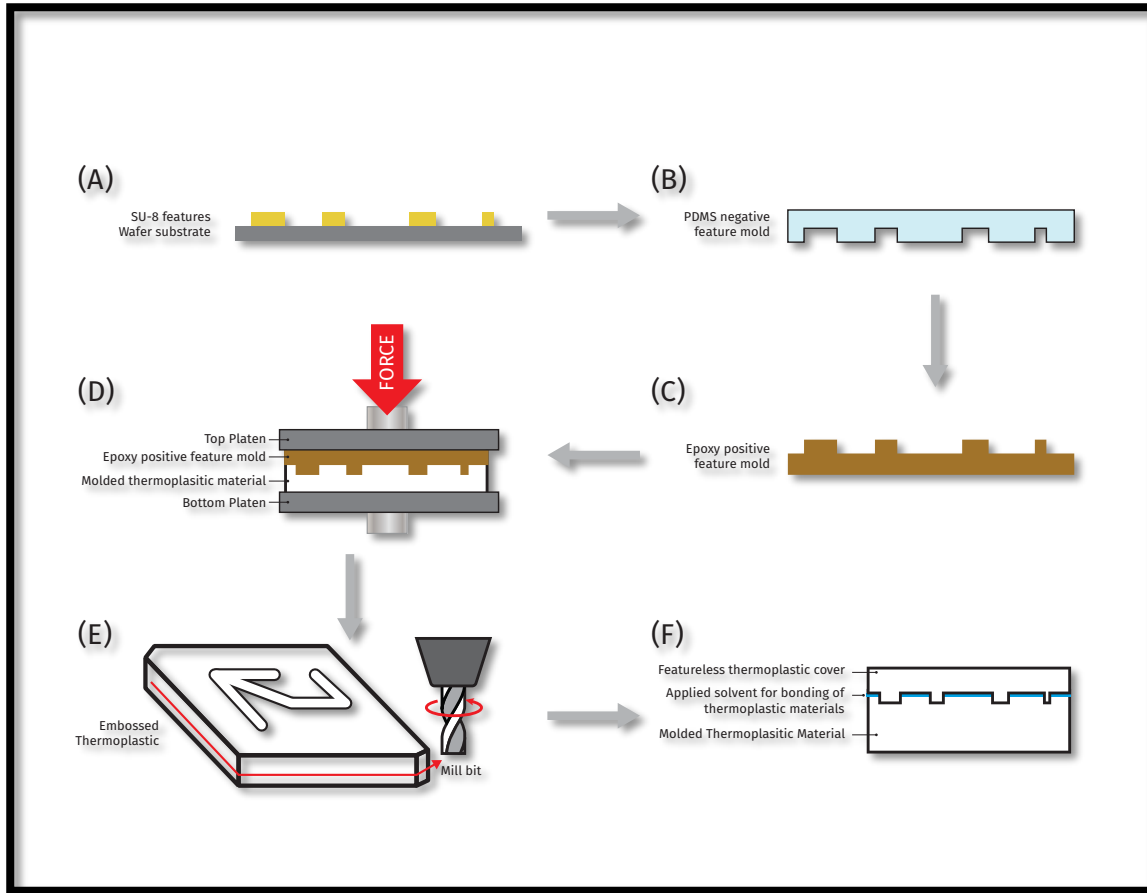


Figure 1.2: Flowchart of microfluidic device fabrication process, showing what is produced at each stage. The process involves (A) the fabrication of an SU-8 master mold, (B) fabrication of a negative-relief feature PDMS mold, (C) fabrication of a positive-relief feature epoxy mold, (D) hot embossing a thermoplastic material with the fabricated epoxy mold, (E) milling a perimeter around the embossed features, and (F) bonding a cover to the embossed thermoplastic material.

While the process has been successfully applied to both PMMA and COP, various technical challenges needed to be addressed. I will methodically work through all technical challenges throughout the following chapters and provide an analysis of my findings, which will ultimately provide an avenue of circumvention for future researchers and members of industry. The work presented in this thesis will be structured in the following manner:

Chapter 2: Background information will be provided for the reader that will outline the specific industrial needs to be addressed. A literature review will also be provided on the materials PDMS, PS, PMMA and COP. A comparison between materials will also be provided. A literature review of photolithography and soft lithography will also be provided in order to give the reader the necessary tools to understand the technical aspects of these methodologies. Additionally, a review of the different plastic fabrication techniques will be discussed. These fabrication techniques include epoxy mold-making, hot embossing, milling and bonding of the device to a surface cover. Lastly, remaining challenges will be addressed and this will provide the framework for the following chapters.

Chapter 3: The photolithography and master fabrication process will be described in full. This process will be discussed beginning from the designing of photolithography masks and will finish with the development of a fabricated master mold. Photolithography was performed on both silicon wafer and Pyrex wafer substrates through frontside and backside UV exposure, respectively. This process was characterized and optimized for specific feature heights and required precise spin speeds to be used. Multi-height features were aligned during UV exposure with the use of an EVG mask aligning system. Lastly, SU-8 feature draft angle control was studied through the use of different exposure energies.

Chapter 4: Soft lithography was studied for the purpose of creating a negative-relief feature mold from the positive-relief feature master wafer. This was then turned into a

positive-relief epoxy mold. Troubleshooting was required to optimize the quality of the epoxy mold for hot embossing. Centrifugation was incorporated into the epoxy mold making protocol, in order to eliminate bubbles trapped within the bulk of the epoxy. An epoxy mold making jig was created in order to help alleviate some of the burden associated with time and human error seen during fabrication. Micromilling of epoxy features was incorporated into the protocol in order to provide gradual 3-dimensional ramp features where necessary.

Chapter 5: Hot embossing of materials PMMA and COP was characterized and optimized for a Carver Press hot embosser and EVG hot embosser. High fidelity transfer of features was the focus during the optimization experimentation and various hot embossing parameters were looked into to achieve this goal. Epoxy mold deformation was also characterized under certain hot embossing conditions. A comparison between hot embossing with silicon wafers and epoxy molds is discussed. Throughput capabilities were also studied over the course of a 40-hour, 5-day workweek in order to determine the number of hot embossed thermoplastic devices that can be produced over this time period.

Chapter 6: Milling of specific device perimeter geometry, as well as backside feature incorporation, was examined. This required a high degree of accuracy when aligning embossed features with the milling machine coordinates. This was achieved through the incorporation of alignment marks into the original photomasks and the creation of a milling machine alignment jig. Tolerance of certain features was also incorporated into

the original design. Milling throughput capabilities were studied in order to determine the greatest volume of devices that can be provided over a week.

Chapter 7: A conclusion on the work previously discussed is provided. This includes a comparison between hot embossing and other device fabrication techniques as a potential for rapid prototyping of thermoplastic microfluidic devices. Epoxy mold hot embossing is compared to silicon wafer hot embossing and a cost comparison is also provided between fabrication techniques. Future work is discussed in order to provide the reader with future steps that should be taken.

Chapter 2

Background and Literature Review

2.1 Choosing Device Material

2.1.1 PDMS

The use of polydimethylsiloxane (PDMS) as a material for fabrication and rapid prototyping of microfluidic devices has been widely adopted in the field and has accommodated a wide variety of experimental setups [5]–[12]. The use of PDMS in its application in microfluidics has been reviewed in the past [13]. PDMS has been used in a multitude of different journal articles that have applied its use in specific devices with specific applications [14]–[25]. Its use has been involved in the fields of micro- and nano-fabrication [26], [27]. Microfluidic devices made of PDMS are fabricated through soft lithography. This process involves the use of a master mold, which is typically fabricated with the use of a silicon wafer substrate and photolithography processes [12]. PDMS has its advantages, which include its optical clarity, cost and turnaround time of prototyping, gas permeability and its application in valve fabrication [28]. This material has been involved in much of the literature in the field of microfluidics but there are limitations as well. A comparison will be provided between PDMS and thermoplastic materials in Section 2.2.5 after the thermoplastic materials PS, PMMA and COP have been introduced in Section 2.2.2, Section 2.2.3 and Section 2.2.4, respectively.

2.1.2 PS

Polystyrene (PS) is a thermoplastic material that has been widely used in biology and tissue culture studies [28]. PS has a glass transition temperature of $\sim 100^{\circ}\text{C}$ [4] and can be used for the molding of thermoplastic microfluidic devices. PS is one material that offers the potential to produce microfluidic devices at a larger scale that can be disposable, which is a need of biologists [28], [29]. Polystyrene requires the need to fabricate a mold that can resist high temperatures and pressure, create inlet and outlet ports, as well as resolve challenges associated with bonding of thermoplastic materials [28]. These challenges have been addressed through the fabrication method developed by Young et al. in which an analysis of hot embossing capabilities in PS was presented [4]. Alternatively, PS microfluidic devices have also been fabricated through the use of hot embossing with PDMS-based hot embossing molds [30] and through micromilling techniques [31]. The use of this material for thermoplastic microfluidic device fabrication and rapid prototyping was the basis for the development of this thesis. This material has its advantages in producing prototyping microfluidic devices that are amenable to mass production fabrication downstream. Although PS has been reported to leach plasticizers, it has strong potential for its cell adhesion, protection against evaporation in cell culture and has been largely characterized [28].

2.1.3 PMMA

Polymethylmethacrylate (PMMA) is another thermoplastic material that has been used in the fabrication of microfluidic devices. This thermoplastic material has a glass transition temperature of 105°C [32], which makes it a suitable candidate for certain fabrication

techniques including hot embossing and injection molding. Hot embossing of microfluidic devices in the thermoplastic PMMA has been studied before and has proven to be a good candidate for microfluidic device fabrication [32], [33]. It can also have micromilling applied to it for microfluidic device prototyping and has had the resultant surface roughness characterized due to this fabrication technique [31], [34], [35]. Due to this material's brittleness, micromilling can produce burrs, which are small plastic remnants after milling has been performed [36] and are often limited to edges and not surfaces [31]. Bonding of PMMA thermoplastic microfluidic devices has been shown to be achievable and contact angles with water has been shown to be 70 degrees [32]. This material was selected as one material to study throughout experimentation for the purposes of rapid prototyping. Hot embossing and milling fabrication techniques were both applied to this thermoplastic material to produce prototyped devices in this project. The thicknesses of PMMA used throughout experimentation varied, depending on the design that was being fabricated, and ranged from 1.5mm-4.5mm.

2.1.4 COP

Cyclo-olefin polymer (COP) was the second thermoplastic material that was used throughout experimentation for prototyping devices in this project. The glass transition temperature for COP is 130°C [37], making it another suitable thermoplastic material for hot embossing and injection molding fabrication techniques. COP has been studied and characterized as a potential material for hot embossing thermoplastic microfluidic devices [37], [38]. COP offers good optical properties, good chemical properties [38], [39] and good bulk properties for ease of fabrication [38], [40]. Another important quality that

COP possesses is that it exhibits low autofluorescence [38], [41]–[43], which makes it a good candidate for fluorescent imaging. Fluorescent and phase contrast imaging are important properties that need to be considered when designing microfluidic devices with a specific material for cell culture [38]. COP also has strong chemical resistance and low water absorption [38], [43], which is a good quality when considering the device sterilization with chemical solvents and studying processes in aqueous environments. COP has also been characterized as a potential material for microfluidic device fabrication by means of micromilling techniques [31]. COP is a more ductile thermoplastic material and as such will produce burrs during micromilling, which is most prevalent along edges and faces [31]. Hot embossing and milling were both used as fabrication techniques for this thermoplastic material.

2.1.5 Comparison of Different Materials for Microfluidic Device Fabrication

Berthier et al. [28] have performed a critical review of microfluidic materials, focusing on a comparison between PDMS and PS. Here, we summarize a few major points raised in the review. PDMS as a material for fabricating microfluidic devices has been widely used in the field. However, there are a number of concerns when using PDMS as the material of choice in microfluidic devices. One issue is with deformation, as PDMS has an elastic modulus of \sim 1-3 MPa, which is approximately 3 orders of magnitude lower than other thermoplastic materials [28]. This lower elastic modulus may cause deformations in the channel dimensions under certain conditions, such as pressure-driven flow [28], [44]. This can be curbed through fabrication under different conditions that

include mixing parameters, curing temperature and time [28], [44], [45]. However, this raises concerns by introducing alternative fabrication conditions and providing a higher degree of difficulty when comparing experimental results over multiple laboratories [28]. Another concern is its permeability to water vapor, which can reach values of ~1,000-6,000 $\mu\text{m}^2/\text{s}$ [46], [47], compared to other materials such as PS that has a reported water vapor permeability of ~43 $\mu\text{m}^2/\text{s}$ [48]. This permeability of PDMS is not always a negative as it also is permeable to gases such as O_2 and CO_2 , which is helpful to cell culture [28]. Oxygen permeability of PDMS has reported diffusion coefficients of ~2,000-4,000 $\mu\text{m}^2/\text{s}$ [49], [50] whereas PS is ~2 $\mu\text{m}^2/\text{s}$ [48]. PDMS also has the potential to absorb hydrophobic compounds [51], which can affect results in cell culture through the uptake of small molecules like soluble factors that play a role in cell signalling [28]. Another issue with PDMS is its potential to leach uncrosslinked oligomers that can incorporate into cellular membranes [52]. This result can be minimized through several cycles of Soxhlet extraction with ethanol, which can reduce the amount of uncrosslinked oligomers in the bulk material [53]. PDMS has also been shown to recover its hydrophobic properties after oxygen plasma treatment to convert its inherent hydrophobic surface to a hydrophilic surface [28]. The PDMS polymer chains have the ability to diffuse to from the bulk material to the surface, which affects its shelf life as a microfluidic device and can cause issues associated with practicality as a material for long-term use [28], [54].

Of particular importance to the work presented in this thesis is the selection of a material that is amenable to mass production downstream. A good prototype device will show the same properties and provide the same results as what would be seen when a more permanent manufacturing process is employed. Injection molding has the capabilities of producing microfluidic devices at the cheapest cost of price per part [55] and is the most likely fabrication technique that will be used for mass production. In order to achieve prototyped devices that will be more representative of microfluidic devices produced through injection molding, it is suggested that thermoplastic materials be used [4]. The limit with fabrication techniques of thermoplastic microfluidic devices is the time required to produce a single device and the quantity that can be produced over the course of a week [4], [33], [37].

2.2 Photolithography and Soft Lithography

2.2.1 Photolithography – Silicon Master Fabrication

Photolithography is a fabrication process that has been used for decades. The first negative series photoresists were introduced in the 1960s [56]. The photolithography process involves a UV light source and a photosensitive polymer to transfer patterns onto a substrate material [57]. Through the use of a photolithography mask, that selectively allows irradiation of certain regions of the photoresist, photochemical processes are initiated that alter the physical and chemical properties of the exposed area [57]. This photochemical process is a free-radical-initiated photocross-linking of the photoresist polymer [56]. There are multiple different photoresists that are available, including

Riston , Ordyl BF 410, Etertec 5600, DF 4615 and DFR-15. However, SU-8 photoresist is the most widely used for high-aspect-ratio lithography. SU-8 is a negative tone, chemically amplified resist, which contains acidic groups and a photoacid generator. Irradiation generates a low concentration of a strong acid that acts as a catalyst of the cross-linking process. Heating of the polymer causes cross-linking and a regeneration of the acid catalyst [57]. There are multiple different SU-8 photoresists available, each with their own specific fabrication protocols and achievable feature heights. A table of the different SU-8 photoresists is provided in Table 2-1.

SU-8 type	Viscosity (cSt)	Thickness (μm)	Soft bake min at 65 °C	Soft bake min at 95 °C	Post-exposure 65 °C	Post-exposure 95 °C	Development (min)
SU-8 2	45	1.5–5	1	1–3	1	1	1
SU-8 5	290	5–15	1	3–5	1	1–2	1–3
SU-8 10	1050	10–30	2–3	5–7	1	2–3	2–5
SU-8 25	2500	15–40	3–5	5–15	1	2–4	3–6
SU-8 50	1250	40–100	5–10	15–30	1	4–10	6–10
SU-8 100	51 500	100–250	10–30	30–90	1	10–20	10–20
SU-8 2002	7.5	2–5	1	2	1	1	1
SU-8 2005	45	6–7	1	2	1	1	1
SU-8 2007	140	8.5–10	1	2	1	1–2	2–3
SU-8 2010	380	13–15	1	2–3	1	2	2–3
SU-8 2015	1250	21–25	1–2	2–5	1	2–3	3–4
SU-8 2025	4500	41–75	1–3	3–9	1	3–7	5–7
SU-8 2035	7000	35–110	2–5	5–20	1	3–10	5–10
SU-8 2050	14 000	50–165	3–5	6–30	1	5–12	6–12
SU-8 2075	22 000	110–225	3–5	9–45	1	7–15	7–12
SU-8 2100	45 000	100–260	5–7	20–60	1	10–15	10–20

Table 2-1 SU-8 characteristic processing times (in minutes) for different variants and film thicknesses [57].

The process by which photolithographic silicon master molds are fabricated is iterative, depending on the number of feature heights required by the design. The process can be outlined as follows:

1. The SU-8 photoresist is spun onto the substrate material at a predetermined RPM to achieve the desired feature height
2. The wafer is soft-baked at 65 °C for a specific time and then at 95 °C for a specific time before being brought down to room temperature

3. The SU-8 is selectively exposed to UV light
4. The wafer is heated, post-exposure, at 65 °C for a specific time and then at 95 °C for a specific time before being brought down to room temperature
5. Steps (1) – (4) are repeated, depending on the number of different feature heights required for the design
6. The wafer is rinsed with an SU-8 developer, containing propylene glycol methyl ether acetate [57], that removes uncrosslinked SU-8 photoresist

2.2.2 Soft Lithography

Soft lithography is a process by which PDMS is poured over top a master mold for the purpose of creating a negative-feature PDMS mold from the positive-feature master. PDMS is known for its ability to mold to features and subsequently release after curing, having achieved mold configurability down to the nanoscale [12]. A flow chart of the soft lithography process to produce a microfluidic device in PDMS is shown in Figure 2.1

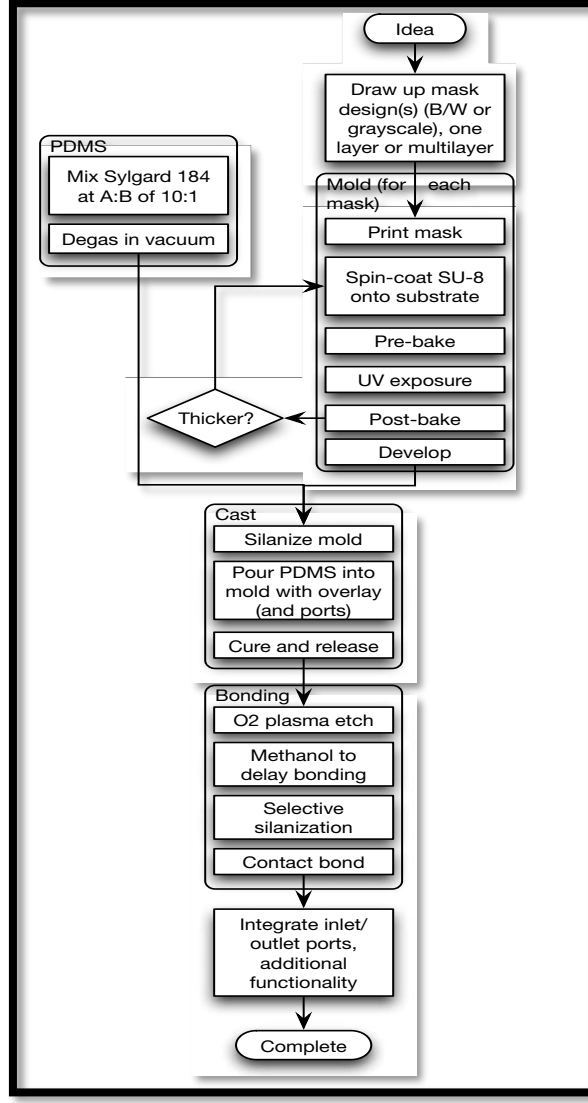


Figure 2.1: Process of making microfluidic devices with PDMS [12].

Typically, the siloxane elastomer base and curing agent are mixed together at a ratio of 10-to-1, respectively [12]. However, increasing the ratio of curing agent in the mixture has been shown to increase the rigidity of the resultant PDMS [58]. There is also the potential to change the mechanical properties of the PDMS by modifying the curing cycle [12]. Mixing in other materials can also alter the mechanical properties of the PDMS [59] or introduce other features that are not achievable with the two components of the

PDMS alone [60]. Coating the PDMS with other media has shown to provide similarly broad possibilities in the performance of the PDMS [61]. Typically, the PDMS has a working life of two hours after mixing, having its viscosity increase with time, so soft lithography must be performed within this window [12]. Once the PDMS is poured over the positive-relief feature master mold, the PDMS can be hardened through direct exposure to heat by means of a hot plate or oven [12].

2.3 Microfabrication of Plastics

2.3.1 Epoxy Mold Making

Epoxy mold making directly follows the fabrication of a PDMS negative-relief feature mold through soft lithography. There are multiple different ways to produce molds for the purposes of hot embossing including electroplating of nickel or nickel alloys [62], deep reactive ion etching (DRIE) in silicon [63], KOH wet etching in silicon [64] with subsequent soft lithography [65], [66] and CNC machining [67]. There are multiple drawbacks to these methods, which include expense of fabrication for electroplating [63], surface roughness and minimum feature size of CNC machining [63], as well as limited lifetime of molds with KOH wet etching in silicon and subsequent soft lithography. Epoxy molds have been used due to their ease of fabrication and relatively lower cost [63]. Epoxy molds have been used for hot embossing of thermoplastic microfluidic devices and have shown to provide a quick avenue for prototyping [6], [37], [63]. There are different types of epoxy that have been used for fabrication of hot embossing molds including EC-415 [4] and Weidling C [37]. The epoxy is mixed in a 10-to-1 ratio of resin

and hardener, respectively. This mixture is then poured directly onto the surface of the negative-relief feature PDMS mold and is hardened according to a specific protocol provided by the manufacturer [4].

2.3.2 Hot Embossing

Hot embossing of thermoplastic microfluidic devices is carried out by the process of heating the thermoplastic material and hot embossing mold between two platens and subsequently applying a force that presses the positive-relief features of the mold directly into the thermoplastic material. The hot embossing machine, mold and thermoplastic material are subject to change [4], [37], [63] but the process remains the same. Hot embossing setups have also included a smooth surface substrate placed below the thermoplastic material and a soft material above the hot embossing mold to create an even pressure distribution across the mold [4]. Hot embossing of PS [4], PMMA [35], [63], [68], [69] and COP [37] have been studied under certain hot embossing conditions. Vacuum conditions between the hot embossing platens have also been looked into as a potential way to mitigate error sources associated with air bubbles being trapped between the hot embossing mold and the thermoplastic material [37]. Planarity of the platens is also a concern in order to assure a uniform emboss and to avoid wedge-errors in the replicated piece [37]. Typically the parameters that have been studied during hot embossing characterization have included the embossing temperature, the embossing force and the time spent applying the embossing force before cooling the thermoplastic material (dwell time) [4], [37], [63]. Figure 2.2 shows an illustration, published by Young et al. [4] that describes epoxy mold making and hot embossing for PS.

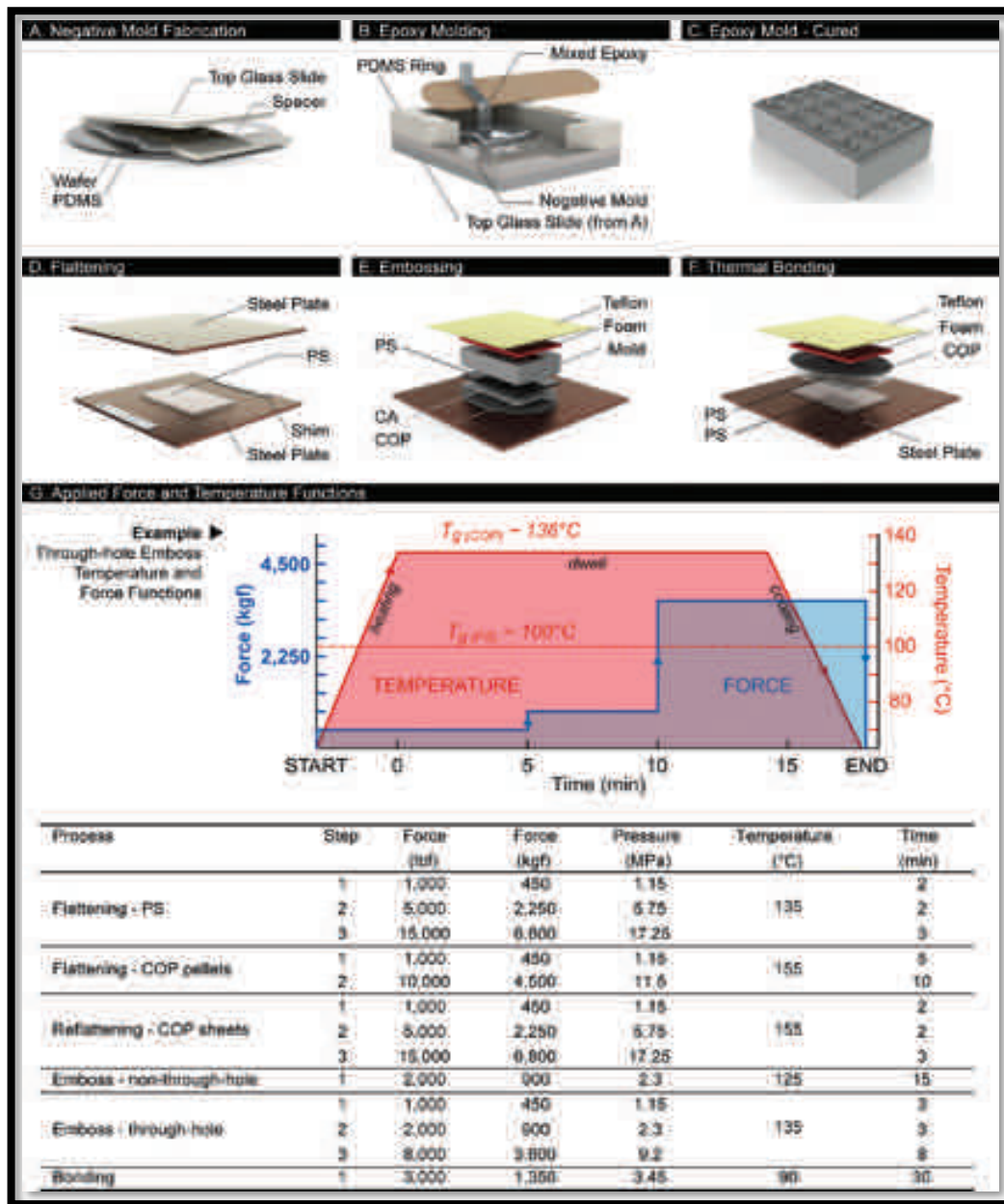


Figure 2.2: Polystyrene microfabrication process. (A) Fabrication of a PDMS slab of uniform thickness to replicate the SU-8 master. (B) Casting of the epoxy in a PDMS cavity composed of the replicate of the SU-8 mold and a PDMS ring. (C) Cured epoxy mold. (D) Flattening of the PS sample to a desired thickness by use of metal shims. (E) Hot embossing of the PS sheet for through-hole fabrication (remove CA and COP for non-through-hole approach). (F) Thermal bonding of two PS sample pieces. (G) Fabrication recipes for different hydraulic press procedures. Pressure is nominal value calculated on the basis of mold surface area of 50-75mm. Force-temperature functions used for through-hole embossing are shown as an example. Temperature curve consists of heating, dwell, and cooling phases. In the dwell phase, force may be successively ramped over time. During cooling, the final applied force during dwell was maintained to prevent sink marks in the embossed part[4].

2.3.3 Milling

Milling of various materials has been a long understood and practiced process, dating back to 1818 [70]. This process involves the removal of material from a starting material through the rotation of an endmill that cuts directly into the workpiece [31]. The endmill has a cylindrical shape and has sharp ridges that are located at the surface of the cylinder around the central axis. These sharp ridges gradually move upwards along the central axis, creating a corkscrew topology. With high-speed rotations, the endmill can be guided to cut the starting material. Originally, milling was employed through manual methods of driving the endmill but has since been advanced to employ the use of computer numerical control (CNC), which allows for computer-aided design models to be directly converted [31]. This helps increase the accuracy of the milling process and has allowed milling to produce features that range in size from several meters to several microns [31], [70]. There are also a wide number of different endmill shapes, materials and sizes that have increased the potential milling features that can be created [31]. Micromilling, milling with the use of endmills that have diameters in the micrometer-range, has been studied for PS, COP and PMMA and has shown that surface roughness associated with milling is typically proportional to the milling feed rate [31]. Along these lines, a smoother milling surface will be produced with a lower feed rate (i.e. how quickly the spinning endmill moves across the starting material). This is an important consideration when looking for a balance between milling time and device quality. Figure 2.3 shows a typical micromilling process, a milling machine and a device made by micromilling.

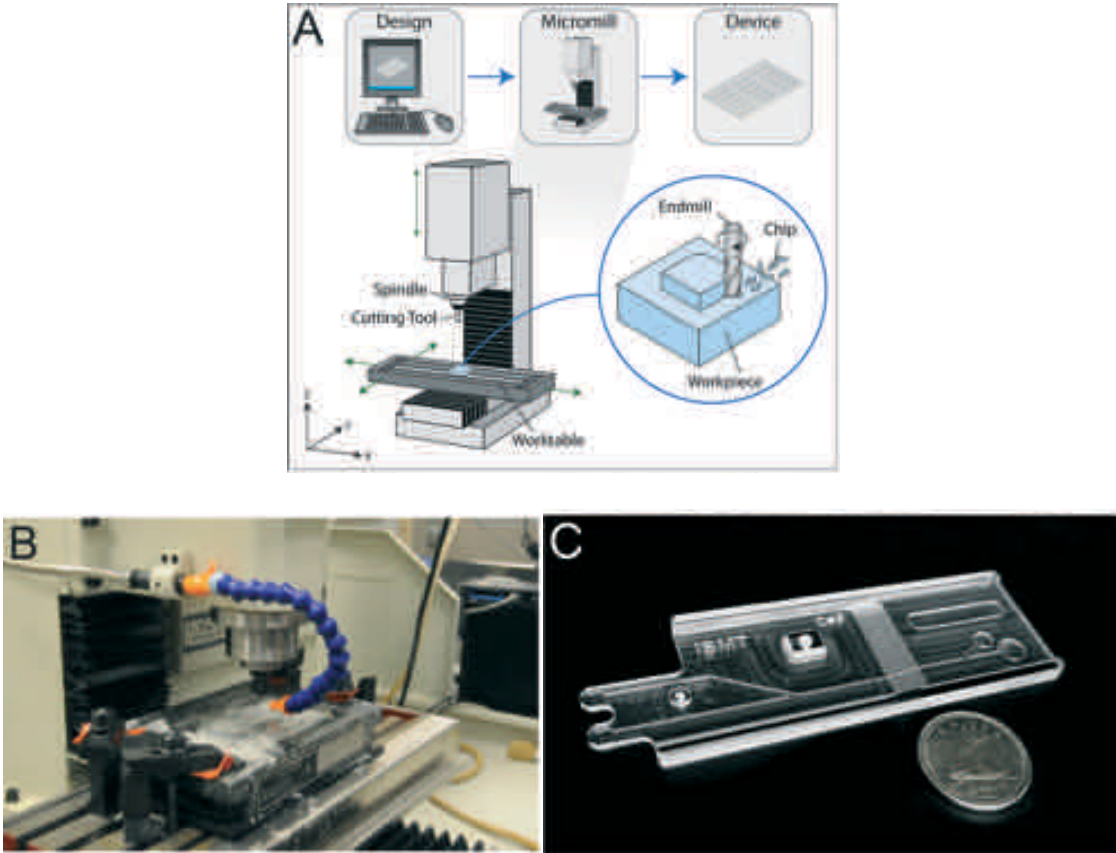


Figure 2.3: (A) A schematic showing the basic components of a CNC mill, which can use computer-aided design (CAD) models to produce finished devices. The mill consists of a worktable (to provide motion in the XY-plane), a cutting tool (to remove material from the workpiece), and a spindle (to hold the cutting tool, spin the cutting tool, and provide motion along the Z-axis). (B) A photograph showing a CNC micromill during operation. (C) A photograph of a micromilled thermoplastic device that contains a variety of feature geometries and sizes [31].

2.3.4 Bonding

Bonding of thermoplastic microfluidic devices involves the sealing of microfluidic features with a backing layer in order to create an enclosed channel through which fluid may be flown. The bonding of microfluidic devices can be achieved through either direct or indirect methods. Indirect bonding methods involve the use of an adhesive layer, while direct bonding methods do not require the use of an additional materials to create a sealed microchannel and thus produce homogeneous sidewalls [39]. Indirect adhesive

bonding can be achieved with the use of a pressure sensitive film [71] or with the use of a thermally sensitive lamination film [72]. Pressure sensitive adhesive films make use of a polymer layer that can flow at room temperature and can come in a solvated liquid form or a dry lamination film [39]. Direct bonding methods include both thermal fusion bonding and solvent bonding [39]. Thermal fusion bonding involves heating the two thermoplastic layers to near or above the glass transition temperature and applying a force to promote contact [39]. This has been looked into as a bonding method for PS [4], [68], PMMA [8], [10], [42], [73] and COP [37], [73]–[77]. Solvent bonding of thermoplastics involves selectively solubilizing a polymer, with the use of particular solvents, to promote polymer chain entanglement across the interface of the two thermoplastic layers [39]. When choosing the thermoplastic material and the solvent for the purposes of solvent bonding, it is important to consider their respective solubility parameters, δ , according to the equation

$$\delta = \sqrt{\frac{H^\circ - RT}{v}}$$

where H° is the latent heat of vaporization, R is the gas constant, T is the absolute temperature and v is the molar volume of the solvent. The further apart solubility parameter values are for the thermoplastic material and the solvent, the longer the two will need to be in contact with one another to produce a sufficient solvent uptake. Table 2-2 lists solubility parameters, δ , for a variety of thermoplastics and solvents.

Thermoplastic	δ [(J/cm ³) ^{1/2}]
PTFE	12.6
PE	16.3
PP	16.3
COC	17.7
PMMA	20.1
PS	18.7
PVC	19.4
PC	19.4
PET	21.8
Solvent	δ [(J/cm ³) ^{1/2}]
Cyclohexane	16.7
Methylene dichloride	19.8
Ethylene dichloride	20.0
Acetone	20.4
<i>n</i> -Hexanol	21.8
Isopropanol	23.4
Acetonitrile	25.1
Ethanol	26.0
Dimethyl sulfoxide	26.7
Methanol	29.6
Water	47.7

Table 2-2 Solubility parameters for selected thermoplastic polymers and organic solvents [78].

2.4 Remaining Challenges

There has been research conducted in the fabrication of thermoplastic microfluidic devices, as well as specific material selection. However, there is the need to further this work in order to provide an avenue for rapid prototyping of thermoplastic microfluidic devices on a scale that extends beyond the small-volume production normally seen in research laboratories. This medium-volume production of thermoplastic microfluidic

devices will help to provide a solution to the gap that currently exists in the field. Moreover, there needs to be a consolidation between hot embossing and milling techniques that can provide a balance between device quality and throughput capabilities. The following chapters will provide an analysis, characterization and optimization of various components throughout the entire process involved in microfluidic device fabrication. This will help to provide future researchers and manufacturers with information on how to produce thermoplastic microfluidic devices at a scale that exceeds low-volume production while avoiding costs associated with mass-volume production methods, such as injection molding.

Chapter 3

Photolithography

3.1 Introduction

Photolithography is a fabrication method that is used to pattern thin films or the substrate on which they reside [57]. This is achieved by exposing a wafer substrate that has been coated with a photoresist material to an irradiated light source. This exposure to an irradiated light source physically and chemically alters the properties of the exposed areas, which in turn affects the solubility of the exposed region [57].

Lithography fabrication processes have been utilized by the electronic industry that has looked for ways to produce increasingly smaller structure dimensions [27], [79]–[87]. Advancements have allowed for 2-dimensional lithography processes to be extended to include 3-dimensional features, which have been applied to a number of different areas of research and development. These areas include the fabrication of biosensors [88]–[93], drug delivery systems [94], scaffolding for tissue engineering [95]–[103] and bioinspired surfaces [104]–[107].

There have been a number of photoresists used for photolithography, however SU-8 has been the most widely accepted, particularly for the purpose of high aspect ratio master fabrication [57]. This negative photoresist was introduced by MicroChem in 1996 and

has been used for its high chemical and mechanical stability, which provide useful conditions for soft lithography in microfluidics [89]. There are a number of different SU-8 types, each with their own characteristic achievable film thicknesses and processing times.

There has been much established work done to understand the general characteristics and particularities of SU-8 photoresist photolithography fabrication [57]. However, there are areas that require improvement for the purpose of rapid prototyping of thermoplastic microfluidic devices. Repeatable microfluidic device fabrication in thermoplastic materials requires an alternative fabrication process from that used when creating PDMS-based microfluidic devices. Hot embossing is one such method and will be described at length in Chapter 5. Of particular interest to this chapter is the concept of demolding after hot embossing has been performed on the raw thermoplastic material. Briefly, thermoplastics are a solid material that become pliable and moldable above a certain temperature, the glass transition temperature, T_g . Hot embossing is performed with a positive-relief feature mold being pressed into the thermoplastic at a temperature above the glass transition temperature. Once hot embossing has been performed, the material is brought back to a temperature below its glass transition temperature, the positive-relief feature hot embossing mold is separated from the thermoplastic. Due to its solidity, the thermoplastic will not easily maneuver around edges of features on the hot embossing mold. In order to account for this difficulty of demolding, considerations must be made when fabricating SU-8 features that will affect hot embossing performance downstream.

These considerations come in the form of SU-8 feature cross-sectional draft angles, which will directly affect the ease of demolding during hot embossing.

Other considerations must be accounted for when fabricating more complex, multi-layer microfluidic devices. These considerations will be discussed throughout Section 3.2, Section 3.3, Section 3.4 and Section 3.5. They are as follows:

1. Characterization of spin speed parameters for desired SU-8 feature heights within a tight tolerance
2. Precise alignment of SU-8 features on a multi-layer device during UV exposure
3. Photolithography method and substrate material selection required to achieve SU-8 features with positive draft angles
4. Energy of exposure required to achieve SU-8 features with positive draft angles that fall within the realm of those seen through injection molding processes, for direct comparison of prototyped device performance to potential mass produced device performance

3.2 Materials and Methods

3.2.1 Photolithography Masks

Throughout the course of prototyping various designs for different sets of photomasks were required. However for the purpose of simplicity only the first design requested for prototyping will be discussed in detail here.

The first design required 3 different feature heights. These 3 different feature heights of the microfluidic device design each required their own specific photolithography mask. These multiple photolithography masks were constructed in Adobe Illustrator. All dimensions of the microfluidic design were constructed to scale by specifying in Adobe Illustrator that measurements should be made in millimeters. Assuring appropriate dimensions and alignment was an important quality assurance step prior to the production of a hard copy version. This was performed through modifying the transparency of each mask to 30% opaqueness on Adobe Illustrator and overlaying each mask in order to assure that features intersected and overlapped as expected. In addition to the features of the microfluidic design, alignment marks were also incorporated into the photomasks in order to help with the specific alignment of the features during UV exposure downstream. These alignment marks came in the form of crosshairs at opposite ends of the mask along the diagonal trajectory from one another. An additional alignment feature was a large rectangular frame enclosing the microfluidic features, which served the dual purpose of marking the maximum outer boundary where features could be included. The multiple soft copy versions of the masks were then emailed to the photomask printing company CAD/Art (CAD/Art Services, Inc., Bandon, OR, USA). The masks were saved in .eps format, as per the request of CAD/Art and were converted into a file format compatible with their equipment. Upon the completion of one last quality check, after the file conversion made by CAD/Art, the photolithography masks were printed on a transparency material and shipped.

3.2.2 SU-8 Negative Photoresist

The type of photoresist used throughout experimentation was an SU-8 negative photoresist (MicroChem Corp., Westborough, MA, USA). Depending on the feature heights required, different series of the SU-8 were used. Most notably SU-8 100 was used to obtain 100 μm feature heights, of which there were 3 for the first design. Other designs employed the use of both SU-8 50 and SU-8 10 to achieve feature heights that fall more closely within the range of those particular series of SU-8 photoresists. Photomasks were designed and printed in such a way to account for the chemical nature of negative-type photoresists. Negative SU-8 photoresists crosslink under exposure of UV light and remained uncrosslinked if UV exposure is not introduced. In lieu of this, photomasks were designed in such a way that microfluidic features were left transparent and featureless areas of the photomask were made opaque. An additional feature of the SU-8 being used is its propensity to absorb light of shorter wavelengths. Wavelengths below 350 nm will over-crosslink the SU-8 and produce a T-topping cross-sectional shape. In order to circumvent this undesired result, a UV filter (Omega Optical, Inc., Brattleboro, VT, USA) was purchased to minimize light exposure with wavelengths below 350 nm. The UV filter that was used has a transmittance of ~0% at wavelengths of ≤ 325 nm. The regions of the SU-8 that were not exposed to UV light were washed away during development in fabrication steps downstream.

3.2.3 Silicon Wafers

Silicon wafers were one particular substrate material that was used to fabricate SU-8 feature master molds. The fabrication protocol of SU-8 feature master molds with silicon

wafer substrates began with the centering of the silicon wafer (WRS Materials, San Jose, CA, USA) on the SU-8 spinner (Specialty Coating Systems, Indianapolis, IN, USA). This was to ensure that tangential velocity of the spinning silicon wafer was uniform at all points along the perimeter of the wafer. Once centering was achieved, SU-8 was dispensed onto the surface of the silicon wafer and spun at an acceleration of 100 RPM/second for 5 seconds and held at 500 RPM for 10 seconds, allowing the SU-8 to spread across the surface of the wafer. The RPM was then accelerated at 300 RPM/second up to a predetermined RPM according to the feature height that was hoped to be achieved. The RPM was then lowered over 5 seconds back down to zero and the silicon wafer with the first layer of SU-8 was brought over to the hot plates (Torrey Pines Scientific Inc., Carlsbad, CA, USA) for a pre-exposure soft baking step. The design had 3 layers at 100 μm each, for a theoretical total height of 300 μm . Figure 3.1 shows the 3 separate photomasks. With this in mind, the wafer was first put on a hot plate at 65°C and held for 10 minutes. The silicon wafer was then brought over to the second hot plate, which was held at 95°C, and left for 60 minutes. After 60 minutes, the wafer was brought back to the 65°C hot plate in order to bring the wafer back to room temperature in a stepwise fashion. The wafer was left on the 65°C hot plate for 5 minutes and then placed onto a workstation while the mask aligner was prepared for the first exposure. The wafer was then put into the mask aligner and the first layer photolithography mask was placed over top of the SU-8. The photolithography mask and SU-8 were placed in close contact through one of two methods, depending on the particular mask aligner that was used, which will be discussed shortly. The UV filter was then placed on top of the area of the photolithography mask that contained the microfluidic features. The wafer

was then exposed to UV light, which had a predetermined energy. Once UV exposure was complete, the photolithography mask was separated from the silicon wafer and spun SU-8. The wafer was then brought over to the hot plates for a post-exposure bake. The wafer was placed on to the hot plate held at 65°C and was left for 1 minute. The silicon wafer was then placed on the 95°C hot plate and held at this temperature for 10 minutes. In order to reduce the temperature of the silicon wafer in a stepwise fashion back to room temperature, the wafer was placed on the 65°C hot plate after the 95°C hot plate step had completed. After 5 minutes on the 65°C hot plate, the wafer was placed on the workbench. The wafer was then brought over to the SU-8 spinner again and the process repeated for each additional feature height that was required.

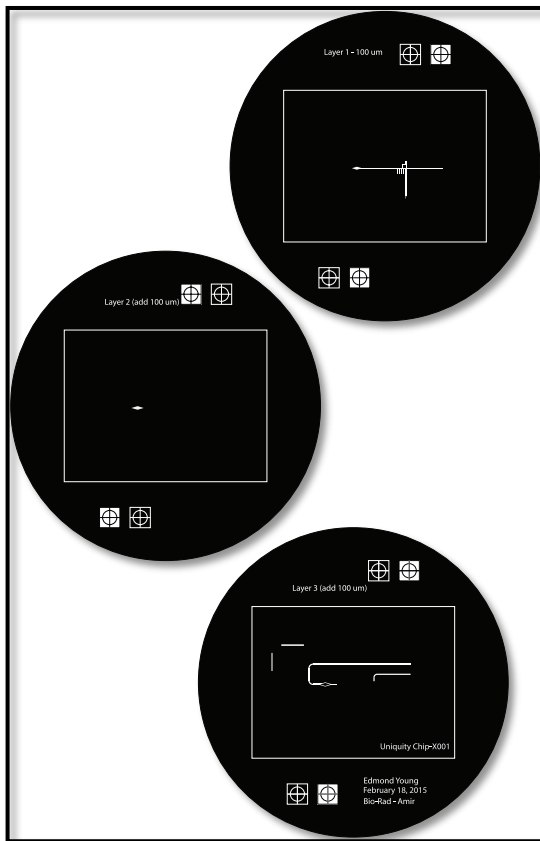


Figure 3.1: 3 photolithography masks that were used to fabricate the 3-layer SU-8 master mold.

3.2.4 Pyrex Wafers

Pyrex glass wafers (University Wafer, Boston, MA, USA) was another substrate that was used to support SU-8 layers of master molds. The fabrication of master molds with the use of Pyrex wafer substrates followed nearly the same protocol as that used for silicon wafer substrates. The optical transparency of glass wafers allowed the use of backside lithography for creating draft angles that could not be easily created with normal frontside lithography. The Pyrex wafer was centered on the SU-8 spinner and had SU-8 negative photoresist poured onto its surface. The wafer and SU-8 were then accelerated at 100 RPM/second over 5 seconds and held at 500 RPM for 10 seconds. The wafer was then accelerated at 300 RPM/second up to a predetermined RPM depending on the feature height that would ideally be achieved. Then the wafer was brought back to rest over 5 seconds. The Pyrex wafer with spun SU-8 was brought to the 65°C hot plate and left for 10 minutes. The wafer was then transferred to the 95°C hot plate and left for 60 minutes before it was brought back to the 65°C hot plate for an additional 5 minutes in order to cool back to room temperature in a stepwise fashion. The wafer was then brought over to the mask aligner in order to expose with UV light. Once exposed, the wafer was brought to the 65°C hot plate and held for 1 minute. The wafer was then brought to the 95°C hot plate and held for 10 minutes before it was brought back to the 65°C hot plate again for 5 minutes and then placed onto the workbench. Once the Pyrex wafer reached room temperature, it was brought back to the SU-8 spinner and the process was repeated 2 more times, for a total of 3 times. Figure 3.2 shows a schematic of the photolithography process for (a) Silicon wafers and (b) Pyrex wafers.

PHOTOLITHOGRAPHY MASTER WAFER FABRICATION

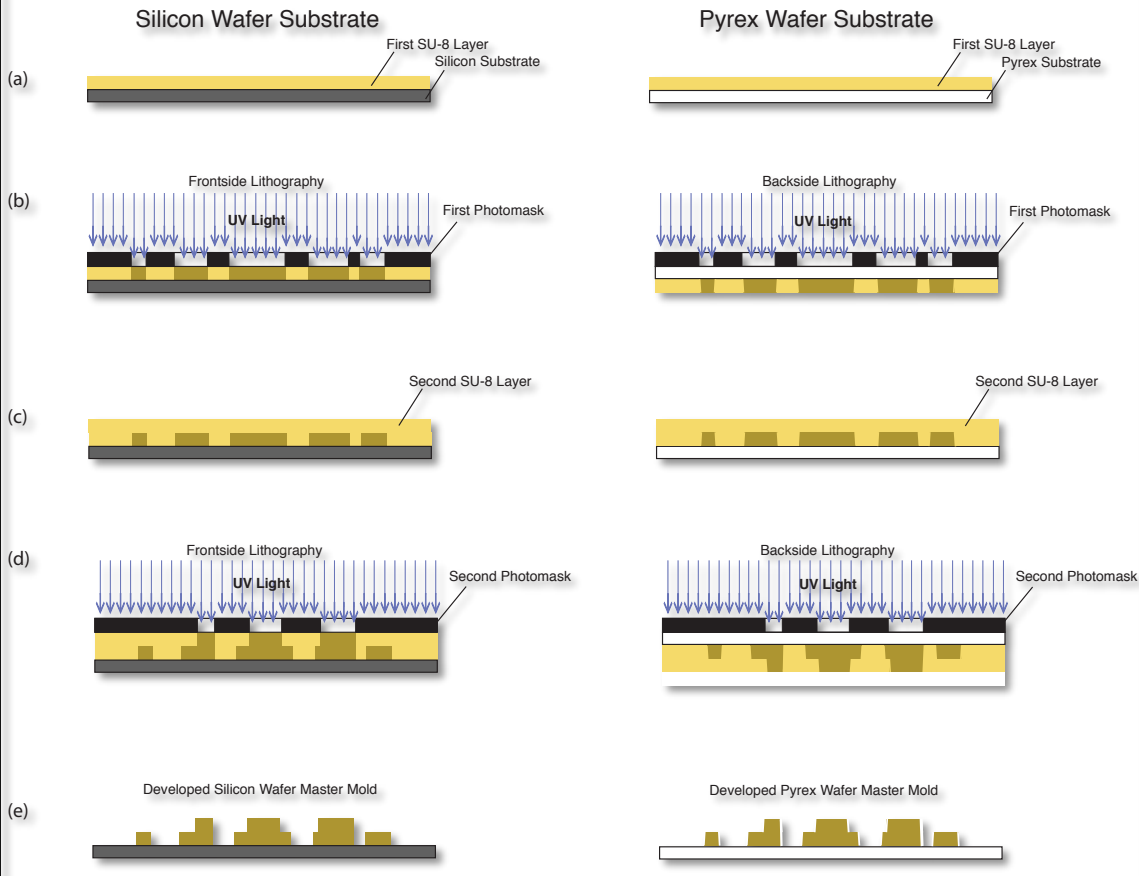


Figure 3.2: A comparison between SU-8 fabrication processes involving a silicon wafer substrate and a Pyrex wafer substrate. (a) shows the first layer of SU-8 being spun onto the substrate material and (B) shows the first layer being selectively exposed to UV light, where the silicon wafer substrate is being exposed through frontside lithography and the pyrex wafer substrate is being exposed through backside lithography. (C) shows a second layer of SU-8 being spun on top of the first layer of SU-8 and (D) shows the second layer of SU-8 being selectively exposed to UV light through frontside lithography for the silicon wafer substrate and through backside lithography for the Pyrex wafer substrate. (E) shows the developed silicon and Pyrex wafer master molds.

The novel component of Pyrex glass wafers is that they are a transparent substrate material. This was a useful feature in that it allowed for the option to perform UV exposure under two different conditions. The first method of UV exposure was through frontside lithography, as was performed with the silicon wafer substrate, in which a

photomask was placed directly onto the spun SU-8 photoresist and was exposed according to this top-down setup. The second method, which was unique to the Pyrex glass wafer substrate, is to expose the SU-8 photoresist through backside lithography. This was performed by placing the photomask directly onto the bottom surface of the Pyrex glass, opposite to the SU-8 photoresist, and having the SU-8 exposed with UV light in a bottom-up setup. This ulterior UV exposure setup showed interesting results when considering SU-8 feature draft angles, which will be discussed below and was an important point to consider for downstream hot embossing processes.

3.2.5 Mask Aligner System

Two separate mask aligner systems were tested throughout experimentation. The first mask aligner and UV exposure system was used primarily throughout the earlier stages and was an OAI Mask Aligner System Model 30 (OAI, San Jose, CA, USA). This system was a more manual system compared to the EVG 620 mask aligner (EV Group, Florian am Inn, Austria), which was used throughout the majority of experimentation. The OAI Mask Aligner System Model 30 required a glass slide to be place directly on top of the photolithography mask, in order to create a close contact between mask and SU-8 for UV exposure. Another aspect of the OAI Mask Aligner System Model 30 was the manual aligning method required for a multi-layer device, compared to the EVG system. In contrast, the EVG 620 system was developed in such a way that the photolithography mask could be taped directly to a provided class cover, which could be programed to provide a specified contact mode between mask and SU-8. The contact mode that was used was a hard contact, which put the mask and SU-8 in direct contact while also

applying a controlled force. Hard contact mode resulted in a resolution of 1-2 μm , according to the EVG 620 mask aligner operations manual. Another aspect of the EVG 620 mask aligner system was its relative ease of use and precision in aligning of features for a multi-height device, compared to the OAI Mask Aligner System Model 30. The issue of alignment and a comparison between the OAI Mask Aligner System Model 30 and the EVG 620 mask aligner will be discussed shortly.

3.3 Optimization of Spin Speed for Precise Feature Heights

A large number of wafers were used in order to try and achieve feature heights within tolerance. Of particular importance was the first feature height, which was required to be within 5 μm of the 100 μm theoretical value. There were multiple sources of potential error and achieving feature heights within these tolerances was not simply a matter of following the suggested values listed on the MicroChem SU-8 datasheet. Sources of potential error were attempted to be minimized, including levelling of the SU-8 spinner as well as levelling of the hot plates used for pre-UV exposure soft baking and post exposure baking. A concerted effort was also made in order to assure that the wafer was precisely centered on the SU-8 spinner to the highest achievable level within the limitations of the unaided eye. Throughout the course of a year there was a fluctuation in humidity and also temperature, which may have played a factor in the fluctuation in feature heights at any particular spin speed. Recorded humidity fluctuated from a low value of 17% to a high value of 54%. Temperature also fluctuated from a low value of 19.1°C to a high value of 25°C. In order to achieve feature heights within tolerance, multiple wafers were used on any given day in order to fabricate multiple SU-8 master

molds at different maximum RPMs. The first fabricated SU-8 master mold would follow the spin speeds recommended on the MicroChem SU-8 datasheet. This provided an initial reference for comparison of feature heights versus spin speeds. Once this SU-8 master mold was fully fabricated, and subsequently developed, measurements were made of feature heights for all three layers of the multilayer device. With these recorded measurements, adjustments could be made to the maximum RPM values that were used for each individual layer in order to accommodate for deviations from the theoretical values. Once the next master wafer mold was fabricated, measurements were again made on each of the individual feature heights. If feature heights were still not within tolerance, additional master molds were fabricated with adjusted maximum RPM values. This process was repeated until feature heights within tolerance were achieved.

The length of time that a wafer was held at the maximum RPM value was thought to be a potential source of variability in feature heights. Throughout early experimentation, a hold time of 30 seconds was employed during the time that the wafer was spun at the maximum RPM value. This hold time of 30 seconds was chosen based on the recommendation of MicroChem as seen on their datasheet. As experimentation continued, the hold time was increased to 40 seconds and then subsequently to 45 seconds. The purpose of this increase in hold time was to address the concern that the quantity of SU-8 dispensed between different wafers, as well as between layers on any particular wafer, was not held at a constant value. There was no automated SU-8 dispensing system and pouring of SU-8 was performed through pouring into a measuring cup, followed by pouring directly onto the wafer. Attempts were made to try and

dispense the same quantity of SU-8 onto the wafer before spinning, however the use of measuring cups did not help entirely. This was due to a certain volume of SU-8 remaining in the measuring cup after the pouring. It was hypothesized that an increase in hold time at maximum RPM would help towards reaching a negligible flow of SU-8 off the wafer. As a direct result, the remaining SU-8 on the wafer would reach a lower limit in thickness, which could be consistently achieved from one master fabrication to another. This was hypothesized after consideration of the fluid dynamics derivation, with appropriate boundary conditions. If one were to take the radial continuity equation and simplified momentum equation

$$-\rho r \omega^2 = \mu \frac{\partial u_r^2}{\partial z^2}$$

and employ the following boundary conditions

$$\frac{du_r}{dz} = 0 \text{ at } z = 0$$

$$u_r = 0 \text{ at } z = 0$$

we can solve for the rate of change of film thickness according to the equation

$$Q = 2\pi r \int_0^{H_R} u_r(z, R) dz = -\pi R^2 \frac{dH'}{dt}$$

which can be integrated to give

$$\frac{H(t)}{H_0} = (1 + \frac{4\rho\omega^2 H_0^2}{3\mu} t)^{-1/2}$$

This unfortunately did not help to address the issue of fluctuation in feature heights for a given spin speed and a variability persisted. Data was collected for the RPM values, SU-8 type used, humidity, temperature and hold time. This data is presented in Figure 3.3

below to give the reader a sense of the variability that was observed throughout experimentation.

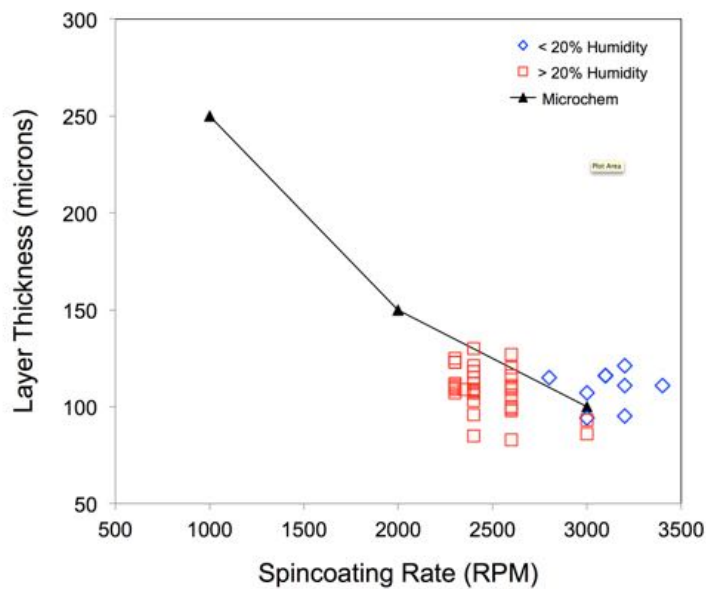


Figure 3.3: Graphed data of SU-8 layer thicknesses achieved under different spincoating rates (RPM). Plotted data points were separated by recorded clean room humidity and theoretical MicroChem values were also plotted for comparison.

Although there was variability associated with spin speeds and resultant feature heights, this did help to strengthen the case for the use of epoxy mold fabrication for the purposes of hot embossing. The fabrication of a master wafer mold with features that are required to be within a tight tolerance is a difficult task and the manufacturer should take every precaution to ensure its preservation once it has been attained. The fabrication of a secondary mold for the purposes of hot embossing not only helps address issues of throughput by allowing for parallelization, but also helps to protect the original master wafer mold from being placed in potentially damaging conditions such as those seen during the hot embossing process.

3.4 Alignment of Multi-Height Features during UV Exposure

3.4.1 OAI Mask Aligner System Model 30

Preliminary UV exposure and mask aligning to lower level feature layers was performed on the OAI Mask Aligner System Model 30 (OAI, San Jose, CA, USA). This mask aligner system was located in the Toronto Microfluidics Foundry cleanroom in the Mechanical and Industrial Engineering department at the University of Toronto. This mask aligner system produced high quality SU-8 polymerized features, with a vertical side wall, upon exposure to the UV light.

The OAI Mask Aligner System Model 30 was designed to accommodate wafers up to 6” in diameter. There was a feature that provided the user a higher degree of manual aligning control through the use of a fine adjustment mask aligner, which provided incremental movement in the x-,y- and theta-direction. This fine adjustment mask aligner was designed to accommodate 4” wafers and did not provide an avenue for higher diameter wafers to be aligned through its use. The design that was being worked with throughout experimentation required a 6” wafer substrate and a 6” photolithography mask. As an outcome, mask aligning using the OAI Mask Aligner System Model 30 was performed through a careful manual adjustment of the photolithography mask. Once the photolithography mask and SU-8 features were aligned, a glass cover was placed over top of the photolithography mask as a weight to provide a tighter contact between the mask and SU-8. The setup was then brought over to the OAI Mask Aligner System Model 30 and was exposed to the UV light source for a calculated amount of time.

The specific amount of time that the SU-8 was exposed was predetermined and depended on a number of considerations. The first consideration was the required energy of exposure recommended by the MicroChem datasheet for the SU-8 type being used and the feature of desired. An SU-8 feature of 100 μm with the use of SU-8 100 would require an energy of 550 mJ/cm^2 . The second consideration was the measured UV intensity of the OAI Mask Aligner System Model 30 light source on the particular day of fabrication. This was measured with an OAI308 power meter (OAI, San Jose, CA, USA) by placing its sensor under the UV light source and exposing it for 10 seconds. With this measurement and the recommended value for the energy of exposure, the time of exposure could be calculated according to the equation

$$t = \frac{E}{I}$$

where t is the time of exposure in seconds, E is the energy of exposure and I is the UV light intensity.

The OAI Mask Aligner System Model 30 provided a quick and easy method of UV exposure and worked well for simpler designs that required only one exposure step, but it had its limitations. The OAI Mask Aligner System Model 30 did not provide much use in terms of ease of alignment for multi-layered devices with wafers at 6" in diameter and often manual aligning over multiple feature layers would introduce a human-associated error that was not within tolerance. The design required the third 100 μm layer channel to be aligned with the first 100 μm channel of the same width. With any misalignment between the first and second layer, or the second and third layer, this precise alignment of device features would not be seen and would not be accepted outside of the tolerance

required. This proved to be a difficult task to perform manually and other mask aligner systems were looked into.

3.4.2 EVG Mask Aligner

3.4.2.1 Silicon wafer

The EVG 620 mask aligner system (EV Group, Florian am Inn, Austria) was introduced into the Toronto Microfluidics Foundry cleanroom in the Mechanical and Industrial Engineering department at the University of Toronto and subsequent experimentation was performed on this system.

The EVG 620 mask aligner system provided a more robust mask aligner and UV exposure option, compared to the previously used OAI Mask Aligner System Model 30. One difference was that the new mask aligner and UV exposure system offered different wafer holders that could be incorporated into the system, which allowed different sized wafer substrates to fit in the appropriate location for alignment. There was a specific 6" wafer holder, which was used for fabrication of the prototyped design created by Bio-Rad Laboratories. There were also multiple mask holders that could be interchanged to accommodate for the size of mask that was being used. The EVG mask aligner system offered a mask holder that could comfortably fit a 6" photolithography mask design. The mask holder was a 7"x7" piece of glass, which required that the previously printed 6" diameter photolithography masks be manually aligned roughly to the SU-8 features. This rough manual aligning could be circumvented through fabrication 7"x7" chrome masks. The EVG mask aligner also provided a graphical user interface where fine alignment

could be performed. This was achieved with the use of two parallel objectives that were placed overtop of the exposed photolithography mask region, providing an image directly onto the EVG mask aligner monitor screen. Three fine adjustment knobs on the EVG mask aligner allowed the user to perform x-,y- and theta-direction movements during alignment of the mask aligner and SU-8 features.

Alignment was performed in a stepwise process. This alignment of the photolithography mask to SU-8 features was achieved by first introducing the photolithography mask into the EVG mask aligner. The objectives were then focused on two distant regions of the photolithography mask that laid along the same horizontal line. The theta adjustment knob was rotated until the photolithography features became aligned with the objectives, which were along a horizontal axis to one another. This ensured that the photolithography mask was parallel to the objectives. Once this theta-directed alignment of the photolithography mask was completed, the mask was vacuum sealed to the mask holder and fixed in position. The substrate with SU-8 features was then loaded into the substrate holder and brought to a close contact with the photolithography mask. The separation distance between the photolithography mask and SU-8 could be specified through the graphical user interface provided by EVG. The objectives then focused on a plane intermediate to the SU-8 features and photolithography mask features. Due to their close proximity to one another, both features could be focused on simultaneously. The x-, y- and theta-adjustment knobs were used to align the wafer substrate and SU-8 features to the photolithography mask. Once alignment between wafer features and photomask features was achieved, UV exposure could begin.

UV exposure of the SU-8 could be performed by specifying the desired energy of exposure, in units of mJ/cm^2 , directly into the graphical user interface of the EVG mask aligner system. This energy could be adjusted from one exposure to the next, which provided the user with the ability to test different energies and the effects that they had on cross-sectional feature quality.

The EVG mask aligner system did not come with an installed UV filter for UV exposure. This proved to be an issue, as wavelengths below 350 nm will over-crosslink the SU-8 and produce a T-topping cross-sectional shape, as discussed above. A UV filter (Omega Optical, Inc., Brattleboro, VT, USA) was purchased to minimize light exposure with wavelengths below 350 nm, which addressed the issue of T-topping. The UV filter was placed directly overtop the photolithography mask after alignment had been performed and before UV exposure was initiated.

3.4.2.2 Pyrex Wafer

Alignment of photolithography mask features to the SU-8 features on a Pyrex substrate was performed in a nearly identical process, compared to the alignment performed with the use of a silicon wafer substrate. Both alignments were performed with the use of the EVG mask aligner and followed the same protocol outlined above. First, the photolithography mask was introduced into the EVG mask aligner system and had its features aligned in the theta-direction to ensure that they were parallel to the objectives of

the mask aligner. The wafer was then introduced into the system and the SU-8 features were aligned to the photolithography mask.

One important difference did exist between the mask alignment method for a silicon wafer substrate and Pyrex wafer substrate. The silicon wafer substrate was inserted into the EVG mask aligner system in such a way that the SU-8 features faced upwards and were in close contact with the photolithography mask. The subsequent UV exposure was performed through frontside lithography where the UV light directly contacted the SU-8 after having gone through the photolithography mask. In contrast, the Pyrex wafer substrate was incorporated into the EVG mask aligner system in such a way that the SU-8 features faced downwards and the bottom side of the Pyrex wafer was in direct contact with the photolithography mask. The UV light in this exposure setup passed through the photolithography mask and Pyrex wafer substrate before contacting the SU-8. This backside lithography method was studied for the purpose of cross-sectional SU-8 feature draft angle experimentation, which will be discussed shortly.

The alignment of SU-8 features to the photolithography mask through backside lithography was not without difficulty. The objectives were required to focus on both the SU-8 features and photolithography mask simultaneously in order to achieve a precise alignment with a high degree of confidence from the user. This was achievable with the silicon wafer frontside lithography setup because the SU-8 features and photolithography mask were within close proximity of one another. However, with the employment of the backside lithography method, there was a greater separation between the SU-8 features

and photolithography mask. This separation became greater with each successive spin of SU-8 for the 3-layer design. As a result, there became an increasing level of difficulty associated with confidently aligning SU-8 features with photolithography mask features to the precision achieved with silicon wafer substrate frontside lithography. Figure 3.4 shows the precise alignment of layers 1 and 3 of the SU-8 microfluidic features.

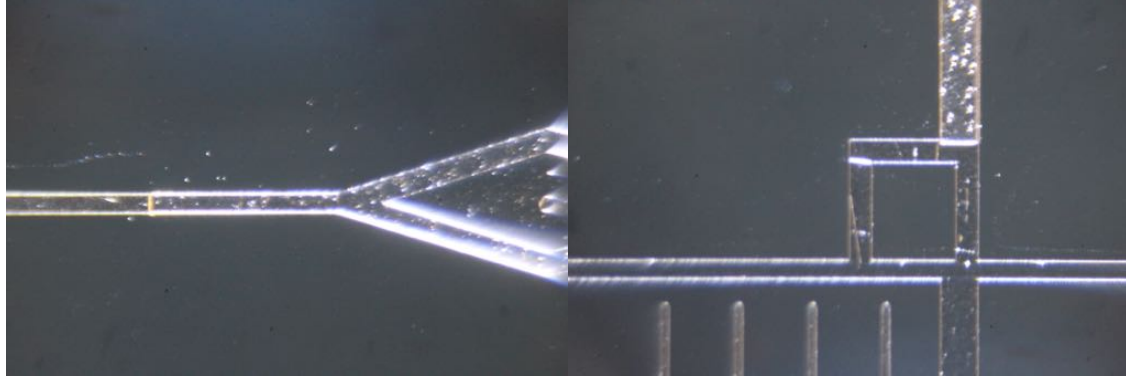


Figure 3.4: Precise alignment of microfluidic device features during UV exposure. The images show the alignment achieved between SU-8 layer 1 and SU-8 layer 3, with respective feature heights of 100 and 300 micrometers.

3.5 Feature Side Wall Draft Angle

3.5.1 Silicon Wafer Substrate

Side wall draft angles can be defined as the angle that the cross-sectional SU-8 feature side wall makes with the normal to the substrate material. A draft angle of zero degrees would be a vertical sidewall, which would be perfectly perpendicular to the substrate material. A negative draft angle would be characterized by a sidewall that makes an angle $<0^\circ$ with the normal to the substrate material and the cross-sectional width of the SU-8 feature closer to the substrate material is less than the cross-sectional width of the SU-8 feature further away from the substrate material. A positive draft angle would be

characterized by a sidewall that makes an angle $>0^\circ$ with the normal to the substrate material and the cross-sectional width of the SU-8 feature closer to the substrate is greater than the cross-sectional width of the SU-8 feature further away from the substrate material. Figure 3.5 shows the cross-sectional geometry of SU-8 features that have (a) a negative draft angle and (b) a positive draft angle. By convention, the draft angle is given a value in degrees where a value of 0° constitutes a vertical sidewall. The degree value becomes increasingly positive as the sidewall takes on a positive draft angle geometry, while becoming more negative if the sidewall takes on a negative draft angle geometry. Positive draft angles are an important aspect of master wafer mold fabrication, as they help improve the ease of demolding after hot embossing downstream in the microfluidic fabrication process. Particularly, a draft angle of $+3^\circ$ to $+5^\circ$ is desired, as this is the range typically seen in injection molding processes. Being able to emulate fabrication conditions seen in injection molding processes will help to provide companies with the most accurate representation of how their design will function under mass production conditions.

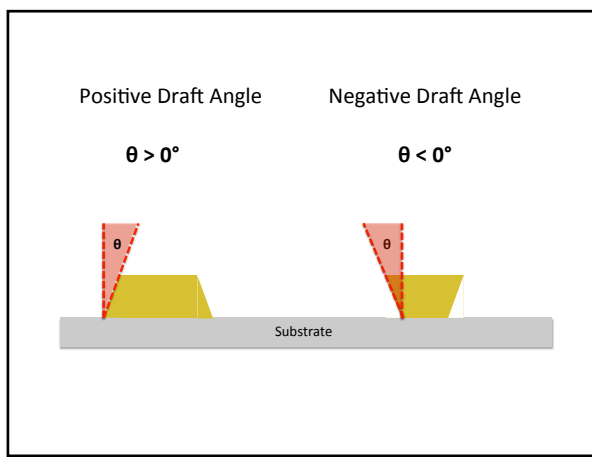


Figure 3.5: Illustration showing the concept of positive and negative draft angles in comparison to the line normal to the surface of the substrate material.

Experimentation on cross-sectional SU-8 feature draft angles was first attempted with the use of silicon wafers as the substrate material. Silicon wafers were the first substrate used for experimentation due to their lower cost of \$0.54 per wafer for an order of 50 wafers, compared to Pyrex wafers that have a cost of \$29.90 per wafer for an order of 25 wafers. Originally, it was noticed that a lower energy of exposure with silicon wafer substrates produced features with negative draft angles, or an undercut, which was a largely undesirable trait. It was hypothesized that increasing the energy of exposure should help to improve the draft angle to a vertical sidewall and eventually to a positive draft angle. This hypothesis was tested and with UV exposure energies of 375 mJ/cm^2 , 420 mJ/cm^2 and 420 mJ/cm^2 for layers 1, 2 and 3, respectively, vertical sidewalls were achieved. Energies were then further increased in an attempt to further improve draft angles and ultimately achieve positive draft angles. Eventually, with 3 successive exposure energies of 1000 mJ/cm^2 , for the 3 separate SU-8 feature layers, a positive draft angle was realized for the first layer. Vertical sidewalls still persisted for the second and third layer, so the energy of exposure was further increased for these two layers. The next 3 attempted exposure energies for layers 1, 2 and 3 were 1000 mJ/cm^2 , 2500 mJ/cm^2 and 4000 mJ/cm^2 . Again, these energies of exposure showed a positive draft angle for the first layer but vertical sidewalls for layers 2 and 3. An attempt to test the ability to control the draft angle degree was made by fabricating a single layer device with an exposure energy of 5000 mJ/cm^2 , with a hope that the draft angle would be even more positive than observed for the case where the energy of exposure was 1000 mJ/cm^2 . The cross-sectional feature geometry proved to be the same under both conditions. Vertical

sidewalls were achievable with silicon wafer frontside lithography, however there was an interest in having further control on the lithography fabrication process and tuning draft angles to a value that would fall within injection molding values. Figure 3.6 shows cross-sectional images of PDMS microfluidic features where the SU-8 used to produce the PDMS features were exposed under different energies.

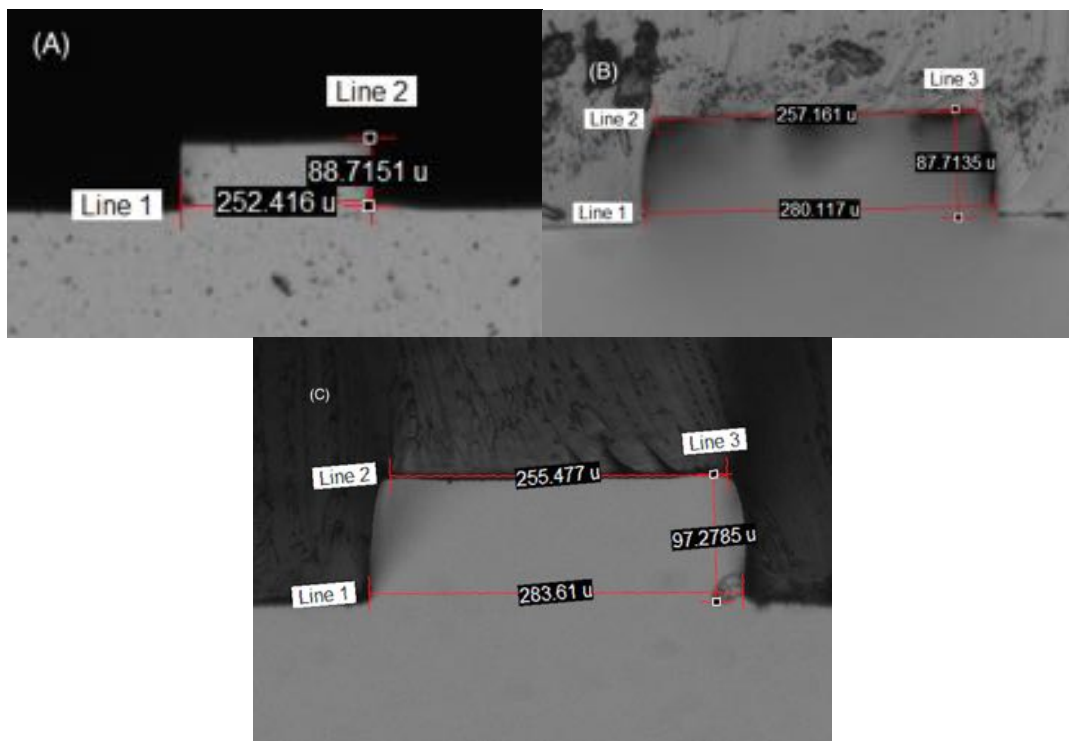


Figure 3.6: Cross-sectional PDMS image of microfluidic feature exposed with an energy value of (A) 420 mJ/cm^2 , (B) 1000 mJ/cm^2 and (C) 5000 mJ/cm^2 .

3.5.2 Pyrex Wafer Substrate through Backside Lithography

Pyrex wafers were tested as the next choice of substrate material due to their optical clarity, which would make them a perfect candidate for potential backside lithography. Backside lithography, as discussed previously, was focused on as a potential way to produce positive draft angles. The hypothesis was that a lower energy of exposure during frontside lithography produced negative draft angles, which was an undesirable outcome.

However, if the setup was reversed and backside lithography was employed then a lower energy of exposure would produce a positive draft angle under this new fabrication condition. Figure 3.7 shows the comparison of two different PDMS channels that were fabricated from two separate energy conditions producing a (a) $+9^\circ$ draft angle and a (b) $+3.6^\circ$ draft angle.

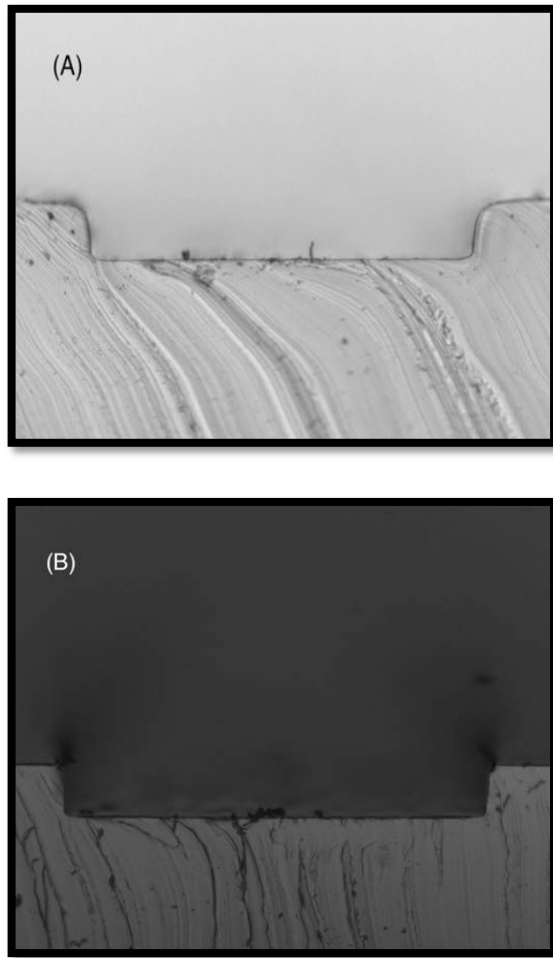


Figure 3.7: Comparison of draft angles of SU-8 features that were exposed through backside lithography at (A) 250 mJ/cm^2 with a draft angle of $\sim+9^\circ$ (B) 275 mJ/cm^2 with a draft angle of $\sim+3.6^\circ$.

This hypothesis of backside lithography with lower energies of exposure was tested. The first wafer that was fabricated was a single $100 \mu\text{m}$ layer of SU-8 and an initial exposure

energy of 300 mJ/cm² was chosen due to the fact that 375 mJ/cm² showed to produce vertical sidewalls under frontside lithography conditions. This initial exposure energy condition gave a vertical sidewall, so lower energies of exposure were tested next. The following two wafers were single 100 μm SU-8 layers each and exposed to energies of 80 mJ/cm² and 150 mJ/cm², respectively. Both wafers had SU-8 features removed during development of the wafers. These were considered to be too low of exposure energies and did not provide enough polymerization of the SU-8 to properly harden and adhere to the Pyrex wafer substrate. The next Pyrex wafer master mold that was tested was again spun with a 100 μm SU-8 layer and the energy of exposure that was tested was 250 mJ/cm². After development, measurements were made and the draft angle showed to have an average value of +8.7°. An energy of exposure between 250 mJ/cm², which gave a draft angle of +8.7°, and 300 mJ/cm², which gave a vertical sidewall, was thought to provide a draft angle that would fall within the values of +3° to +5°, which would be within injection molding values. The next Pyrex wafer was spun with a 100 μm thick SU-8 layer and exposed through backside lithography at 275 mJ/cm². After development, measurements were made and the draft angle showed to have an average value of +3.5°. The next step was to create a 3-layer device and see if this draft angle value persisted for taller SU-8 features. A Pyrex wafer substrate was created where all 3 layers were exposed through backside lithography at 275 mJ/cm². After development, measurements were made on the draft angle of the 300 μm SU-8 features. The measurements showed that the 300 μm SU-8 features had an average draft angle of +3.6°. Figure 3.8 is a graph showing the results of the draft angle experimentation.

SU-8 feature side wall draft angle versus the energy of UV light exposure

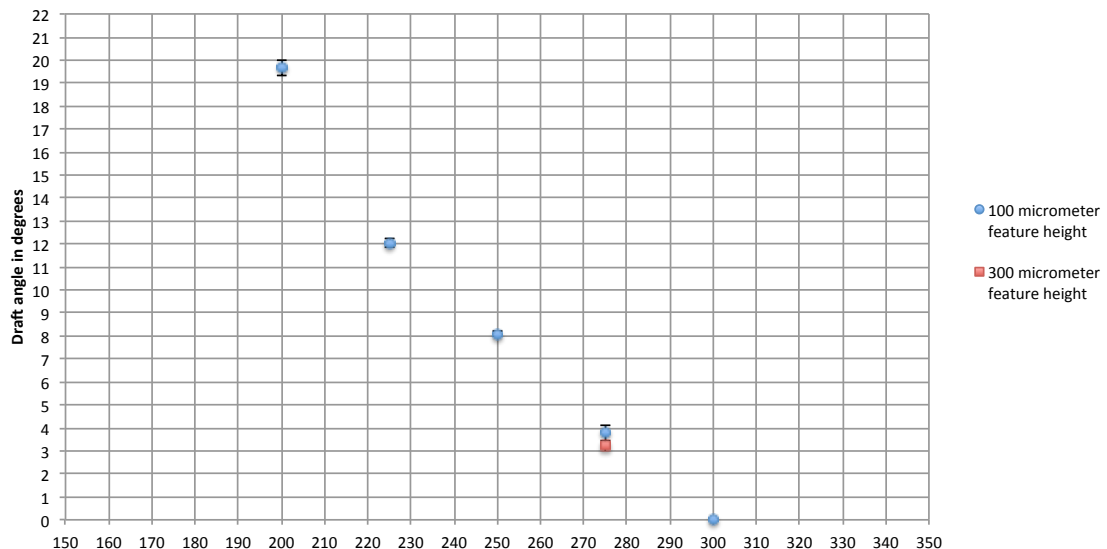


Figure 3.8: Plotted data of draft angles achieved through backside lithography with a Pyrex wafer substrate under varying UV energy exposures. Error bars represent standard deviations, with n=3 for 100 μm feature heights and n=6 for the 300 μm feature height.

Chapter 4

Soft Lithography and Epoxy Mold Making

4.1 Introduction

Rapid prototyping of devices is an important component of any research and development initiative. Testing and modifying potential designs through numerous iterations helps achieve desired results and allows manufacturers to settle on a product that has been effectively tested against any number of preconceived conditions. While PDMS device fabrication has been adopted as a rapid prototyping material for research laboratories, spanning a broad category of applications [108]–[113], it has its limitations. These include its low stiffness under certain preparation conditions [114], permeability to water vapour [115], its potential to absorb small hydrophobic molecules [51], its recovery of hydrophobic characteristics [54] and its potential to leach uncrosslinked oligomers into the channel solution [52]. There are also concerns associated with PDMS device prototyping due to an increased level of difficulty in corroborating results between PDMS devices and previously used, more conventional methods [116], [117].

The relative speed and ease-of-use when dealing with PDMS makes it an enticing fabrication technique. PDMS devices have been used in a multitude of applications including fabrication of modular self-aligning blocks [5], study of hematologic cancers through cytomics [118] and the study of specificity of breast cancer metastasis to bone

[119]. The use of PDMS in microfluidics has its place, but for the purpose of prototyping in industry, with a specific end goal of mass production, its limitations outweigh its benefits. Thermoplastic prototyping allows for a direct understanding of the properties and conditions that will be present in the distributed product downstream. There is an increased complexity in fabrication of thermoplastic devices when compared to PDMS and there are several possible fabrication methods that come with certain advantages and disadvantages [120]. One particular fabrication method is hot embossing features directly into a thermoplastic of choice.

Hot embossing offers a relatively straightforward fabrication protocol and the ability to produce high quality thermoplastic microfluidic devices. In order to produce a hot embossed device, there needs to be a hot embossing stamp fabricated beforehand. There is more than one way to produce a hot embossing master mold structure. These master molds have been previously fabricated through machining of the features directly into the surface of the mold [120]. However, there are inherent disadvantages associated with this process. Firstly, machine marks on the surface of the master mold will directly transfer into the embossed thermoplastic and affect the optical clarity of the microfluidic device. Secondly, micromachining has limitations in its ability to produce small-scale features. Thirdly, there is a complexity and cost associated with the removal of these micromachined marks through polishing techniques [4].

As a direct continuation, micromilling is another potential standalone thermoplastic microfluidic device fabrication technique that allows for rapid prototyping.

Micromilling, while providing a quick fabrication route, has its limitations in producible feature size. There is a minimum feature size of $< 3 \mu\text{m}$ with the use of a milling machine that costs upwards of \$200,000. For a milling machine with a cost of \$15,000, minimum feature sizes will be approximately $25 \mu\text{m}$ [31]. Additionally, micromilling leaves rough surface marks that will have an effect on the mammalian cell growth and will affect optical clarity during microscopy.

A previously developed hot embossing device fabrication protocol [4] has already helped to address some of the conventional limitations of the hot embossing process. This technique uses an aluminum-filled epoxy as the master mold for hot embossing. This epoxy casting material offers a number of benefits over previously used hot embossing molds. One benefit of this particular fabrication technique is that it allows for the production of thermoplastic devices with feature sizes down to the resolution of silicon master mold features. This offers a larger range of potential applications compared to other thermoplastic device fabrication processes. There is also the added benefit of employing readily understood soft lithography techniques in the master mold fabrication process and thus reducing complexity with the hot embossing master mold fabrication process. Also noteworthy is the surface quality seen as a direct result of the epoxy mold fabrication process, compared to previously discussed micromachined molds. The epoxy can be mixed to appropriate ratios and directly poured onto a PDMS negative-relief feature mold and hardened according to a curing protocol. This will provide channel surface roughness to the degree seen in the silicon wafer master mold, greatly reducing costs compared to CNC micromachined aluminum hot embossing molds [4].

Despite the improvements already introduced into the hot embossing and mold fabrication process in general, there is still room for further characterization and optimization. This further improvement is particularly in regards to both the repeatability and quality of the fabricated epoxy molds. The objective of this chapter is to address these concerns and provide a course of circumvention for future manufacturers. These areas of improvement, which will be described at greater length in Section 4.2 and Section 4.3, are as follows:

1. Create a high quality PDMS negative-relief feature mold with a uniformly flat surface for the use of epoxy mold fabrication
3. Eliminate bubbles trapped within the bulk of the epoxy material
4. Make an epoxy mold fabrication jig
5. Incorporate micromilling to create additional 3-dimensional features, or modify existing features, directly on an epoxy mold

4.2 Materials and Methods

4.2.1 PDMS Negative-Relief Feature Mold Fabrication

A measuring cup was placed onto a scale (Ohaus Corporation, Parsippany, NJ, USA), which was subsequently zeroed. PDMS elastomer base and curing agent (Dow Corning Corporation, Midland MI, USA) were then mixed in a 10:1 ratio, specifically 25g:2.5g by

mass. The PDMS was then put into a degasser (Bel-Art Products, Wayne, NJ, USA) and left for 30 minutes until all bubbles had been removed from the bulk of the PDMS.

A rectangular PMMA (McMaster Carr Supply Company, Elmhurst, IL, USA) frame was milled using a PCNC micromilling machine (Tormach Inc., Waunakee, WI, USA) and cleaned with isopropyl alcohol (Sigma-Aldrich Corporation, St. Louis, MO, USA). The previously fabricated silicon wafer master mold was also cleaned with isopropyl alcohol and dried with a compressed nitrogen gas (The Linde Group, Munich, Germany). Once all debris had been removed from the surface of the silicon master, it was placed onto a clean transparency (ACCO Brands, Lincolnshire, IL, USA), feature-side facing upwards. The milled rectangular PMMA frame was placed onto the top, feature-side surface of the silicon master in such a way that the middle opening of the frame was centered around the microfluidic features of the silicon master. The setup was placed on top of a levelled hot plate (Torrey Pines Scientific Inc., Carlsbad, CA, USA) and left at room temperature until the PDMS had finished degassing. Once the PDMS was bubble-free, it was removed from the degasser and brought over to the hot plate. The PDMS was poured slowly and carefully over top the silicon master mold features and was contained within the middle opening of the PMMA rectangular frame. Any bubble formation that transpired during the pouring step was addressed through the use of a 0.5-10 μ L pipette tip. The 0.5-10 μ L pipette tip was carefully used to dislodge any bubbles and drag them to the periphery of the PDMS-filled opening. Once all bubbles had been removed, a 5"x4" glass slide of thickness 1.2 mm (Ted Pella Inc., Redding, CA, USA) was carefully placed over top of the middle opening of the PMMA rectangular frame. This provided a

top cover to the PDMS-filled space above the features of the silicon master mold. Once this was done, the hot plate was set to 75°C and left for 2 hours. The hot plate was then allowed to cool to room temperature and the setup was moved to a separate workspace. The silicon wafer was carefully dislodged from the PMMA rectangular frame and PDMS negative-relief feature mold and glass cover. The PMMA frame was then removed from the PDMS negative-relief feature mold and glass cover. The hardened PDMS was never removed from the glass slide cover, in order to eliminate any possibilities of bubbles being trapped between the interface of the PDMS and substrate in succeeding steps.

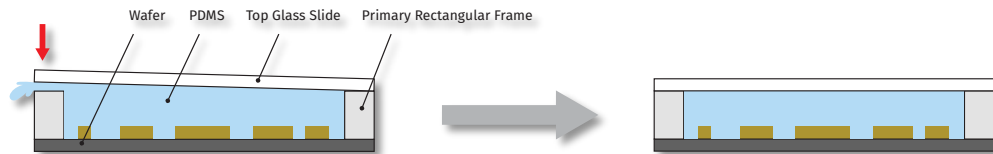
4.2.2 Epoxy Fabrication Protocol

A PDMS rectangular ring was created with the mixing of PDMS elastomer base and curing agent (Dow Corning Corporation, Midland MI, USA) in a 10:1 ratio, or 60g:6g by weight. This was then put in the degasser (Bel-Art Products, Wayne, NJ, USA) for 30 minutes until all bubbles have been removed from the bulk of the PDMS. The PDMS was then poured into an 86mmx128mm OmniTray (Thermo Fisher Scientific Inc., Waltham, MA, USA) with an aluminum block placed directly in the center. The aluminum block was previously milled down to an appropriate size such that its height was just shallower than the height of the OmniTray. The PDMS filled the OmniTray to the top and a 5"x4" glass slide of thickness 1.2 mm (Ted Pella Inc., Redding, CA, USA) was placed over top the opening of the OmniTray. This setup was then brought over to a hot plate (Torrey Pines Scientific Inc., Carlsbad, CA, USA) and allowed to cure for 2 hours at 75°C. The epoxy resin and hardener were then mixed in a 10:1 ratio, or 160g:16g by weight. The epoxy that was used throughout experimentation was EC-415

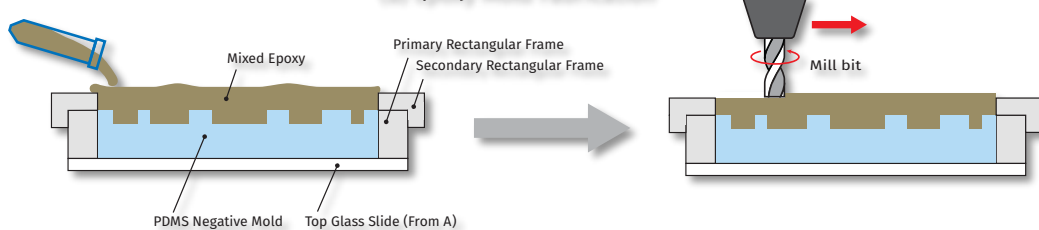
aluminum-filled epoxy (Adtech Plastic Systems, Madison Heights, MI, USA). The PDMS rectangular ring and negative-relief feature mold, which was attached to a glass substrate, were placed in the degasser for 30 minutes in order to eliminate any trapped gasses from within the bulk of the PDMS. The PDMS rectangular ring was then placed around the center of the negative-relief feature PDMS mold. The mixed epoxy was poured into overtop of the PDMS negative-relief feature mold and filled the volume up to the top of the PDMS rectangular ring. A polystyrene (Goodfellow Cambridge Ltd., Huntingdon, England) rectangular sheet, with dimensions slightly larger than that of the PDMS rectangular ring, was placed over top the PDMS ring as a cover. The setup was then placed into the oven (Binder GmbH, Tuttlingen, Germany) for 52°C for 24 hours. After the 24 hours, the temperature was ramped to 66°C and held for 3 hours. Following these 3 hours, the setup was removed from the oven and the hardened epoxy was separated from all other components. The hot embossing epoxy mold was then put back into the oven for the final 8-hour temperature-conditioning step of the protocol. The 8 hour temperature condition step consisted of 2 hours held at 93°C, 2 hours held at 121°C, 2 hours held at 149°C and 2 hours held at 176°C. The heat ramping from one temperature in the oven protocol to the next should not exceed 13°C per hour and cooling should not exceed 27°C per hour. Figure 4.1 illustrates the epoxy mold making process. Figure 4.2 is a photograph of microfeatures on a typical epoxy mold.

Epoxy Mold Fabrication

(A) PDMS Mold Fabrication



(B) Epoxy Mold Fabrication



(C) Releasing Cured Epoxy Mold

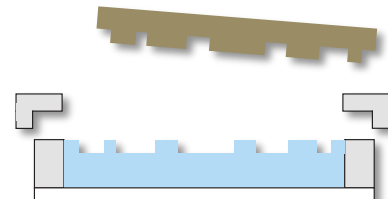


Figure 4.1: Epoxy mold fabrication process with (A) PDMS being poured over the SU-8 features in order to create a negative-relief feature PDMS mold, (B) aluminum-filled epoxy being poured over the PDMS negative-relief feature mold and subsequently being cured and having its back surface milled to create a uniformly thick epoxy and (C) the epoxy mold being released from the PDMS mold.



Figure 4.2: Image taken of a fabricated epoxy mold with positive-relief microfluidic features.

4.2.3 Elimination of Bubbles from Bulk Epoxy Material

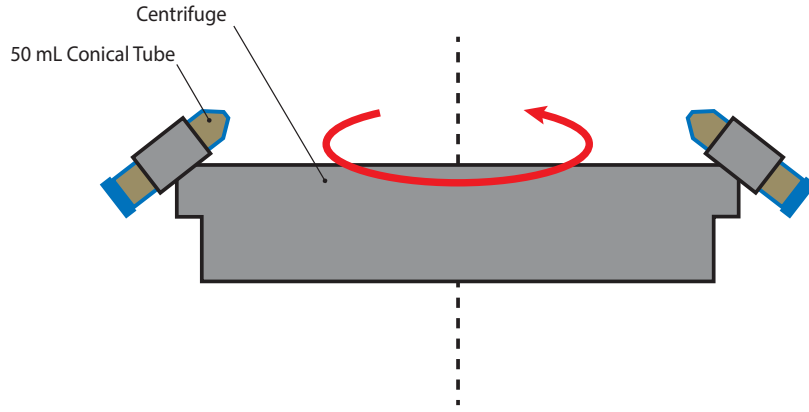


Figure 4.3: 50 mL conical tubes filled with mixed epoxy being centrifuged in an upside-down orientation in order to isolate all bubbles that are trapped within the bulk of the epoxy to the bottom end of the conical tube.

In order to eliminate bubbles from within the bulk of the epoxy hot embossing mold, there was the requirement to incorporate some additional steps in the fabrication protocol. The EC-415 aluminum filled epoxy (Adtech Plastic Systems, Madison Heights, MI, USA) was mixed in a 10:1 ratio of resin to hardener, or 160g:16g by weight. Once the

epoxy was thoroughly mixed, it was poured into two 50 mL conical tubes (Corning Inc., Corning, NY, USA). The conical tubes were placed top-side facing downwards into a conical tube holder (Eppendorf, Hamburg, Germany). In order to have the conical tube sit correctly in this upside down configuration, the bottom component of the conical tube holder was removed to accommodate the conical tube cap. The upside down conical tube and respective holder were then placed into the Binder oven (Binder GmbH, Tuttlingen, Germany) at a temperature of 70°C and left for 2 minutes. The epoxy was then removed from the oven and placed into an Eppendorf centrifuge (Eppendorf, Hamburg, Germany) and was spun at 750 G-force for 5 minutes. Figure 4.3 shows the setup for spinning the epoxy mold in 50 mL conical tubes in an upside down orientation. Once the centrifugation was complete, the upside down conical tube and holder were again put inside the Binder oven and held at a temperature of 70°C for 3 minutes. The epoxy was then removed from the oven and, due to the raised temperature, had a lower viscosity that helped with ease of pouring over the PDMS. The epoxy from within the two conical tubes was then poured over the PDMS negative-relief feature mold and was contained by the PDMS rectangular ring. The pouring step was carefully monitored to avoid pouring of the centrifuged bubbles, which were congregated at the tapered bottom of the conical tube. Figure 4.4 shows a photograph of epoxy bubbles that have collected after centrifugation.



Figure 4.4: Image showing congregated bubbles revealed after mixed epoxy had been centrifuged. The bubbles are at the opening of the conical tube because the 50 mL conical tube was centrifuged in a right side up orientation for ease of imaging purposes

4.2.4 Epoxy Mold Fabrication Jig

An epoxy mold fabrication jig was developed in order to help produce thin epoxy molds with consistent dimensions. The epoxy fabrication method, with the incorporation of the jig, is as follows. A PDMS negative-relief feature mold was created by pouring PDMS over a silicon master into the center opening of a milled rectangular PMMA frame, as before. The PDMS was then covered with a glass slide over top of the center opening of the PMMA rectangular frame. The setup was then placed on a hot plate and was left at 70°C for 2 hours. A 4.5 mm thick PMMA (McMaster Carr Supply Company, Elmhurst,

IL, USA) rectangular ring was then milled with the use of a PCNC micromilling machine (Tormach Inc., Waunakee, WI, USA). The dimensions of the center opening of the rectangular frame were the same as the dimensions specified for the rectangular frame used to contain the PDMS as previously described. The outer edge dimensions were 5 mm longer in both length and width, compared to the PMMA rectangular ring used to contain PDMS. L-shaped components were also milled using 1.5 mm thick PMMA (McMaster Carr Supply Company, Elmhurst, IL, USA). These two L-shaped components were subsequently glued to the 4.5 mm thick rectangular frame at specific locations such that their inner edges would securely fit the dimensions of the PDMS negative-relief feature PMMA frame. The L-shaped components were also glued at the position where the center opening of the PDMS negative-relief feature PMMA frame and the center opening of the 4.5 mm thick PMMA frame were aligned with one another. Once the PDMS had fully cured on the hot plate, the hot plate was turned off, allowing the PDMS to cool to room temperature. The silicon wafer was then carefully separated from the PMMA rectangular frame and PDMS negative-relief feature mold, which was anchored to the glass slide substrate. The 4.5 mm thick PMMA rectangular frame, with precisely glued L-shape components, was then secured on top of the PMMA rectangular frame enclosing the PDMS negative-relief feature mold. The aluminum filled epoxy was prepared as previously described and was poured directly onto the surface of the PDMS negative-relief feature mold. The epoxy was contained with the use of the 4.5 mm thick PMMA rectangular frame and was poured up to the top of this container. Enough epoxy was poured so that there was a slight convex meniscus over the top opening of the 4.5 mm thick PMMA rectangular frame. No cover was placed on this top surface. The

aluminum-filled epoxy setup was then placed into a Binder oven and left at 52°C for 24 hours. Following this 24 hour curing step, the oven was then set to 66°C and left for 3 hours. The epoxy setup was then removed from the oven and secured directly to the PCNC micromilling machine. The glass slide substrate at the bottom end of the setup was secured to the levelled granite block of the micromilling machine, exposing the top epoxy surface to the endmill. The top surface of the epoxy was then milled, in order to achieve a flat surface that is parallel to the positive-relief feature side surface of the epoxy mold. Once the milling of the top surface of the epoxy mold was complete, the epoxy was separated from the PDMS negative-relief feature mold and 4.5 mm thick PMMA rectangular frame. The lone epoxy was then put back into the oven to continue with the oven baking protocol. The final steps of the curing protocol consisted of 2 hours held at 93°C, 2 hours held at 121°C, 2 hours held at 149°C and 2 hours held at 176°C. The heat ramping from one temperature in the oven protocol to the next did not exceed 13°C per hour and cooling did not exceed 27°C per hour. Figure 4.5 shows images taken from various steps in the epoxy mold fabrication process with the use of the epoxy mold fabrication jig.

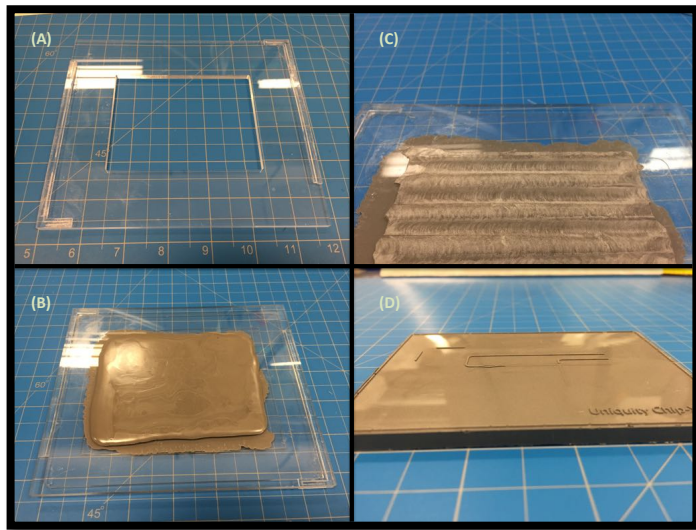


Figure 4.5: Images taken throughout the epoxy mold fabrication process including (A) epoxy mold fabrication jig by itself, (B) aluminum-filled epoxy poured onto the PDMS mold located at the center of the epoxy mold fabrication jig, (C) milled epoxy backside of epoxy mold after curing process had completed and (D) released epoxy mold sitting flat on a cutting table.

4.2.5 Micromilling 3D Features

Micromilling of 3-dimensional ramp features were incorporated into the overall design and were implemented once the hot embossing epoxy mold had finished baking in the oven. Once the oven had cooled down to room temperature, the epoxy mold was removed. The epoxy then had double-sided tape (Scotch Brand, St. Paul, MN, USA) attached to its backside, featureless surface. The epoxy was brought over to the PCNC micromilling machine and was taped directly to the granite block (Standridge Granite Corporation, Santa Fe Springs, CA, USA). The aligning of the x,y-coordinates to the micromilling x,y-coordinates was an important step and required careful adjustment until the user felt that alignment was within tolerance. Next an endmill with a 1/32" diameter was inserted into the milling shank (Lyndex Corporation, Mundelein, IL, USA). The

channel feature that was to be milled had a diameter of 600 μm . A way to help improve tolerance in the alignment step would be to use an endmill with a larger diameter, however this would produce a rougher milled surface. The zeroing of the milling x,y-coordinates was performed in a 2-step process. The first step required the endmill to be carefully placed in the center of the channel that would eventually be milled. This was then selected as the $y=0$ point. The endmill was then carefully brought over to the point where the endmill dropped from the taller feature to the shallower feature and was rested snuggly against the taller feature's vertical sidewall. This point was then selected as the $x=0$ point. The $z=0$ point was selected as the point where the endmill sat directly on top of the shallower channel feature. These coordinates are a direct result of previously produced 3D CAD files where the origin was selected for micromachining. The endmill was then brought upwards in the z-direction a distance of approximately 2 millimeters in order to avoid any damaging of features during the initialization of the micromilling program. Figure 4.6 shows the milling of a ramp feature directly into the epoxy mold. We were initially concerned that milling the epoxy directly would result in chipping of the epoxy mold due to the material's brittle nature. However, we observed that this was not the case and milling was easily implemented without chipping issues.

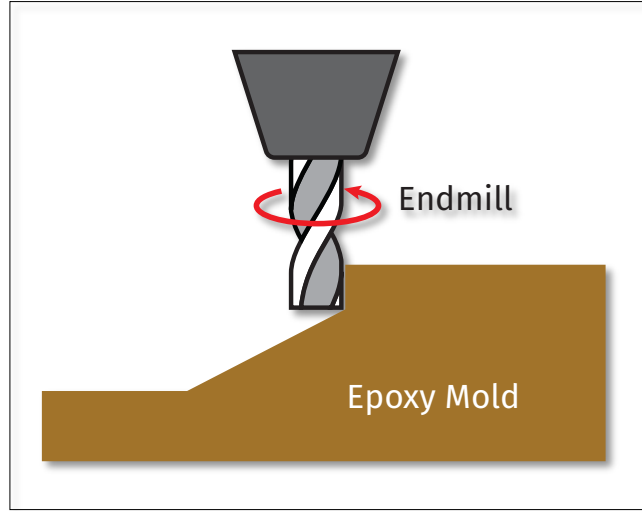


Figure 4.6: Endmill cutting directly into an epoxy mold feature.

4.3 Results

Through the implementation of the 4 previously mentioned methods, there has been a marked improvement in the quality of produced hot embossing epoxy molds. There was a need to improve each component of the epoxy mold fabrication process and as a result there has been

1. An improvement in epoxy mold channel quality and surface smoothness
2. A consistently bubble-free bulk epoxy mold material
3. Incorporation of advanced 3-dimensional features
4. A repeatable epoxy mold fabrication process with uniform thickness

A milled PMMA rectangular frame to successfully contain all PDMS proved to repeatedly produce a high quality PDMS negative-relief feature mold and the glass slide

cover allows the PDMS to cure and adhere to its surface, which eliminated any separation between the PDMS-glass interface. This was an important step to overcome because, with the continuous adherence between the PDMS negative-relief feature mold and the glass slide substrate, there was the complete elimination of air bubbles becoming trapped in this interface. If there were any air bubbles that were trapped between the PDMS mold and the glass slide substrate, this would directly affect the surface of the epoxy mold through direct translation. Any surface deformations in the epoxy mold surface would have adverse effects in hot embossing quality and subsequent device bonding. The continuous contact between PDMS and glass slide substrate effectively eliminated this source of error for potentially producing lower quality microfluidic devices.

The incorporation of heating and subsequent centrifugation of the mixed aluminum-filled epoxy prior to pouring over the PDMS negative-relief features helped to eliminate trapped bubbles within the bulk of the epoxy. This was important in moving towards a high quality epoxy mold that would not be weakened with pockets of air bubbles. The heating of the mixed epoxy for a brief period helped to lower the viscosity of the epoxy and the immediate centrifugation allowed the bubbles to be directed towards the bottom of the conical tube, away from the opening where the epoxy would eventually be poured. This greatly reduced bubbles from within the bulk of the epoxy but it required that the volume of epoxy that was poured from each conical tube only reached a certain point. Evacuating all of the epoxy from a particular conical tube would dispense the congregated bubbles and users should be careful to avoid this potential.

With the limitations seen with the photolithography process in terms of what 3-dimensional features could be fabricated on the master wafer mold, there was a need to incorporate micromilling directly into the epoxy mold fabrication process. Through micromilling of features, gradual gradients in height were incorporated into the microfluidic design. The photolithography process produced a microfluidic design that had multi-height features that transitioned from one to another in sharp, instantaneous drops in height. Once the hot embossing epoxy mold was created, micromilling allowed the design to have another degree of complexity. Micromilling of height gradients was also applied directly to the SU-8 features on the master wafer mold. This was tested under differing RPMs and feed rates and eventually produced ramps directly on the SU-8 features as well. Although there is the potential to mill ramps directly onto the SU-8 features, it is not recommended to go this route. The master wafer mold is disproportionately difficult to fabricate within tolerance, compared to the epoxy hot embossing mold. It is of paramount importance to the production process that the master wafer mold is preserved once it is fabricated. In contrast, the hot embossing epoxy mold is cheaper and comparatively easier to fabricate. In addition, the epoxy mold is more robust and was never once seen to have features fracture under the different tested RPMs and feed rates, which were also tested on the master wafer mold.

There was also a great importance placed on being able to produce high quality hot embossing epoxy molds that could be repeatedly and reliably fabricated. The first design protocol employed the use of a PDMS rectangular frame to confine the poured aluminum-filled epoxy to the portion of the PDMS negative-relief feature mold that

contained the microfluidic channels. This was a great first step towards a repeatable and reliable epoxy mold fabrication protocol in that it was quick to fabricate and easy to demold from the cured epoxy. The PDMS-PDMS interface between the negative-relief feature mold and rectangular frame produced a tight seal and there was no leaking of epoxy during baking as a result. There was a need to address the large quantity of PDMS that was being used to create the rectangular frame. Another concern with this initial epoxy mold fabrication protocol is the inherent flexibility of PDMS as a material. When the PDMS rectangular frame was placed on the surface of the negative-relief feature mold, there was a degree of human-associated error in maintaining consistently repeatable dimensions. This would have an effect downstream during hot embossing where a pressure is applied to the epoxy according to the equation

$$P = \frac{F}{A}$$

where F is the applied force of the hot embossing machine and A is the surface area of the epoxy on which the force is applied. In order to produce epoxy molds with consistent dimensions there was the need to move to a harder material. The designed and tested epoxy mold-making jig addressed these concerns by incorporating the use of the hard thermoplastic PMMA. Though there was mild leaking of epoxy between the PMMA-PMMA interface of the newly designed epoxy mold making jig, this proved to have no effect on the ability to demold the epoxy once it had hardened. In addition to the consistent dimensions seen, there was also the benefit of being able to successfully mill across the backside, featureless surface of the epoxy in order to produce an epoxy with a uniform thickness. This once again has a positive influence on producing high quality hot embossed devices, due to a more uniform contact between the platens of the hot

embosser and the epoxy mold. This uniform contact creates a more even pressure distribution. Figure 4.7 shows the improvements made to the epoxy mold with the incorporation of the additional epoxy mold fabrication steps, as well as the use of an epoxy mold fabrication jig.

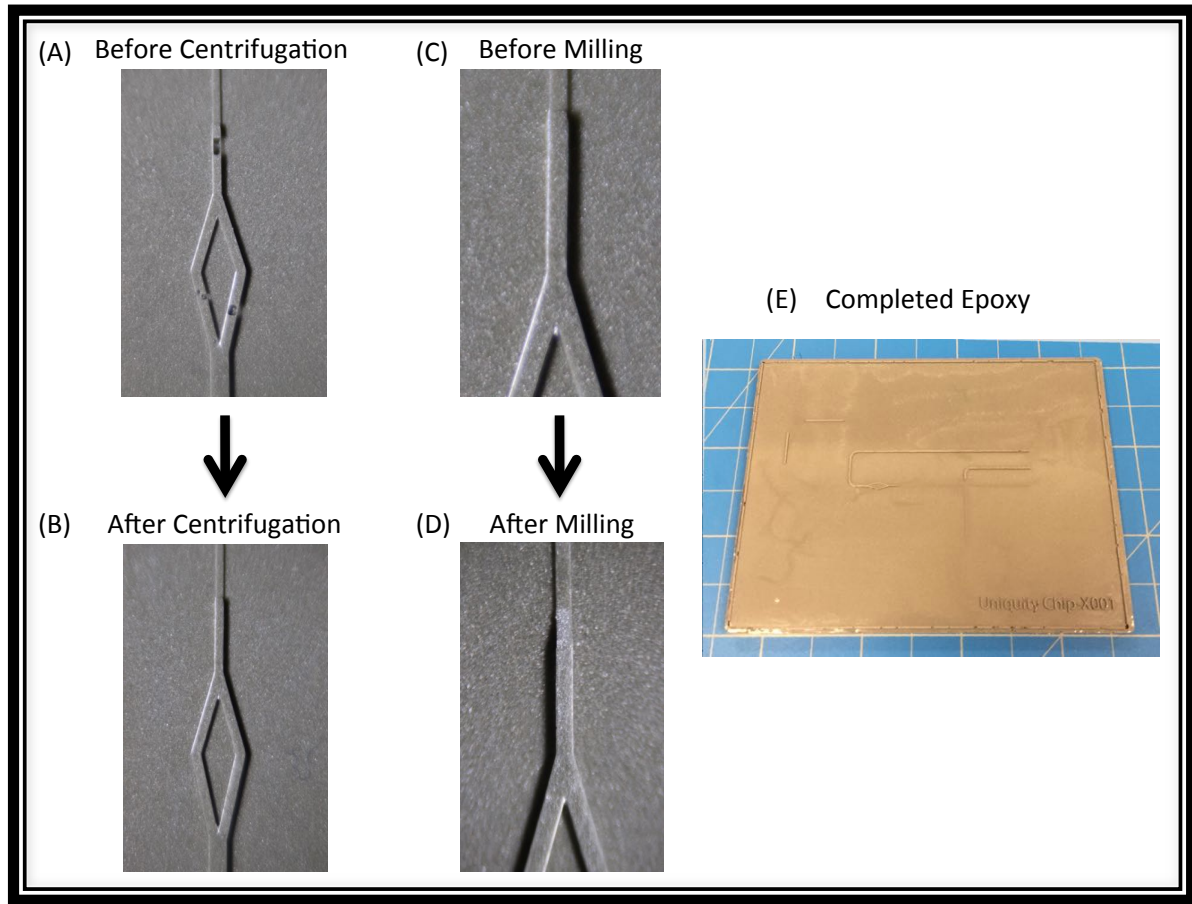


Figure 4.7: Images of taken of epoxy mold features including (A) epoxy mold feature before centrifugation step was introduced, (B) epoxy mold feature after centrifugation step was introduced, (C) epoxy mold feature before milling step was introduced, (D) epoxy mold feature after milling step was introduced and (E) image of epoxy mold created with the use of epoxy mold fabrication jig.

Chapter 5

Hot Embossing Capabilities

5.1 Introduction

One method of fabricating thermoplastic microfluidic devices is through the use of hot embossing. The use of thermoplastic microfluidic devices over other types, including silicon and glass, has to do with its large breadth in material properties, surface chemistries and its potential as a disposable alternative when considering its use as a biomedical device [63]. Hot embossing as a fabrication method, along with injection molding, has largely been used for the fabrication of thermoplastic microfluidic devices for mass production [68], [121]–[125]. Hot embossing involves the placement of a thermoplastic raw material between two platens, along with a positive-relief feature hot embossing mold directly on top of the thermoplastic material. The platens are raised to an elevated temperature, above the glass transition temperature of the thermoplastic material being hot embossed, and the platens are pressed together at a constant applied force. The positive-relief microfluidic features in the hot embossing mold are directly transferred to the raw thermoplastic material, which will have negative-relief microfluidic channels. The temperature of the platens is cooled and the platens are separated. The embossed thermoplastic material is demolded from the hot embossing mold to reveal a negative-relief feature microfluidic design on its surface.

Certain aspects of the hot embossing mold need to be taken into consideration in order to produce a high quality microfluidic device through direct translation [63]. The mold must be able to withstand multiple embosses and the high temperature and pressure that is involved. When considering property requirements for a hot embossing mold material it is important to look for high stiffness, high strength, reasonably high fracture toughness, good surface finish, good wear resistance and a low cost and straightforward method of fabrication [63]. There are a number of different ways to produce a hot embossing mold, including electroplating of nickel or nickel alloys [62], deep reactive ion etching (DRIE) in silicon, KOH wet etching in silicon [64] with soft lithography [65], [66] and CNC machining [67]. However there are downsides to these fabrication methods including the high cost of electroplating (>US\$ 3000) and a rough surface finish, in combination with a limitation to small feature sizes associated with CNC machining, just to name two examples [63]. For this reason, alternative hot embossing mold fabrication methods have been investigated.

In this chapter, a comparison will be made between the hot embossing capabilities and characteristics of a mold fabricated from a silicon wafer master mold with SU-8 positive relief features and an EC-415 aluminum-filled epoxy, which was achieved through a secondary fabrication method. The secondary fabrication method of the EC-415 aluminum-filled epoxy was through soft lithography and casting of the silicon wafer master mold with positive-relief SU-8 features. It is also important to consider the capabilities of the hot embossing machine being used and the quality of thermoplastic

microfluidic devices being produced. A cross-sectional feature transfer fidelity characterization of thermoplastic materials PMMA and COP was performed on two separate hot embossing machines, the Carver Press and EVG 520HE hot embossers. The purpose of this chapter is to identify the method of producing the highest number of hot embossed thermoplastic microfluidic devices and the discussion will end with a quantified value for the times required for the production of thermoplastic devices on an individual basis and over the course of a full work week.

5.2 Hot Embossing Machines

5.2.1 Carver Press

The Laboratory of Integrative and Microengineered Technologies has purchased a hot embossing machine for fabrication of thermoplastic microfluidic devices. The particular hot embossing machine is a Carver Press (Carver Inc., Wabash, IN, USA) and comes at a price of \$15,645. Figure 5.1 shows an image of the Carver Press hot embossing machine.



Figure 5.1: Image of Carver Press hot embossing machine taken from Carver Inc. website with permission.

The Carver Press hot embossing machine has certain characteristics that should be noted.

The system operates through a touch screen interface where platen temperatures and hot embossing forces can be selected for fabrication of microfluidic devices with thermoplastic materials. There is the option to program hot embossing fabrication protocols with specific steps. This allows the user to come up with a customizable and automated program for ease of use. Both platens can be held at separate temperatures. The system has a reservoir attached directly, allowing for cooling of the platens after hot embossing has been performed. Upon selection of cooling, the reservoir passes water through a chiller (McMaster Carr Supply Company, Elmhurst, IL, USA) and through the platens themselves before returning back to the reservoir. The specific reservoir used by the Carver Press holds a volume of 5 gallons. The temperature of the water reservoir increases over multiple successive embosses and this can increase the waiting time for cooling down of the platens in order to remove the hot embossing epoxy mold and thermoplastic material for demolding. The use of the chilling unit helps to curb this effect and provide a more consistent temperature control. There is also an air valve that should be opened to allow air to pass through the system at the end of the day. This passing of air provides an opportunity to push any excess water, used to cool the platens, out of the system and avoid potential corrosion. The platens and hot embossing chamber is open to the surroundings and does not have the capabilities to ensure a vacuum environment during hot embossing. The platens are separated from the user by a transparent screen that must be closed at the time of use for successful functioning of the hot embossing machine as a safety feature.

The Carver Press operates under a range of temperatures and embossing forces. The working temperature could reach 650°C and can be chosen to accommodate the specific glass transition temperature of the material being embossed. The embossing force can range from 1,000-30,000 lbf and was looked into as a potential parameter that could improve hot embossed thermoplastic microfluidic device quality.

5.2.2 EVG 520HE

The EVG 520HE (EV Group, Florian am Inn, Austria) machine was tested during experimentation and was compared to the Carver Press in terms of produced device quality, hot embossing time required and inherent machine characteristics. These comparisons will be discussed below and a brief description of the hot embossing machine will be provided now. Figure 5.2 shows an image of the EVG 520HE hot embossing machine.



Figure 5.2: Image of EVG 520 HE taken from EV Group website with permission.

The EVG 520HE hot embossing machine was grander in both size and incorporated features, compared to the Carver Press. The EVG 520HE also had a purchase cost of \$780,732. The system was kept in the Centre for Microfluidic Systems Foundry cleanroom. A graphical user interface was the medium by which the user could program hot embossing protocols and log usage. The hot embossing protocol that the user would set had additional features that were not available with the Carver Press hot embossing machine. There was the programmable option to have the environment within the hot embossing chamber achieve a lower pressure, which could reach a low value of 1×10^{-5} mbar. The pressure was set at a value of 1×10^{-1} mbar during experimentation. This provided a vacuum environment to help with the quality of hot embossed thermoplastic devices. The programmable protocol could be modified and reorganized, with additional steps being placed in the middle of a previously made protocol while not having to reproduce the protocol as a result. This was not the case for the Carver Press.

The EVG 520HE machine had platens that could have their temperature set to separate values and could reach 550°C. The platens could accommodate stamp sizes of 200 mm diameter and 15 mm in thickness. There was a temperature stability of +/- 1% and a temperature uniformity of +/- 1.5% due to the closed environment of the hot embossing platen chamber. The platens could be pressed together at a force that ranged from 200 N - 20,000 N. The EVG 520HE had its force values in Newtons, which were converted to lbf through the equality

$$1 \text{ N} = 0.2248 \text{ lbf}$$

in order to provide consistent force values between the Carver Press and the EVG 520HE hot embossing machines. Therefore, the EVG 520HE had applied force capabilities that ranged from 44.962 lbf - 4496.185 lbf. Once the hot embossing had been completed with the EVG 520HE, cooling of the platens was employed through the use of the EVG 520HE chilling unit (EV Group, Florian am Inn, Austria). This chilling unit cooled the platens through a recirculating line of 50% water 50% glycerol. This chilling system is set up in a closed loop and as a result there is no required plumbing to a water supply. Figure 5.3 shows a typical hot embossing process, depicted with open platens similar to those on the Carver Press.

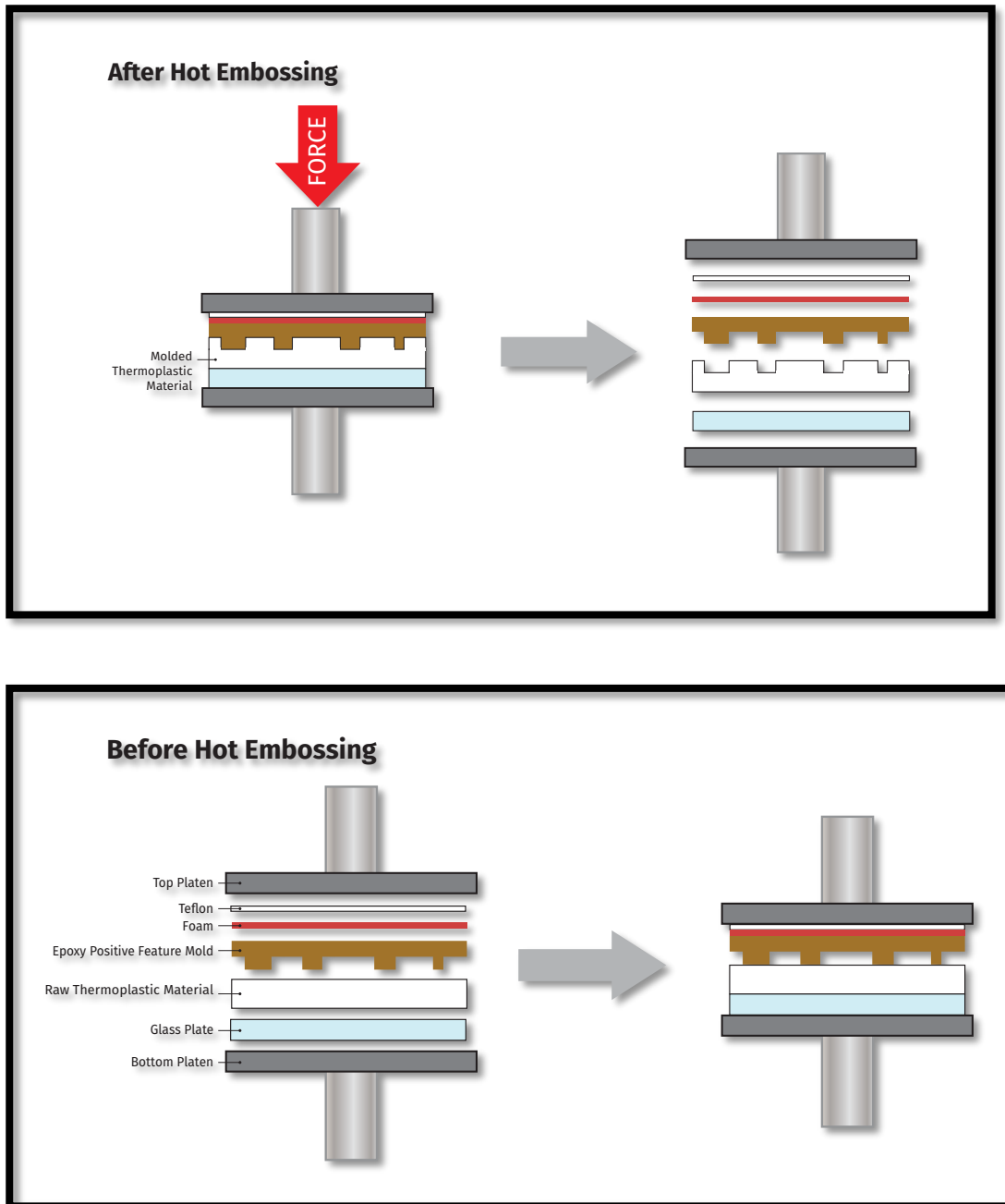


Figure 5.3: Hot embossing being performed on a thermoplastic material with the use of an epoxy mold. All items labelled and presented in the order that they are found during the hot embossing process. After an application of force and temperature, the thermoplastic material is released from the hot embossing machine with a transfer of microfluidic features from the epoxy mold.

5.3 Hot Embossing Protocol

5.3.1 Carver+PMMA+Epoxy

Characterization of feature transfer fidelity was performed on the thermoplastic PMMA (McMaster Carr Supply Company, Elmhurst, IL, USA) with the use of an aluminum-filled epoxy mold and Carver Press hot embossing machine. This characterization was performed to look into the quality of embossed features under different hot embossing parameters. The parameters that were looked at were temperature, hot embossing force and dwell time. The first step in the characterization was to test a range of hot embossing temperatures. A constant hot embossing force of 4,500 lbf and constant dwell time of 5 minutes was used while testing a range of temperatures. The tested temperatures were based off of two considerations. The first is that commercial grade PMMA has a glass transition temperature that can range from 85°C – 165°C. The second is that the working temperature of the aluminum-filled epoxy has a maximum value of 220°C. The temperatures tested ranged from 100°C – 200°C in 10 degree increments. Cross-sectional images were taken and a temperature of 170°C was chosen for further characterization. This temperature provided high feature transfer fidelity while remaining far enough away from the maximum temperature that the aluminum-filled epoxy can be used in. After the temperature was decided, further experimentation was performed in which different hot embossing forces and dwell times were tested. Three embosses were performed with each tested parameters in order to achieve a statistical range. For the feature transfer fidelity characterization of PMMA with an epoxy mold and the Carver Press hot embosser, Table 5-1 lists the parameters that were tested:

CHIP NO.	HEAT TEMP. °C	COOLING TEMP. °C	HEAT DELAY, min	DWELL TIME, min	FORCE, LBF
1	170	60	5	3	3000
2	170	60	5	3	3000
3	170	60	5	3	3000
4	170	60	5	3	4500
5	170	60	5	3	4500
6	170	60	5	3	4500
7	170	60	5	3	6000
8	170	60	5	3	6000
9	170	60	5	3	6000
10	170	60	5	4	3000
11	170	60	5	4	3000
12	170	60	5	4	3000
13	170	60	5	4	4500
14	170	60	5	4	4500
15	170	60	5	4	4500
16	170	60	5	4	6000
17	170	60	5	4	6000
18	170	60	5	4	6000
19	170	60	5	5	3000
20	170	60	5	5	3000
21	170	60	5	5	3000
22	170	60	5	5	4500
23	170	60	5	5	4500
24	170	60	5	5	4500
25	170	60	5	5	6000
26	170	60	5	5	6000
27	170	60	5	5	6000
28	170	60	5	6	3000
29	170	60	5	6	3000
30	170	60	5	6	3000
31	170	60	5	6	4500
32	170	60	5	6	4500
33	170	60	5	6	4500
34	170	60	5	6	6000
35	170	60	5	6	6000
36	170	60	5	6	6000

Table 5-1 Parameters tested for hot embossing characterization of PMMA with the use of the Carver Press

5.3.2 Carver+COP+Epoxy

A similar characterization of feature transfer fidelity was performed with the use of an aluminum-filled epoxy mold and the Carver Press hot embosser. This next characterization was performed with the thermoplastic COP (ZEONOR® 1020R, Zeon Corporation, Tokyo, Japan). The characterization began the same way, in which a constant hot embossing force of 4,500 lbf and constant dwell time of 5 minutes were used while a range of temperatures was tested. Commercial grade COP has a glass transition temperature that can range from 80°C – 180°C, so temperatures were tested within this range. Temperatures were tested from 120°C – 180°C in 10 degree increments from one emboss to the next. A temperature of 170°C was chosen due to the quality of cross-sectional channel features that it produced. After the temperature of 170°C was chosen, different hot embossing forces and dwell times were tested to characterize feature transfer fidelity of embossed features in the thermoplastic COP with the use of an aluminum-filled epoxy mold and the Carver Press hot embosser. Table 5-2 lists the parameters that were tested:

CHIP NO.	HEAT TEMP. °C	COOLING TEMP. °C	HEAT DELAY, min	DWELL TIME, min	FORCE, LBF
1	170	40	5	3	3000
2	170	40	5	3	3000
3	170	40	5	3	3000
4	170	40	5	3	4500
5	170	40	5	3	4500
6	170	40	5	3	4500
7	170	40	5	3	6000
8	170	40	5	3	6000
9	170	40	5	3	6000
10	170	40	5	4	3000
11	170	40	5	4	3000
12	170	40	5	4	3000
13	170	40	5	4	4500
14	170	40	5	4	4500
15	170	40	5	4	4500
16	170	40	5	4	6000
17	170	40	5	4	6000
18	170	40	5	4	6000
19	170	40	5	5	3000
20	170	40	5	5	3000
21	170	40	5	5	3000
22	170	40	5	5	4500
23	170	40	5	5	4500
24	170	40	5	5	4500
25	170	40	5	5	6000
26	170	40	5	5	6000
27	170	40	5	5	6000
28	170	40	5	6	3000
29	170	40	5	6	3000
30	170	40	5	6	3000
31	170	40	5	6	4500
32	170	40	5	6	4500
33	170	40	5	6	4500
34	170	40	5	6	6000
35	170	40	5	6	6000
36	170	40	5	6	6000

Table 5-2 Parameters tested for hot embossing characterization of COP with the use of the Carver Press

5.3.3 EVG+PMMA+Epoxy

A characterization of embossed feature quality was performed next with the EVG 520HE in thermoplastic PMMA using an aluminum-filled epoxy hot embossing mold. The experimental parameters tested were again temperature, hot embossing force and dwell time. A range of temperatures was tested while hot embossing force and dwell time were kept constant at 4,500 N and 5 minutes, respectively. A temperature of 170°C was found to produce the best quality of embossed features while remaining far enough away from the maximal working temperature of the epoxy mold when using the Carver Press hot embosser. A range of temperatures was tested on the EVG 520HE hot embosser that lied around this value of 170°C. The temperatures tested ranged from 145°C – 185°C in 10 degree increments from one emboss to the next. A temperature of 175°C was selected as the optimal temperature and further characterization was performed to look into different hot embossing forces and dwell times. Table 5-3 lists the parameters that were tested during characterization:

CHIP NO.	HEAT TEMP. °C	COOLING TEMP. °C	HEAT DELAY, min	DWELL TIME, min	FORCE, N
1	175	60	5	3	3000
2	175	60	5	3	3000
3	175	60	5	3	3000
4	175	60	5	3	4500
5	175	60	5	3	4500
6	175	60	5	3	4500
7	175	60	5	3	6000
8	175	60	5	3	6000
9	175	60	5	3	6000
10	175	60	5	4	3000
11	175	60	5	4	3000
12	175	60	5	4	3000
13	175	60	5	4	4500
14	175	60	5	4	4500
15	175	60	5	4	4500
16	175	60	5	4	6000
17	175	60	5	4	6000
18	175	60	5	4	6000
19	175	60	5	5	3000
20	175	60	5	5	3000
21	175	60	5	5	3000
22	175	60	5	5	4500
23	175	60	5	5	4500
24	175	60	5	5	4500
25	175	60	5	5	6000
26	175	60	5	5	6000
27	175	60	5	5	6000
28	175	60	5	6	3000
29	175	60	5	6	3000
30	175	60	5	6	3000
31	175	60	5	6	4500
32	175	60	5	6	4500
33	175	60	5	6	4500
34	175	60	5	6	6000
35	175	60	5	6	6000
36	175	60	5	6	6000

Table 5-3 Parameters tested for hot embossing characterization of PMMA with the use of the EVG 520HE

5.3.4 EVG+COP+Epoxy

The final characterization that was performed with the thermoplastic COP and involved the use of an aluminum-filled epoxy mold and the EVG 520HE hot embossing machine. First, a range of temperatures was tested while holding the applied force and dwell time constant at 4,500 N and 5 minutes, respectively. The temperature decided on during characterization for COP with the Carver Press hot embossing machine was 170°C, so a range of temperatures was tested around this value. The tested temperatures ranged from 130°C – 180°C in 10 degree increments from one emboss to the next. The temperature decided on was 150°C, as this provided the highest quality emboss with other parameters held constant. After the temperature was decided, different applied forces and dwell times were tested. Table 5-4 lists the parameters that were tested during characterization:

CHIP NO.	HEAT TEMP. °C	COOLING TEMP. °C	HEAT DELAY, min	DWELL TIME, min	FORCE, N
1	150	60	5	3	3000
2	150	60	5	3	3000
3	150	60	5	3	3000
4	150	60	5	3	4500
5	150	60	5	3	4500
6	150	60	5	3	4500
7	150	60	5	3	6000
8	150	60	5	3	6000
9	150	60	5	3	6000
10	150	60	5	4	3000
11	150	60	5	4	3000
12	150	60	5	4	3000
13	150	60	5	4	4500
14	150	60	5	4	4500
15	150	60	5	4	4500
16	150	60	5	4	6000
17	150	60	5	4	6000
18	150	60	5	4	6000
19	150	60	5	5	3000
20	150	60	5	5	3000
21	150	60	5	5	3000
22	150	60	5	5	4500
23	150	60	5	5	4500
24	150	60	5	5	4500
25	150	60	5	5	6000
26	150	60	5	5	6000
27	150	60	5	5	6000
28	150	60	5	6	3000
29	150	60	5	6	3000
30	150	60	5	6	3000
31	150	60	5	6	4500
32	150	60	5	6	4500
33	150	60	5	6	4500
34	150	60	5	6	6000
35	150	60	5	6	6000
36	150	60	5	6	6000

Table 5-4 Parameters tested for hot embossing characterization of COP with the use of the EVG 520HE

5.3.5 Epoxy Surface Coating with Releasing Agent

A surface coating releasing agent was applied to the feature-side surface of the aluminum-filled epoxy hot embossing mold. The particular releasing agent was Weicon Mould Release Agent (Weicon Inc., Cambridge, ON, CA). The purpose of using a releasing agent was to help with demolding of the epoxy hot embossing mold from the embossed thermoplastic material. It was hypothesized that with the use of a releasing agent, ease of demolding would be improved and the lifetime of the hot embossing epoxy mold would increase. This would be a direct result of positive-relief features on the epoxy mold breaking less often with the use of a releasing agent. The Weicon Mould Release Agent has applications in plastic processing, injection moulding and vacuum thermoforming. This releasing agent prevents sticking on plastics and metals and has a maximum working temperature of 130°C and was sprayed onto the epoxy mold surface from a distance of 10 inches - 12 inches, as per the instructions provided by Weicon. Figure 5.4 shows images of the epoxy mold before and after application of the Weicon Mould Release Agent:

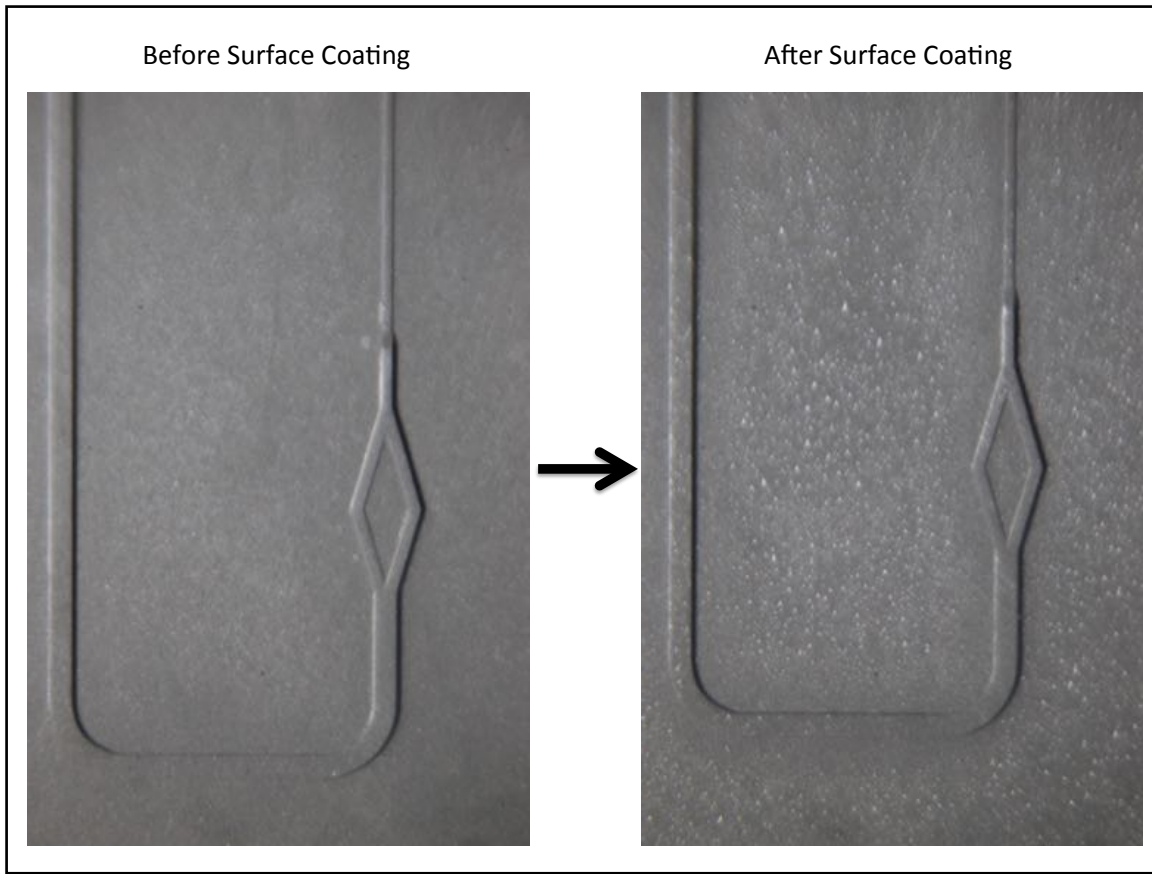


Figure 5.4: Images taken of epoxy mold surface before and after the application of the Weicon Mould Releasing Agent.

This maximum temperature is lower than the temperatures used during characterization of materials PMMA and COP on the Carver Press and EVG 520HE hot embossing machines. This was taken into consideration when hot embossing with the use of the Weicon Mould Release Agent was performed. At a hot embossing temperature of 120°C, dwell time was increased to 30 minutes in order to see a comparable quality of embossed thermoplastic devices.

5.4 Feature Transfer Fidelity

5.4.1 Carver+PMMA+Epoxy

Once embossing was complete on the Carver Press hot embosser with the thermoplastic PMMA using an aluminum-filled epoxy mold, cross-sections were made at specific locations on the embossed PMMA. These cross-sections were performed with the use of a Tormach PCNC micromilling machine. Three of the four locations that were cross-sectioned were at the inlet ports of the microfluidic device. The fourth location was at the opposite end of the device, where the largest channel was turning to lead into the diamond-shaped microfluidic feature. This fourth location was cross-sectioned in order to gain an insight into the cross-sectional feature transfer fidelity from one side of the device to the other side. Figure 5.5 shows the four locations on the device that were cross-sectioned:

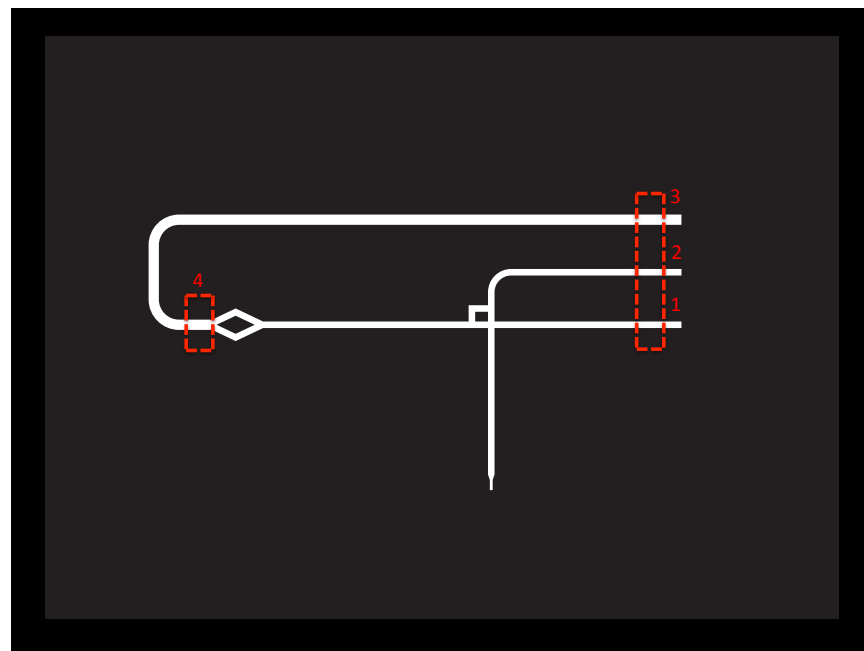


Figure 5.5: The 4 locations where cross-sectional measurements were taken for the characterization of the hot embossing process using thermoplastics PMMA and COP with the use of the Carver Press and EVG 520 HE hot embossing machines.

Once these cross-sections were made for all 36 embossed PMMA devices, cross-sectional images were taken at each of the four locations with the use of a EVOS brightfield microscope (Life Technologies Inc., Carlsbad, CA, USA). A cross-sectional area measurement on each of the 144 images was then performed with ImageJ. Cross-sections were subsequently made on the aluminum-filled epoxy at the same locations as those made for the embossed PMMA. The cross-sections of the epoxy were imaged with the EVOS brightfield microscope and a cross-sectional area measurement was taken for each of the four locations with the use of ImageJ. A cross-sectional feature transfer fidelity was then characterized at each of the four locations under all the different parameters in Microsoft Excel. Cross-sectional measurements were made according to the following discrepancy between the hot embossing epoxy mold and embossed thermoplastic material shown in Figure 5.6:

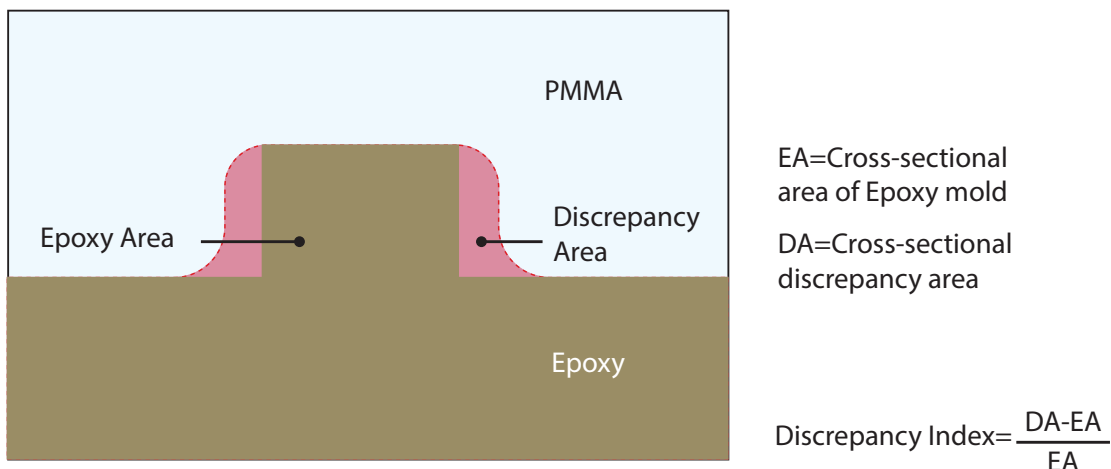


Figure 5.6: Theoretical cross-sectional shape of epoxy mold and embossed thermoplastic PMMA for the purpose of describing how the Discrepancy Index was calculated.

Where Discrepancy Index is a decided upon ratio of comparison between the embossed cross-sectional area and the epoxy cross-sectional area, EA is the epoxy cross-sectional area and DA is the discrepancy area between the embossed thermoplastic material and the hot embossing epoxy mold. Figure 5.7 shows the graphs produced for the four different locations:

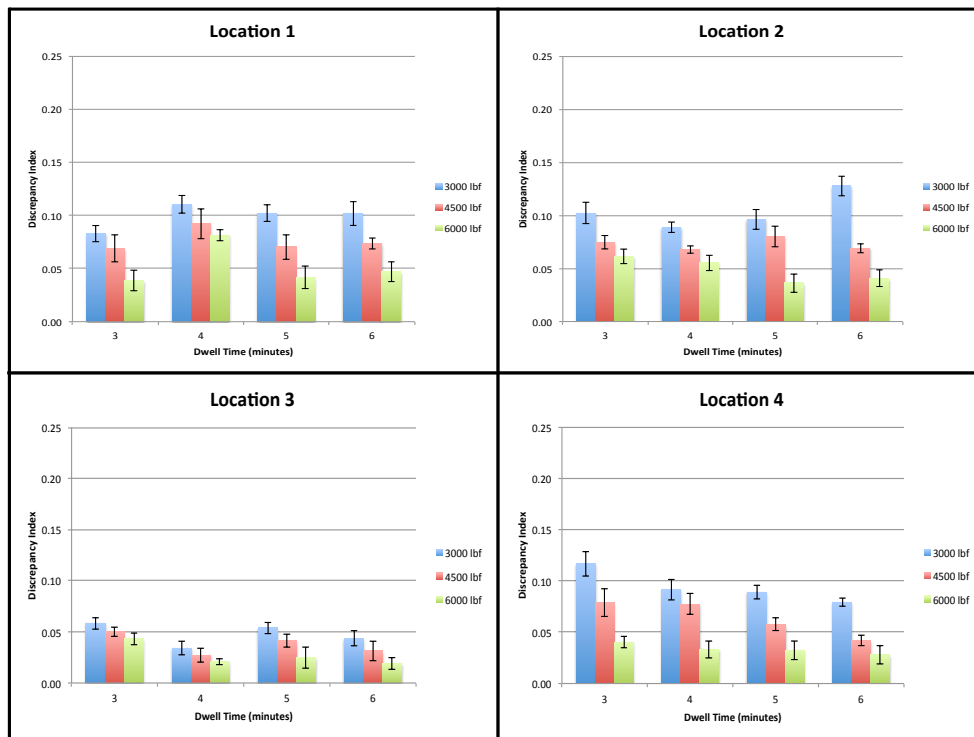


Figure 5.7: Cross-sectional normalized discrepancy graphs of the 4 locations on the microfluidic device where characterization was performed for PMMA using the Carver Press. Sample size of n=3 for all conditions. The maximum Discrepancy Index axis value is 0.25 for Location 1, Location 2, Location 3 and Location 4.

5.4.2 Carver+COP+Epoxy

A cross-sectional feature transfer fidelity analysis was also performed for the embossed COP with the Carver Press hot embosser and aluminum-filled epoxy. The cross-sections

of the COP were made at the same location as those made for PMMA. Three were at the three separate inlet ports and one was through the large channel at the opposite end of the device. Cross-sectional imaging was again performed with the EVOS brightfield microscope and cross-sectional area measurements were made with ImageJ. The aluminum-filled epoxy was also cross-sectioned at the same location as those made for the embossed COP. Cross-sectional images of the aluminum-filled epoxy were taken with the EVOS brightfield microscope and cross-sectional area measurements were then made with ImageJ. Cross-sectional feature transfer fidelity was then characterized with the use of Microsoft Excel according to the Discrepancy Index equation previously discussed. Figure 5.8 shows the graphs for the four separate locations are as follows:

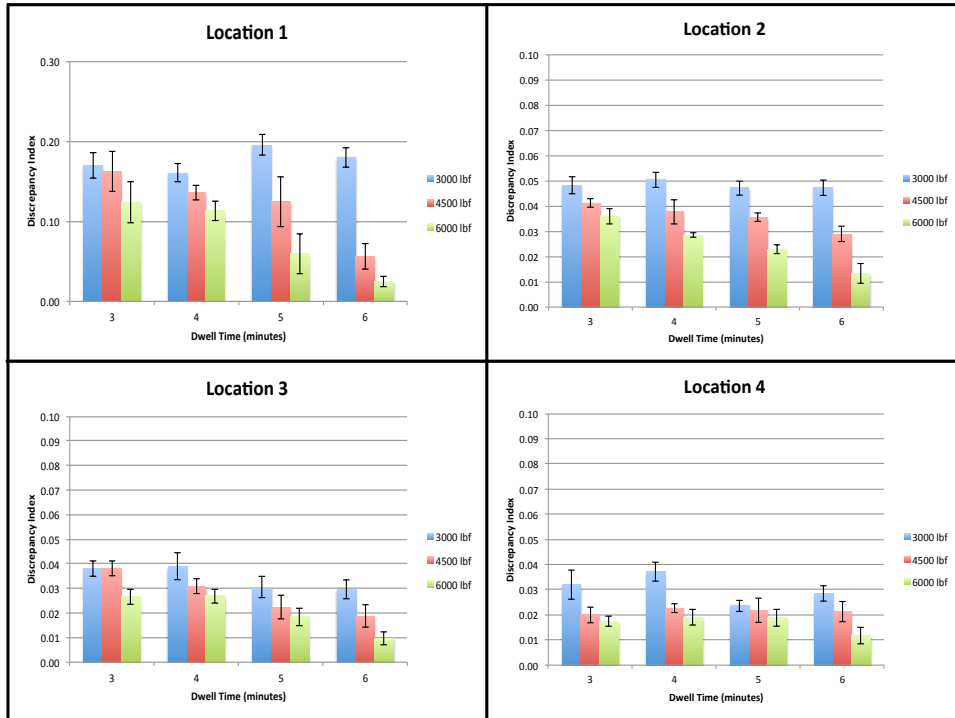


Figure 5.8: Cross-sectional normalized discrepancy graphs of the 4 locations on the microfluidic device where characterization was performed for COP using the Carver Press. Sample size of n=3 for all conditions. The maximum Discrepancy Index axis value is 0.50 for Location 1 and 0.10 for Location 2, Location 3 and Location 4.

5.4.3 EVG+PMMA+Epoxy

After embossing of the 36 devices in PMMA was performed with the EVG 520HE hot embosser using an aluminum-filled epoxy, cross-sectional analysis was performed. The cross-sections of the embossed PMMA were at the same four locations mentioned previously in order to remain consistent. Cross-sectional images were taken with the EVOS brightfield microscope and cross-sectional area measurements were made with ImageJ. Cross-sections of the aluminum-filled epoxy, which was used throughout embossing experimentation, were made at the same location as those made for the embossed PMMA. Cross-sectional images of the aluminum-filled epoxy were taken with the EVOS brightfield microscope and cross-sectional area measurements were made with ImageJ. Cross-sectional feature transfer fidelity of the 144 images was then characterized with the use of Microsoft Excel, where the Discrepancy Index was calculated for all four locations on the 36 embossed PMMA devices. Figure 5.9 shows the graphs for the four separate locations are as follows:

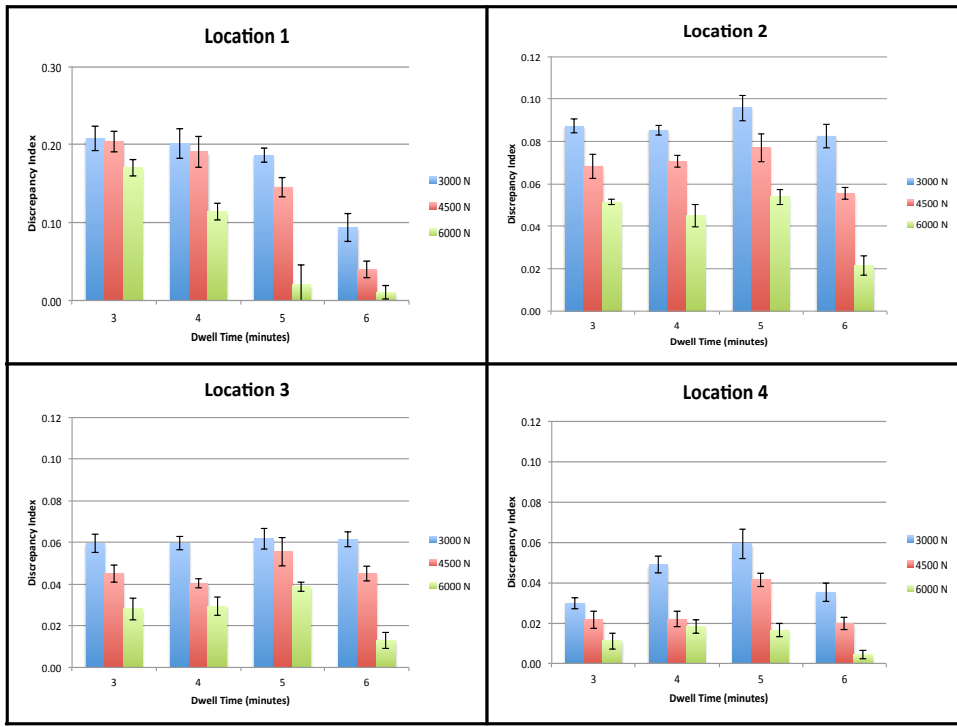


Figure 5.9: Cross-sectional normalized discrepancy graphs of the 4 locations on the microfluidic device where characterization was performed for PMMA using the EVG 520HE. Sample size of n=3 for all conditions. The maximum Discrepancy Index axis value is 0.50 for Location 1 and 0.12 for Location 2, Location 3 and Location 4.

5.4.4 EVG+COP+Epoxy

After the 36 COP sheets were embossed, with the use of the EVG 520HE hot embosser and aluminum-filled epoxy mold, cross-sections were made at the four locations previously discussed. The four cross-sectioned locations were imaged with the use of the EVOS brightfield microscope and cross-sectional area measurements were made with ImageJ. The aluminum-filled epoxy was also milled at the four locations previously discussed. The cross-sections of the aluminum-filled epoxy were imaged with the use of the EVOS brightfield microscope and cross-sectional area measurements were made with ImageJ. Cross-sectional feature transfer fidelity of the 144 images was then performed

with the use of Microsoft Excel, where the Discrepancy Index was calculated for the four locations of all 36 embossed COP devices. Figure 5.10 shows the graphs of the four separate locations are as follows:

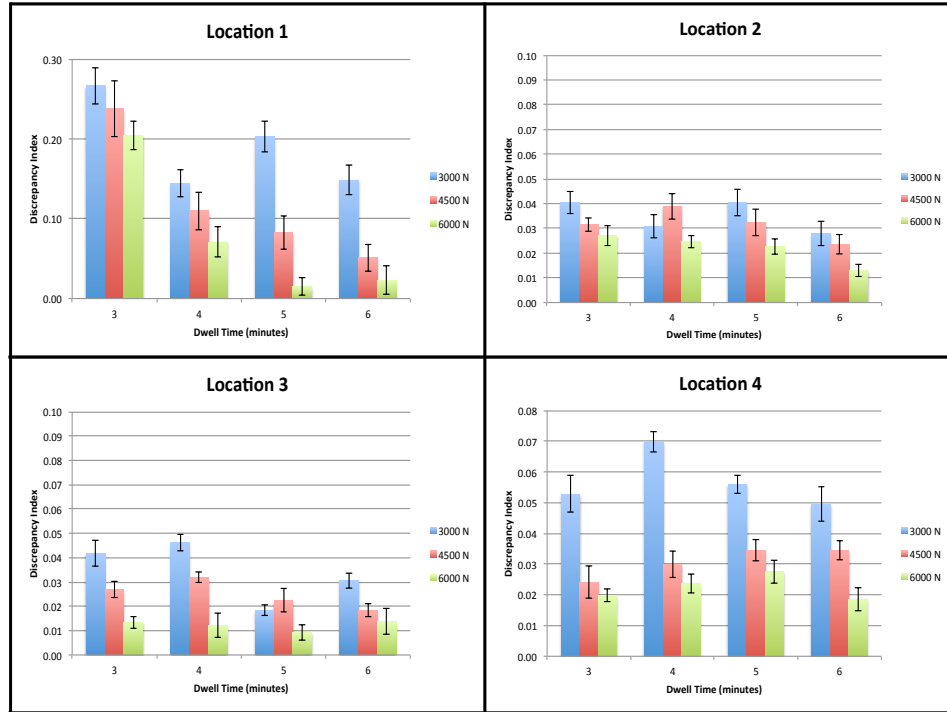


Figure 5.10: Cross-sectional normalized discrepancy graphs of the 4 locations on the microfluidic device where characterization was performed for COP using the EVG 520HE. Sample size of n=3 for all conditions. The maximum Discrepancy Index axis value is 0.70 for Location 1 and 0.10 for Location 2, Location 3 and Location 4.

5.4.5 Statistical Analysis

The results of the characterization experiments were analyzed through a 2-way ANOVA. Each set of parameters was tested 3 times, providing an n=3 sample size. This analysis was performed for each characterization experiment involving the hot embossing of the two thermoplastic materials, PMMA and COP, on the two hot embossing machines,

Carver Press and EVG 520HE. Ultimately, the statistical analysis showed that the quality of the thermoplastic device for both materials on both hot embossing machines was force dependent, through a rejection of the null hypothesis. The statistical analysis also showed that the quality of the embossed thermoplastic material for both materials on both hot embossing machines was dwell time dependent, through a rejection of the null hypothesis.

5.5 Epoxy Mold Deformation

An experiment was run to test whether there was a change in the epoxy mold dimensions after hot embossing was performed. There were two considerations that brought about this experiment. The first was a lack of information on the Young's modulus for the EC-415 aluminum-filled epoxy material. Under different applied forces, the material would alter its length according to the equation:

$$E = \frac{FL_0}{A_0\Delta L}$$

which would affect the relative displacements between the microfluidic channel features on the epoxy mold surface. The second consideration was the recorded value of 10.3×10^{-6} in/in•F for the coefficient of thermal expansion. There was a question as to whether the epoxy mold might deform over multiple embosses and this was studied. Figure 5.11 shows a theoretical example of the epoxy mold deforming under high temperature and pressure hot embossing conditions.

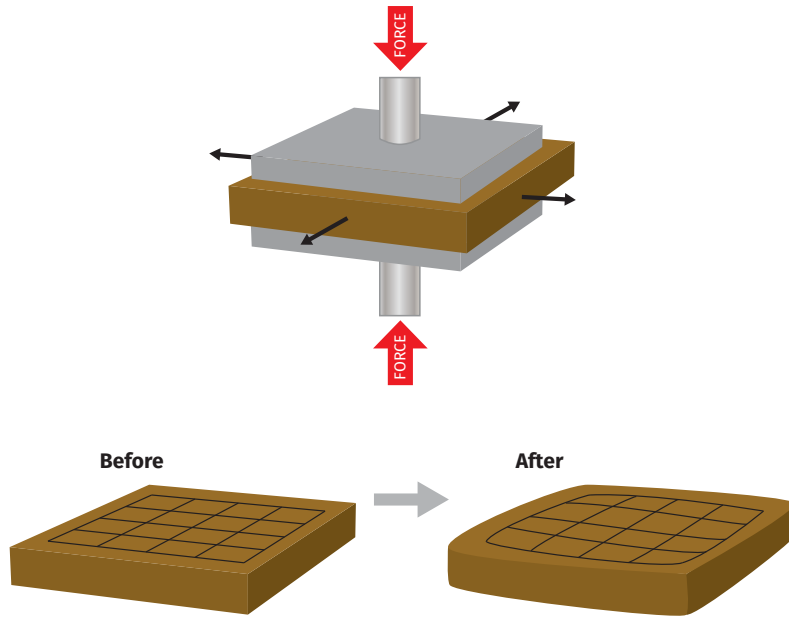


Figure 5.11: Hypothesized result of epoxy mold surface grid after hot embossing was performed at a high compressive force.

An epoxy mold was created with no microfluidic features on its surface so as to provide a smooth surface on both the top and bottom side of the epoxy. A 2-dimensional grid pattern was programmed in SolidWorks (Dassault Systemes, Velizy-Villacoublay, France). The grooves of the grid were 800 μm wide and 400 μm deep. The epoxy molds were aligned to the milling machine and the grid pattern was milled directly into the surface of the epoxy mold. Figure 5.12 shows an image of the epoxy grid surface with a calliper placed next to it for measurement purposes.



Figure 5.12: Grid pattern milled directly into epoxy mold surface

After milling was complete, the epoxy was brought over to a levelled granite block and had its grid surface imaged with a calliper placed directly into its surface. Next the epoxy was placed directly into the platens and hot embossing was performed under the maximal conditions that previous hot embossing experiments were performed under. The hot embossing process was:

1. Raise platens temperature to 170°C
2. Hold at 170°C for 5 minutes
3. Close platens and apply force of 6000 lbf
4. Hold platens closed for 5 minutes
5. Cool platens to 40°C and open platens

After this process was complete, the epoxy was brought over to the levelled granite block and an image was taken of the grid surface with a calliper placed directly on its surface. This was repeated for a total of 4 times per epoxy and 2 separate epoxies were tested. The results are shown in Table 5-5:

Epoxy	Emboss Number	Closing Speed (%)	Heating Temp. (°C)	Thermal Confluence Time (min)	Force (lbf)	Dwell Time (min)	Cooling Temp. (°C)	Length Pre-emboss	Length Post-Emboss
E1	1	20	170	5	6000	5	40	69.99	70.00
E1	2	20	170	5	6000	5	40	70.00	69.99
E1	3	20	170	5	6000	5	40	69.99	70.00
E1	4	20	170	5	6000	5	40	70.00	70.00
E2	1	20	170	5	6000	5	40	70.02	70.02
E2	2	20	170	5	6000	5	40	70.02	70.01
E2	3	20	170	5	6000	5	40	70.01	70.02
E2	4	20	170	5	6000	5	40	70.02	70.01

Table 5-5 Measurements made of two separate epoxy mold grids after multiple hot embosses

This experiment showed that under the maximal conditions used during hot embossing there was no noticeable deformation of the epoxy dimensions. This was an affirmation that over multiple embosses, the displacement of channel features from one another will be minimal. Increased temperatures and pressures could be applied to the epoxy mold in order to further characterize any potential deformation. However, the conditions chosen were specifically applied as they provided input into whether deformation would be seen when using parameters at the upper limit of those used for hot embossing of PMMA and COP during cross-sectional feature transfer fidelity characterization. With these hot embossing conditions there will be a consistency of produced microfluidic device dimensions.

5.6 Comparison Between Epoxy and Silicon Masters

5.6.1 Silicon Master Hot Embossing

Hot embossing was performed on the EVG 520HE hot embosser with the use of a silicon master mold for pressing the microfluidic features into the thermoplastic material. This was looked into as a comparison between silicon master molds and aluminum-filled

epoxy molds for the purposes of hot embossing quality characterization and hot embossing parameter optimization. Figure 5.13 shows a typical hot embossing setup where the epoxy mold in Figure 5.3 has been replaced with an SU-8 master wafer mold.

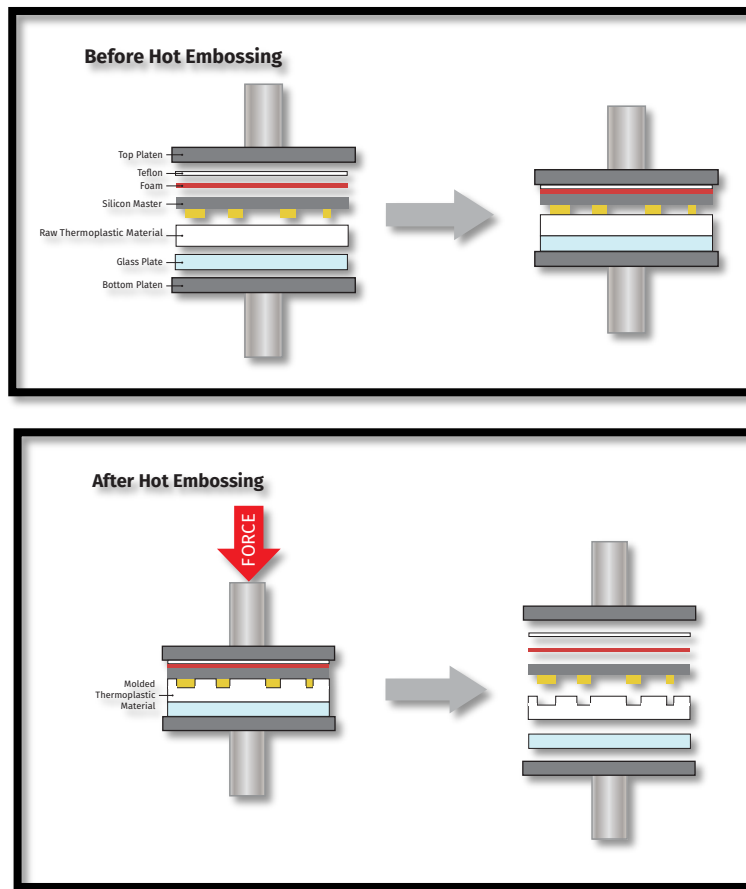


Figure 5.13: Hot embossing being performed on a thermoplastic material with the use of a silicon wafer with SU-8 features. All items labelled and presented in the order that they are found during the hot embossing process. After an application of force and temperature, the thermoplastic material is released from the hot embossing machine with a transfer of microfluidic features from the silicon wafer master mold.

A large number of silicon master molds had been accumulated during the process of fabricating a silicon master mold that fell within the tight tolerances of Bio-Rad Laboratories' expectations. These silicon master molds were used for initial experimentation on the hot embossing capabilities with the use of silicon master molds.

The thermoplastic material PMMA was also used for initial experimentation and the specific thickness of PMMA that was used was 1.5 mm thick. This thickness provided much higher flexibility to maneuver around the silicon wafer master mold positive-relief features post-emboss, compared to the thicker 4 mm thick PMMA raw material that was required. An initial concern was that the SU-8 features attached to the silicon wafer master mold might not be as firmly adhered to the silicon substrate, compared to the positive-relief features of the aluminum-filled epoxy mold. A thinner raw thermoplastic material could help to alleviate some of the burden of demolding during this initial testing. Figure 5.14 shows the delamination of the SU-8 features from the wafer substrate during demolding from the thermoplastic material after hot embossing has been performed.

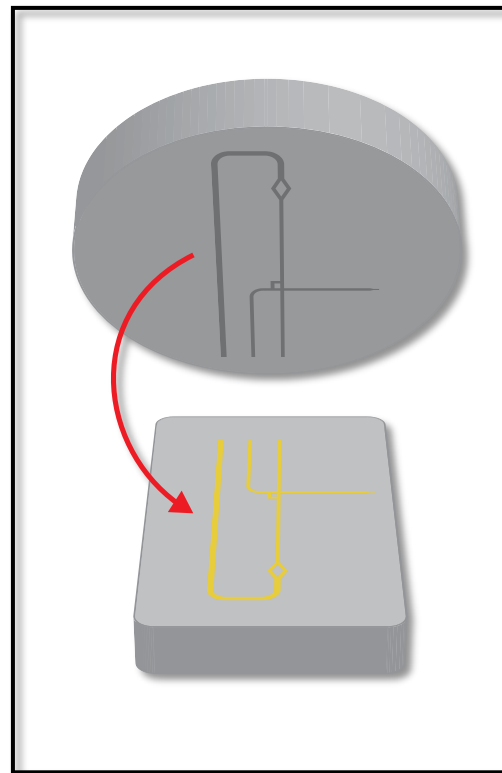


Figure 5.14: SU-8 features being removed from the silicon wafer substrate and becoming embedded in the thermoplastic material during demolding.

Experimentation began with the use of the silicon master molds previously mentioned without any additional modifications or coating of releasing agents on its surface. The hot embossing parameters that were used for hot embossing were those used with the epoxy mold on the EVG 520HE system. These initial hot embossing parameters were 6000 N, 170°C and 5 minutes dwell time. The microfluidic design that was initially used on the silicon wafer was the first layer of the 3-layer design. This layer had microfluidic features that were 100 μm tall and 250 μm wide. Only a single layer was used initially in order to test the capabilities of a simple design for embossing purposes before moving onto a more complex, multi-layer design. These first tests on hot embossing with the use of a silicon wafer master mold proved to be unsuccessful, as features removed from the silicon wafer substrate during demolding.

Next, Pyrex wafer master molds with a single feature height were used for hot embossing experimentation. The parameters used for hot embossing were the same as those previously mentioned. The purpose of using a Pyrex wafer master that was fabricated through backside lithography was that the SU-8 features had positive draft angles and it might potentially help during demolding. No additional modifications were made to the Pyrex wafer master mold and demolding again proved to be unsuccessful due to the removal of SU-8 features.

After having tested both silicon wafer master molds and Pyrex wafer master molds without any additional processing, the use of a spun layer of releasing agent was tested with silicon wafers that had been previously fabricated. These silicon wafers were again

one feature height and the releasing agent that was used was provided by EVG. The two separate solutions were spun at 1000 RPM for 60 seconds, according to the specified protocol. The same addition of a layer of releasing agent was also applied to a second design provided by Bio-Rad Laboratories, which consisted of a single SU-8 layer with feature widths of 450 μm and feature heights of 50 μm . These wafers were tested under the same hot embossing conditions and this proved to be unsuccessful.

It was decided that further experimentation should be limited to the second design provided by Bio-Rad Laboratories, due to its lower aspect ratio for SU-8 features. New silicon wafers were fabricated, however an SU-8 seed layer was spun and exposed to UV light before an additional layer of SU-8 was spun, which was exposed using the mask for Design #2. The purpose of this additional seed layer was to anchor the SU-8 microfluidic features to a layer that was made of the same material. It was thought that if both the microfluidic feature layer and the layer that it is directly attached to were both made of SU-8, then there would be a stronger bond between these layers, which could potentially help with the adhering of SU-8 microfluidic features during demolding. After the developing of the silicon wafer master molds, a layer of releasing agent was coated on its surface. These silicon master molds were then tested, using the same hot embossing parameters mentioned above. The SU-8 microfluidic features did not entirely lift off during demolding but not all features remained anchored to the SU-8 seed layer.

Lastly, silicon wafer master molds were again fabricated with an SU-8 seed layer and a 50 μm layer with Design #2 microfluidic features. After development, an additional hard

baking step was applied to these wafers. The hard baking step involved heating the silicon wafer master mold in 20 degree incremental ramp ups, being held at each temperature for 5 minutes before increasing the heat further. The silicon wafer master molds were held at a high temperature of 200°C on the hot plates for an hour, before lowering the temperature in 20 degree incremental ramp downs and holding the silicon wafer master molds at each temperature for 5 minutes. This hard baking step allowed hot embossing to be performed at a higher temperature and potentially allowed for further cross-linking of the SU-8 material. Hot embossing was then performed with parameters of 6000 N, 200°C and 5 minutes dwell time. SU-8 microfluidic features stayed adhered to the seed layer for 3 embosses before they started to demold.

It was at this point that further experimentation was thought to not provide any further information. A discussion and comparison of hot embossing with the use of silicon wafer master molds and aluminum-filled epoxy molds will be provided in Section 5.6.2.

5.6.2 Epoxy Mold Hot Embossing

5.6.2.1 Start-up Optimization & Epoxy Mold Robustness

A comparison can be drawn at this time between silicon wafer master molds and aluminum-filled epoxy molds for the purpose of hot embossing and characterization of different thermoplastic materials with different hot embossing machines. Start up optimization is a necessary step required for a manufacturer interested in producing thermoplastic microfluidic devices through hot embossing. While the literature provides information on parameters used by specific research groups with specific hot embossing

machines and hot embossing molds, there is still an initial stage where these parameters must be tested and tuned to the particular equipment available.

This start up characterization and optimization requires a means to produce thermoplastic microfluidic devices without the continuous need to fabricate silicon wafer master molds, which is a timely and costly process. The timely nature of this process is a result of repeated silicon wafer master mold fabrication until parameters have been chosen that produce SU-8 feature heights and draft angles that are within the tolerances of those required. Once a master mold has been fabricated within tolerances, it would be unwise to use this as a hot embossing mold where it might not withstand the conditions applied to it. Aluminum-filled epoxy molds provide a path of circumvention for this issue, as they are a direct translation of the silicon wafer master mold that has been fabricated within tolerances and allow the silicon master to be preserved by applying hot embossing conditions to the aluminum-filled epoxy. Whether positive-relief microfluidic features fracture on the epoxy mold, the silicon master can provide the possibility to continue testing and optimization with device features that are still within tolerance through the fabrication of another aluminum-filled epoxy mold. The second concern of cost ties directly into the concern of characterization and optimization of hot embossing parameters through the use of a silicon wafer master mold. Previous experimentation on hot embossing with a silicon master showed to provide ambiguity in not only the parameters required for high quality feature transfer fidelity of microfluidic features but also features that would preserve the lifetime of the silicon master. If the manufacturer does not choose a set of parameters that fall within the allowable range for preserving the

silicon wafer SU-8 features, or if demolding results in loss of features, then a new silicon wafer will be required. This new silicon wafer master mold will need to be fabricated in a clean room, which costs between \$75-\$180 per hour for industry use depending on the equipment being used at the Toronto Nanofabrication Centre (TFNC). With a 3-layer device, fabrication time can reach up to 6 hours and each silicon wafer master mold can result in a clean room associated cost up to \$1080. With the concern of producing a silicon wafer master mold within tolerances, this can become a costly endeavor. Once an appropriate master wafer has been created, it should be protected. Epoxy hot embossing molds, on the contrary, do not need to be fabricated in a clean room and can be fabricated in a laboratory setting, as demonstrated in Chapter 4. This can help to save costs associated with hot embossing mold fabrication while simultaneously preserving a silicon wafer master mold that has been fabricated within feature height and draft angle tolerances.

5.6.2.2 Multiple Epoxy Molds from Single Silicon Master

Once an appropriate silicon wafer master mold has been fabricated, there is also the potential to create multiple hot embossing epoxy molds from the master wafer, which is illustrated in Figure 5.15. This can be done by following the epoxy mold fabrication process described in Chapter 4. The advantage of this is that the epoxy molds will all be fabricated from the same silicon wafer master mold and there will not be a concern as to whether feature heights on the epoxy mold are within the tolerance required by the buyer. This allows for parallelization of hot embossing, which is only limited by the amount of space and hot embossing equipment available. Once a silicon wafer master mold has

been created, all further epoxy molds created will be produced with desired feature dimensions. On the contrary, there is a larger degree of variability seen in the feature heights achieved through the production of multiple silicon wafer masters. If precise feature dimensions are an important aspect of a particular microfluidic design then there should be a consistency in hot embossing mold fabrication. This is more achievable through the preservation of a single silicon master mold, by means of epoxy mold fabrication, than through fabrication of multiple silicon wafer master molds.

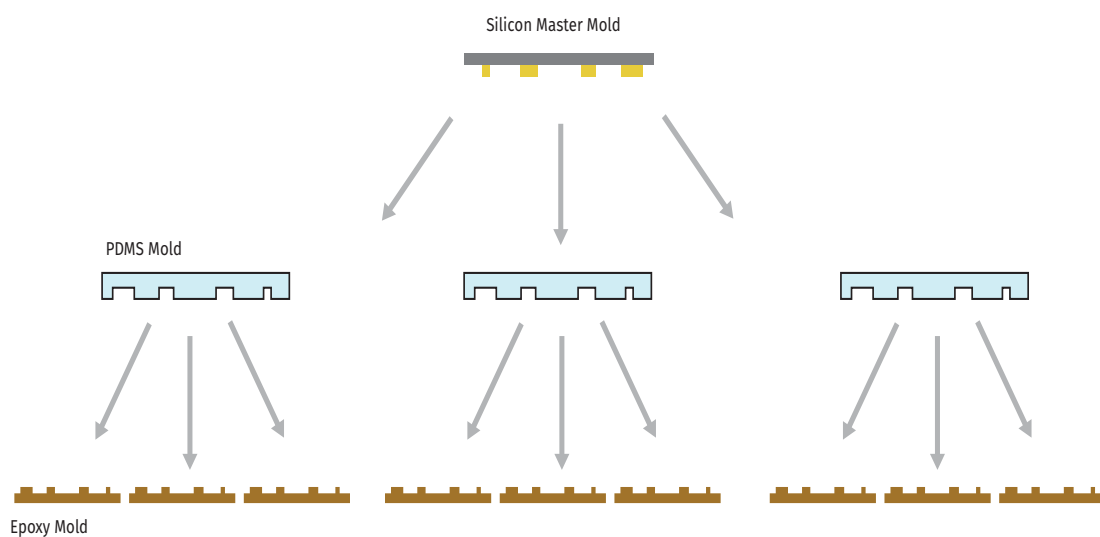


Figure 5.15: Amplification in the number of hot embossing molds that can be created from the use of a single silicon wafer master mold.

5.6.2.3 Preservation of Optimized Silicon Master

A characterization was performed on the preservation of silicon master mold SU-8 feature dimensions. The purpose of this characterization was to study the fidelity of feature dimensions through each stage of the fabrication process of thermoplastic microfluidic devices. Four areas of the 3-layer microfluidic design were examined.

These four areas are the same four that were used during cross-sectional feature transfer fidelity characterization of thermoplastics PMMA and COP with the use of aluminum-filled epoxies and both Carver Press and EVG 520HE hot embossing machines. An example of the measurements made at each stage in the fabrication process is provided in Figure 5.16:

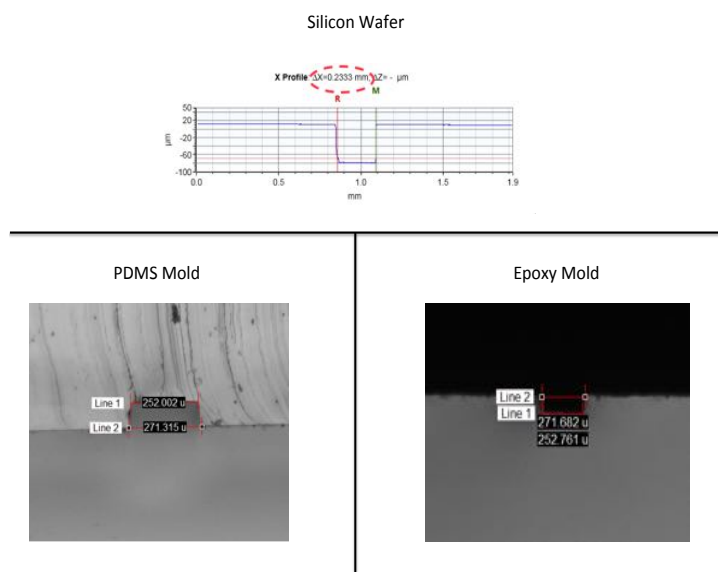


Figure 5.16: Cross-sectional measurements of a microfluidic feature being made on an SU-8 feature from a silicon master mold, a PDMS negative-relief feature mold produced from the same silicon master mold and an epoxy positive-relief feature mold produced from the same PDMS mold.

This analysis was performed on a PDMS mold and epoxy mold that were used for cross-sectional feature transfer fidelity characterization of PMMA and COP on the Carver Press and EVG 520HE hot embossing machines. The resultant data collected from these characterizations elucidates the quality of embossed thermoplastic microfluidic features, which is the last step in the fabrication process. This analysis was performed over 4 separate PDMS and hot embossing epoxy mold locations, stemming from one silicon master. This was performed in order to get a representation of the preservation of

microfluidic feature dimension preservation across a device from the fabrication of the silicon master mold to the fabrication of the hot embossing epoxy mold. This data is provided below in Table 5-6:

	Location 1 (mm)	Location 2 (mm)	Location 3 (mm)	Location 4 (mm)
Silicon Wafer	0.2333	0.4815	0.5816	0.5861
PDMS – Top	0.2520	0.4841	0.5810	0.5879
PDMS - Bottom	0.2713	0.5476	0.5934	0.5951
Epoxy – Top	0.2528	0.4844	0.5813	0.5884
Epoxy - Bottom	0.2717	0.5477	0.5939	0.5959

Table 5-6 Measurements made on the silicon wafer, PDMS negative-relief feature mold and positive-relief epoxy mold at four separate locations on the microfluidic design

Averaging the top and bottom values for the mold width, this table shows that the microfluidic design has an average width discrepancy of 0.0184 mm with a standard deviation of 0.0151 mm from the width seen on the silicon wafer to those seen on the PDMS negative-relief feature mold during soft lithography. Along the same vein, there was an average width discrepancy of 0.0189 mm with a standard deviation of 0.0150 mm from the width seen on the silicon wafer master mold to those seen on the aluminum-filled epoxy hot embossing mold.

5.7 Throughput capabilities

The throughput capabilities of the hot embossing process were affected by a number of factors. The first factor that needed to be taken into consideration was the number of embosses that could be performed with each epoxy mold. This value was primarily

contingent on the use of the Weicon releasing agent, as well as the feature heights of the microfluidic design that was to be embossed. Without the use of the Weicon releasing agent, each epoxy mold lasted an average of 3 embosses for Design #1, where the feature heights reached a value of 300 μm . However, without the use of the Weicon releasing agent, each epoxy mold lasted over 10 embosses for Design #2, where the feature heights reached a value of 56 μm . The embossing was not performed further for Design #2 and the features did not break on the epoxy mold during hot embossing testing of Design #2. With the use of the Weicon releasing agent, each epoxy mold lasted over 10 embosses for Design #1 and ranged from 20-25 embosses per epoxy mold. This value could be further increased with repeated coating of the Weicon releasing agent after each emboss. The Weicon releasing agent provided a thin lubricating layer between the aluminum-filled epoxy and the thermoplastic hot embossed material, which improved the demolding process and preserved the epoxy features as a result. However, with each successive emboss without the reapplication of the Weicon releasing agent, the demolding became more difficult. After 4-5 embosses without reapplication of the Weicon releasing agent, the demolding process was just as difficult as without any Weicon releasing agent.

The Weicon releasing agent was required to be used in temperatures that did not exceed 130°C. Thus, hot embossing conditions were performed at 120°C when the Weicon releasing agent was used. To compensate for the lower temperature, an increased embossing force of 9,000 lbf was applied. Various embossing dwell times were applied, ranging from 5 minutes to 60 minutes. Ultimately, an embossing dwell time of 15

minutes showed to provide a good quality chip by eye while also maintaining an overall embossing time that matched the post-embossing milling time of ~30 minutes.

These hot embossing conditions were used to test throughput capabilities of the hot embossing process over a 5-day workweek. The data provided below in Table 5-7 shows the times that were seen for each emboss over the course of 5 days:

Monday				
Device #	Epoxy #	Begin HE	End HE	Δ HE (min)
1	1	9:00 AM	9:34 AM	34
2	1	9:37 AM	10:11 AM	34
3	1	10:15 AM	10:51 AM	36
4	1	10:55 AM	11:32 AM	37
5	1	11:36 AM	12:13 PM	37
6	1	12:18 PM	12:56 PM	38
7	1	1:06 PM	1:36 PM	30
8	1	1:39 PM	2:15 PM	36
9	1	2:19 PM	2:59 PM	40
10	1	3:03 PM	3:37 PM	34
11	1	3:43 PM	4:17 PM	34

Tuesday				
Device #	Epoxy #	Begin HE	End HE	Δ HE
1	1	9:09 AM	9:47 AM	38
2	1	9:56 AM	10:32 AM	36
3	2	10:36 AM	11:15 AM	39
4	2	11:19 AM	11:58 AM	39
5	1	12:01 PM	12:41 PM	40
6	1	12:43 PM	1:18 PM	35
7	1	1:21 PM	2:04 PM	43
8	1	2:08 PM	2:41 PM	33
9	1	2:44 PM	3:22 PM	38
10	1	3:24 PM	3:59 PM	35

Wednesday				
Device #	Epoxy #	Begin HE	End HE	Δ HE (min)
1	2	9:00 AM	9:30 AM	30
2	2	9:35 AM	9:55 AM	20
3	2	10:00 AM	10:39 AM	39
4	2	10:42 AM	11:17 AM	35
5	2	11:20 AM	11:58 AM	38
6	2	12:02 PM	12:42 PM	40
7	2	12:45 PM	1:26 PM	41
8	2	1:29 PM	2:18 PM	49
9	2	2:20 PM	3:16 PM	56
10	2	3:19 PM	3:59 PM	40

Thursday				
Device #	Epoxy #	Begin HE	End HE	Δ HE (min)
1	2	9:00 AM	9:35 AM	35
2	2	9:38 AM	10:03 AM	25
3	2	10:05 AM	10:45 AM	40
4	2	10:47 AM	11:15 AM	28
5	2	11:20 AM	11:54 PM	34
6	2	12:00 PM	12:36 PM	36
7	2	12:40 PM	1:14 PM	34
8	2	1:20 PM	1:52 PM	32
9	2	2:00 PM	2:36 PM	36
10	2	2:40 PM	3:15 PM	35

Friday				
Device #	Epoxy #	Begin HE	End HE	Δ HE (min)
1	3	9:20 AM	9:59 AM	39
2	3	10:00 AM	10:36 AM	36
3	3	10:39 AM	11:11 AM	32
4	3	11:13 AM	11:57 AM	44
5	3	12:00 PM	12:35 PM	35
6	3	12:39 PM	1:15 PM	36
7	3	1:30 PM	2:06 PM	36
8	3	2:08 PM	2:40 PM	32
9	3	2:45 PM	3:10 PM	25
10	3	3:15 PM	3:50 PM	35

Table 5-7 Times associated with the beginning and ending of each hot emboss performed throughout the week-long throughput test, as well as the time per each hot emboss.

Overall, 51 hot embossed devices were produced over the course of a 5-day, 40-hour workweek. The average hot embossing time over the 5-day workweek was 30.1 minutes per device with a mode of 30 minutes. The number of hot embosses performed each day was capped at the value of devices that could sequentially be milled the same day. On average, hot embossing began earlier in the day and milling was begun after the first hot embossed device was ready to be brought over to the milling machine – approximately 30 minutes after the start of the day. The number of hot embossed devices can be further increased with a hot embossing epoxy mold that contains more than one microfluidic design on its surface, or with the use of more than one hot embossing machine. However, for the purposes of testing throughput capabilities with the use of one manufacturer and one hot embossing machine, a consistent value of 10 devices per day can be fabricated.

Chapter 6

Milling Techniques and Device Finalization

6.1 Introduction

After hot embossing of the microfluidic features into a thermoplastic material, there are some additional post-embossing modifications that need to be included. This includes the milling of complex perimeters and additional features when necessary. The milling of thermoplastic materials runs on the premise that a rotating cutting tool will remove material from the raw workpiece [31]. The milling system includes a worktable, a cutting tool and an overhead spindle in which the cutting tool is held. Milling has a long history, dating back to 1818 [70] and has markedly improved over the years to allow for features with micro-scale resolution [126]. Additionally, milling machines have improved from their traditional mechanical lever control of the x-, y- and z- coordinates to now use computer numerical control (CNC), which helps in the reduction of human error and improvement of repeatability and precision [31]. The inclusion of computer numerical control into the milling process also allows for a quick conversion of computer-aided design (CAD) models into the milling program for rapid testing and iteration. There are limitations in some aspects of the milling process, including the surface finish achievable with milling and the smallest feature sizes achievable [63]. However, hot embossing was used as the fabrication method for the microfluidic features throughout experimentation.

Milling of the device perimeter, along with additional features, could use this technique to its advantage. Milling is a rapid fabrication method, taking less than 30 minutes per device in most cases [31].

The purpose of milling additional features into the microfluidic device, or milling complex perimeters is to allow for a larger variability in achievable microfluidic designs. There is the possibility to take advantage of hot embossing and milling fabrication methods to produce a device that isn't achievable from each fabrication method on its own. However, there are technical challenges that need to be addressed in order to make this a viable option, including the ability to precisely and repeatedly align embossed microfluidic features with the milling machine coordinates. A study on throughput capabilities should also be addressed to see if the milling fabrication process could accommodate the hot embossing throughput over the course of a week.

6.2 Materials and Methods

6.2.1 SolidWorks 3D CAD Design

The first step in the milling and micromilling fabrication process is to create a 3-dimensional CAD design of the geometry that you are interested in milling. The program used to create these 3-dimensional designs throughout experimentation was SolidWorks 3D CAD software. This program allowed for the workup of complex microfluidic device designs as well as additional processing that would be included after embossing of microfluidic features had been achieved. First, a sketch of the milling design was created

in SolidWorks. Precise measurements were made of each dimension of the design in order to assure that the design would hold the same dimensions as those envisioned. Once the sketch model was created, each component of the sketch was extruded to a particular height in order to create a 3-dimensional representation of the milling program that would eventually be run. The SolidWorks 3D CAD program has the capability to include more complex 3-dimensional features, such as ramps, which were created and applied directly to the hot embossing aluminum-filled epoxy mold surface. Once the SolidWorks file was complete according to the envisioned design, the 3-dimensional model was saved and transferred to the SprutCAM software for additional processing.

Figure 6.1 shows a CAD model of the microfluidic design produced in SolidWorks.

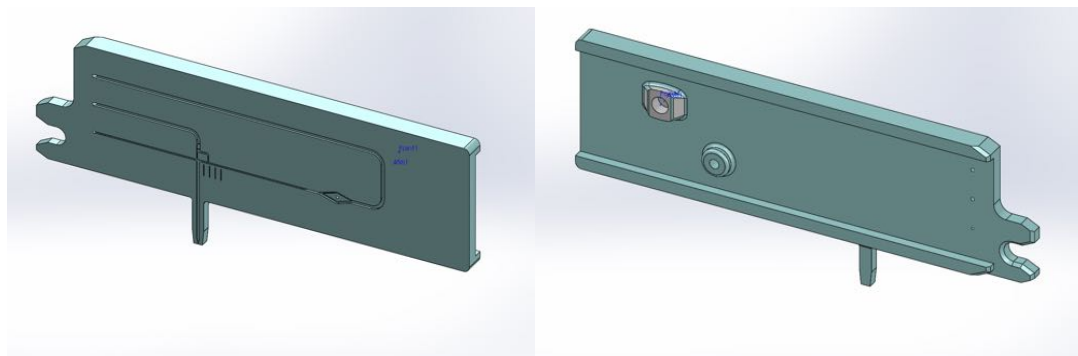


Figure 6.1: Front and back side of microfluidic design produced in SolidWorks.

6.2.2 SprutCAM

SprutCAM software (SprutCAM, Naberezhnye Chelny, Russia) was used to apply further control over the milling program. The file that was created on SolidWorks was first uploaded to the SprutCAM software. Next the location of the origin was specified. This was an important step as it would be the location where the origin was during actual milling with the milling machine. The zero was usually located at the minimum x value,

the maximum y value and the maximum z value of the CAD model. The maximum z value was the most important, as this allowed the user to zero the endmill directly on the surface of their thermoplastic. This was in contrast to choosing the z=0 location as the minimum z value, which would require the user to locate the bottom end of their thermoplastic material. This would be particularly difficult, as there was usually an adhesive layer attaching the thermoplastic material to the sacrificial layer. This adhesive layer has a thickness, which is unaccounted for in the SprutCAM software. After the origin had been selected, particular areas of the design were selected and a specific endmill was chosen to perform the milling of this area. A list of endmills that are available in the laboratory can be selection. Specific aspects of the milling process were also stipulated. This includes selecting the RPM of the endmill, the feed rate, the number of passes that the endmill will make, the depth of each pass, the step size between one pass and the next most adjacent pass, and so on. These are important aspects of the milling process that need to be selected in order to produce a high quality milling process. For example, if RPMs are too high and feed rate too low, the thermoplastic material could melt and if the RPM is too low and the feed rate too high then the endmill could break. It was also important to choose particular values that find a good balance between milling surface finish and total milling run time. Once all values had been selected for all areas, a simulation was run to see whether the milling program would run according to what the user envisioned. If the simulation looked appropriate then the file was saved in a format that is compatible with the Tormach PCNC milling machine.

6.2.3 Tormach PCNC & G-Code

Once the SprutCAM parameter selection had been completed the file was saved as a .TAP extension and was automatically written in a G-code format that is compatible with the Tormach PCNC milling machine. Simply, the G-code is a line-by-line low level computing language that specifies the coordinates that the endmill should move to, also specifying certain parameters such as the RPM and feed rate. The file was uploaded to the Tormach PCNC software. The first step was to acquire all the endmills that would be used throughout the milling process. A sacrificial layer was secured onto a levelled granite block through the use of double-sided tape. The embossed thermoplastic material was then placed onto the sacrificial layer in such a way that the embossed microfluidic features were oriented appropriately to the x-, y- and z- coordinates of the milling machine. This was an important step, as the milling machine cannot adjust its inherent x-, y- and z- direction coordinates so it is up to the user to assure that any embossed features follow these coordinates. A developed automatic alignment method will be discussed shortly. Once the embossed thermoplastic material had been secured to the sacrificial layer, with the use of double-sided tape, the first bit used for the milling program was placed into the milling chuck. The endmill was zeroed in order to specify the origin of the milling program. The endmill was then secured and raised slightly above the embossed thermoplastic material. The program was then run and a coolant was applied to the endmill in order to reduce the temperature during the running of the program and avoid melting of the thermoplastic material. Once the first step of the program was complete, the endmill was removed and the second endmill was inserted into the chuck and zeroed again. This process continued until the entire program was

complete. Once the program was complete, the microfluidic device was removed from the sacrificial layer and cleaned with isopropanol. Figure 6.2 provides an illustration of the endmill milling the device perimeter.

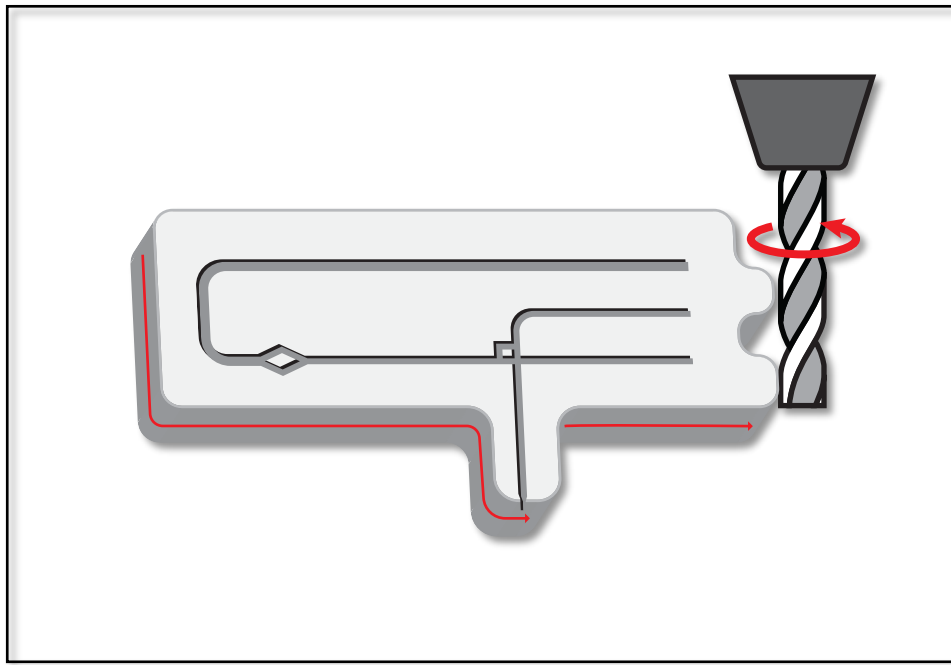


Figure 6.2: Device perimeter being milled after microfluidic features had been embossed directly into the thermoplastic material.

When milling features onto the thermoplastic material, or milling the device perimeter, it was important to consider the appropriate parameters for each step. The size of the endmill played a large role in this decision, as the RPM and feed rate chosen would directly affect both the milled surface quality and whether the endmill would break under the applied conditions. The smaller the endmill size, particularly with diameters of 500 μm or less, the more likely the endmill would break under higher feed rates. Typical endmill rotational speeds were 5000 RPM, with feed rates ranging from 100-300 mm/minute. This would affect surface quality, as lower RPMs and higher feed rates would make milling grooves further apart and the surface would have a less clean finish.

However, if reducing milling time was desired to increase throughput then a compromise must be met when considering these parameters.

6.3 Alignment of Embossed Features with Milling Coordinates

6.3.1 Embossed Alignment Marks

Alignment of embossed microfluidic features to the coordinates of the milling machine is a precise and important step in the fabrication of a thermoplastic microfluidic device. Embossing a raw thermoplastic material leaves a rough, jagged perimeter after demolding has been performed. This needs to be milled away in order to uniformly bond the device to a thermoplastic backing. If the thermoplastic device is envisioned to be incorporated into a separate machine then dimensions must fit within the tolerances of the machine. Design #1 was designed in such a way that it had a complex device perimeter and additional features that would be incorporated onto its backside, opposite the face where the microfluidic features were embossed. The device perimeter and backside features were necessary incorporations into the design, as they were required for the purpose of interfacing the microfluidic chip directly into a separate machine.

There is the need to provide a method of precise alignment of embossed microfluidic feature to the milling machine coordinates, while also minimizing human error and time required to achieve a high level of alignment. Originally, alignment of microfluidic features on the embossed thermoplastic to the milling machine coordinates was performed by eye. This was a time-consuming and laborious process. This method also

did not provide a consistent alignment from one device to the next, which would not fare well for a manufacturer interested in producing rapid prototyping of thermoplastic microfluidic devices for medium-volume production. There was the need to look into methods of improving alignment precision and accuracy, while also minimizing time required to achieve the desired results. Figure 6.3 shows an image of the alignment marks incorporated directly into the epoxy mold.

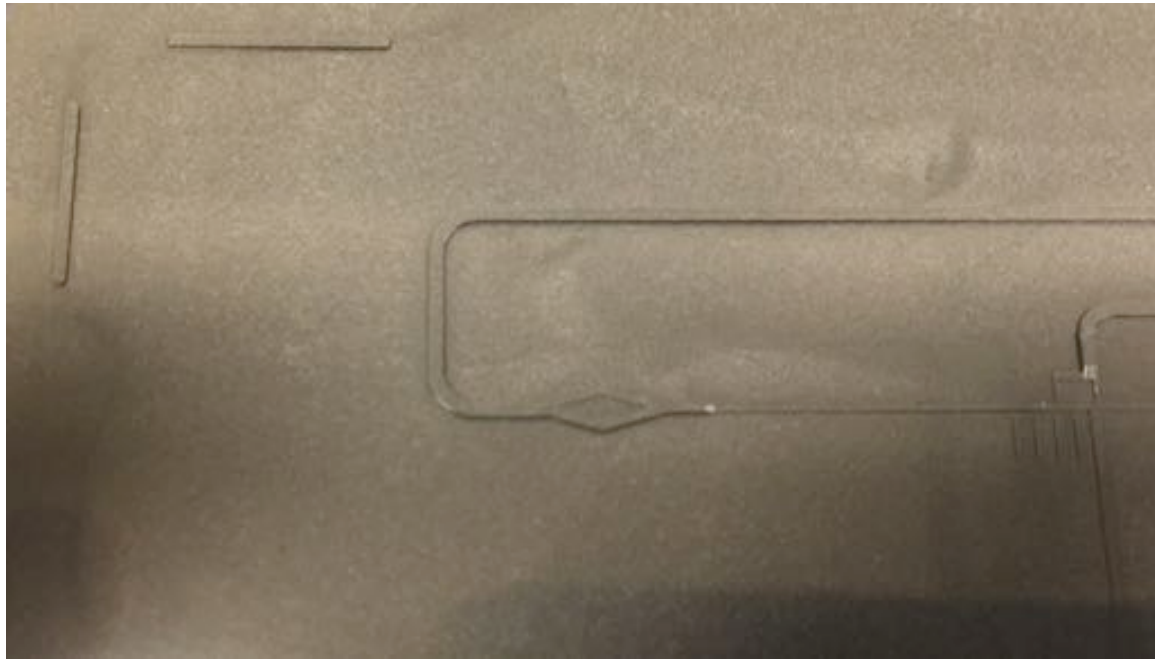


Figure 6.3: Image of alignment marks on the surface of the hot embossing epoxy mold.

Alignment marks were incorporated directly into the microfluidic design that would appear on the surface of the hot embossing epoxy mold. These alignment marks were simply two perpendicular lines with widths of 500 μm that were added to the microfluidic design area of the photolithography mask. The location on the photolithography mask that the alignment marks were added was within the bounds that would eventually lead to their incorporation onto the surface of the epoxy hot embossing mold. The alignment marks were added to the last photolithography mask, photolithography mask #3, in order

to produce alignment marks on the silicon master mold that had feature heights as tall as the tallest features of the microfluidic design. The purpose of choosing the alignment marks to have the tall features, relative to other features on the microfluidic design, was so that they would produce relatively deep trenches after the aluminum-filled epoxy mold had embossed the thermoplastic. Once the embossed thermoplastic had been fabricated, with the incorporation of the two perpendicular alignment marks, this device was brought over to the milling machine.

6.3.2 Precise Alignment of Embossed Features with Milling Coordinates

Precise alignment, with the use of the embossed alignment marks, was achieved on the milling machine by creating a separate milling file that would be applied directly to the sacrificial thermoplastic layer. The sacrificial layer is what the embossed thermoplastic device would be attached to through the use of double-sided tape. A new milling file was created, separate from the file used to incorporate the microfluidic device perimeter and backside features. This milling file, which was applied directly to the sacrificial layer, involved milling a flat rectangular surface and leaving only two positive-relief beams with the same dimensions and relative displacements as those of the alignment marks on the photolithography mask. The milled rectangular surface on the sacrificial layer would have a depth greater than the depth of the embossed alignment mark trenches by 200 μm . The purpose of having the positive-relief beams in the sacrificial layer be 200 μm taller than the trenches of the embossed alignment marks was to account for the thickness of the double-sided tape that would be used to secure the embossed thermoplastic device onto the sacrificial layer. Figure 6.4 shows the embossed thermoplastic material being

directed towards the milled sacrificial layer, with associated positive- and negative-relief alignment marks.

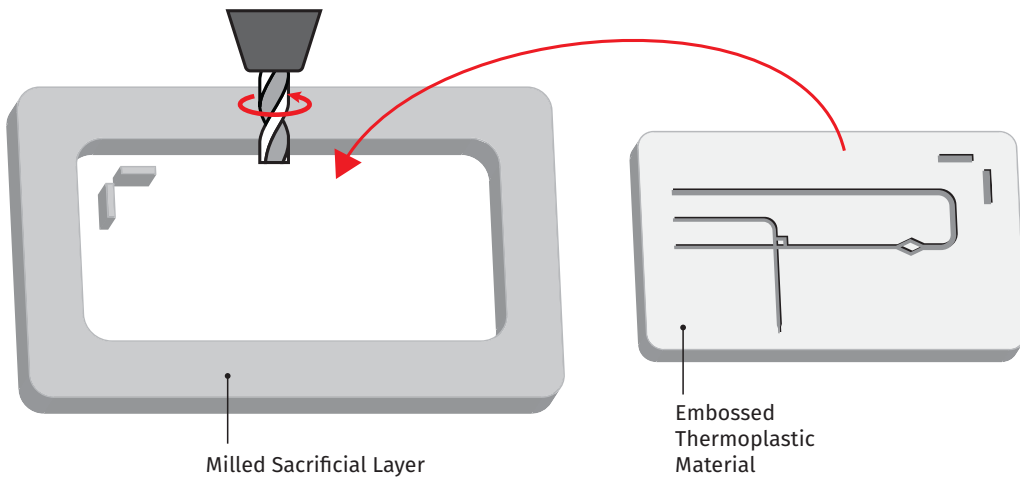


Figure 6.4: Concept of the hot embossed thermoplastic material being transferred to the milled sacrificial layer. The negative-relief embossed alignment marks fit directly onto the positive-relief milled alignment marks in a complementary fashion.

With the incorporation of milling alignment marks directly into the embossed thermoplastic material, and positive-relief alignment beams directly into the thermoplastic sacrificial layer, a much simpler method of alignment was achieved. The alignment marks on the photolithography mask were incorporated in such away that they followed the exact same x-, y- and z- coordinates of the microfluidic features on the photolithography mask. This assured that the alignment marks incorporated on the photolithography mask would account for the coordinates of the microfluidic features, as illustrated in Figure 6.5. The separate milling file that was applied directly to the thermoplastic sacrificial layer surface provided an inherent alignment with the milling machine coordinates. This allowed for rapid alignment between the embossed microfluidic features and the milling coordinates without the need of manual alignment.

This helped to improve accuracy of alignment, precision of alignment and speed of alignment when compared to the previously employed manual alignment method.

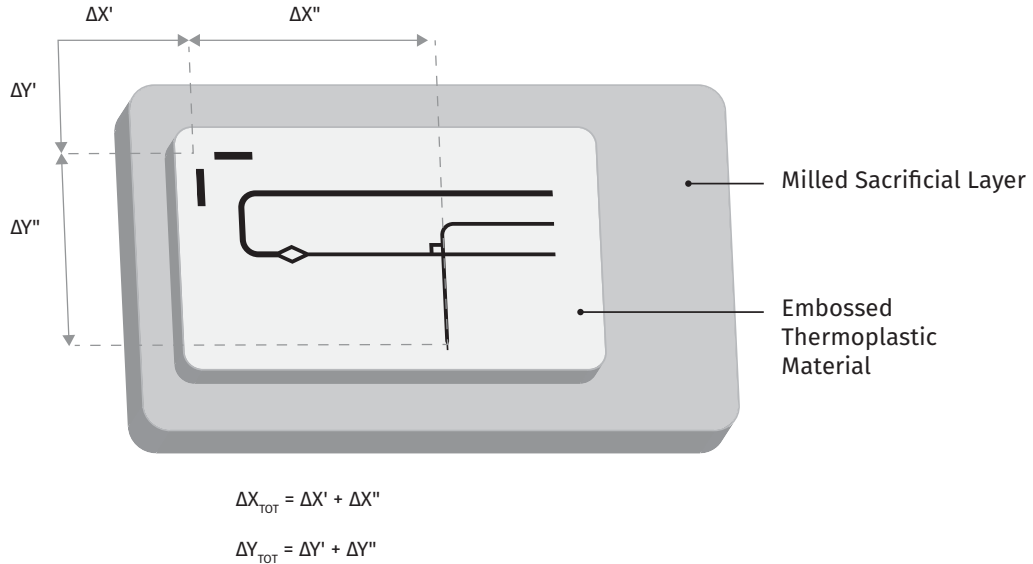


Figure 6.5: Knowledge of the alignment mark coordinates with respect to the milled sacrificial layer origin, and also with respect to the microfluidic features, provided the information necessary to calculate of appropriate zeroing location for milling of backside features.

6.3.3 Tolerance Built into Original Design

Although the incorporation of alignment marks into the embossed thermoplastic material and milling sacrificial layer helps improve the speed and precision when aligning embossed features with milling coordinates, there needs to be secondary precautions taken. Specifically, if there are microfluidic features that have a particularly tight tolerance in terms of the allowable dimensions then there needs to be a safeguard against potential errors in device finalization. One particular example is the “nozzle” microfluidic feature of Design #1, shown in Figure 6.6. The dimensions of this feature

are critical to the device's functionality and must remain within a tight tolerance of the theoretical width and height values of 100 μm each. A deviation in height can only be within 5% of the theoretical value and a deviation in width can only be within the same percentage. When noticing the top-down view of the nozzle geometry and the fact that the device perimeter ends directly at the tip of the nozzle, it becomes apparent that any misalignment or error in the milling protocol can result in a sectioning of the nozzle at an inappropriate location, thus causing the nozzle width dimension to increase beyond the allowable tolerance. One way to circumvent any potential of this negative outcome is to incorporate a "buffer zone" or nozzle extension as a means of protecting this important microfluidic dimension. This was incorporated into the photolithography masks and the nozzle tip was extended by 500 μm . The inclusion of this nozzle extension helped to provide a range of allowable milling coordinates that will mill through the nozzle extension, as opposed to milling through the tapering end of the nozzle itself. This ensured that dimensions at this highly sensitive region would stay within the tolerances required for proper functionality of the microfluidic device. Although this does also inherently produce a range of displacements of the microfluidic features to the device perimeter, along the axis of the nozzle itself, this was limited to the length of the nozzle extension that remains after milling. This remaining length was on the order of 25 μm , which was deemed acceptable. The value could be improved further and would only require a simple re-zeroing of the milling origin by a value of 25 μm in the +y-direction. However, it is imperative that the nozzle remains unscathed during milling and a 25 μm nozzle extension buffer would provide ample room for curtailing any potential of negatively affecting this important microfluidic feature.

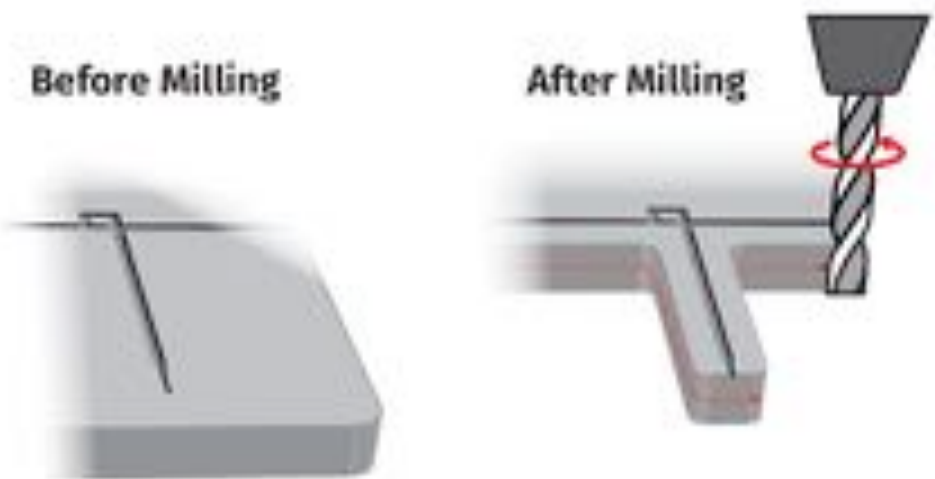


Figure 6.6: Extended nozzle region of the microfluidic design allowed for a buffer when milling was performed in order to assure that the precise cross-sectional dimensions were achieved post-milling.

6.4 Results

The incorporation of embossed alignment features with positive-relief alignment posts, milled directly into the sacrificial substrate layer during milling, improved both the repeatability and throughput capabilities of the post-embossing device milling process. The positive-relief posts that were milled directly into the sacrificial layer were complementary to the embossed alignment marks, which allowed for rapid alignment of embossed features with the milling coordinates. This helped with precision and accuracy, compared to the previously used manual alignment method where embossed features were aligned to the milling machine coordinates by eye. The previously used method had no true safeguard against human error and required an exorbitant amount of time – on the order of 5-15 minutes – to achieve a result that was acceptable. Even with this amount of

time required for alignment, the results were variable. With the use of hot embossed alignment marks and positive-relief alignment marks milled into the sacrificial layer, the time required for alignment was reduced to 10-15 seconds each. The variability seen in the alignment of one chip to the next was on the order of the discrepancy of the width of the embossed alignment features and the width of the positive-relief alignment features of the sacrificial layer. This value remained within the tolerances built into the design and microfluidic features were preserved over the course of multiple runs. Figure 6.7 shows images of the fully fabricated device after milling of additional features has been applied.

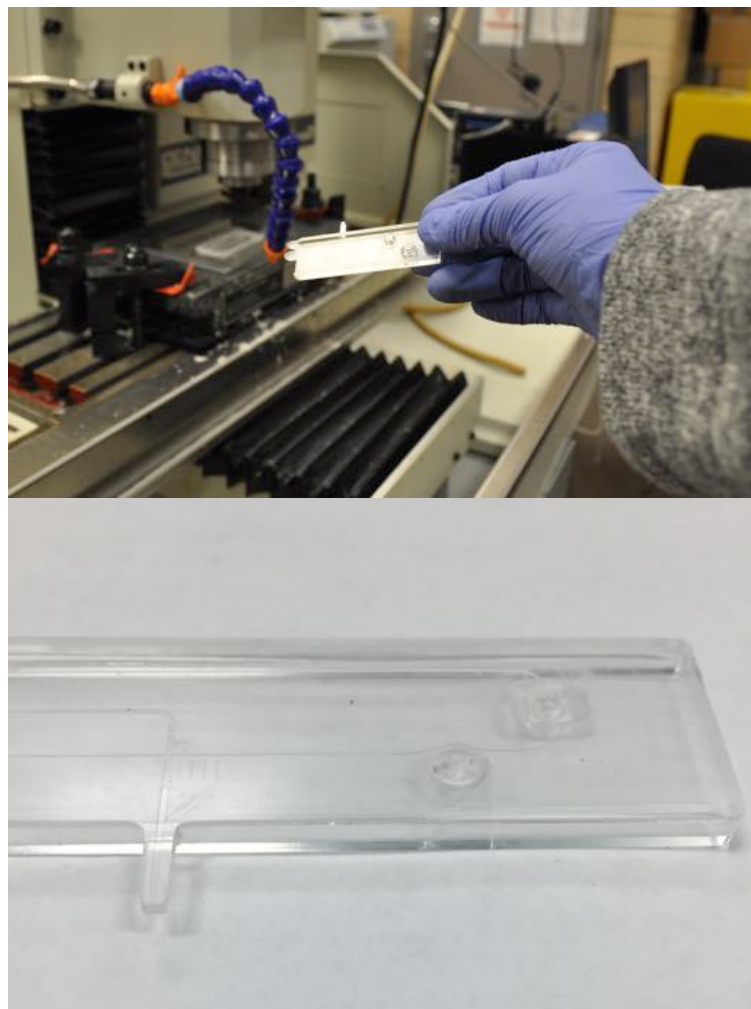


Figure 6.7: Images taken of a finished device that was fabricated through hot embossing of microfluidic features and milling of the device perimeter and additional backside features.

The incorporation of a nozzle extension into the microfluidic design also helped to preserve this feature from being affected during the post-embossing milling procedure. The nozzle extension was milled into as opposed to having the milling being performed directly at the tip of the nozzle, which would have left no room for error. Any variability that was seen in the y-coordinate alignment, caused by a discrepancy in the width of the embossed alignment features and positive-relief alignment features of the sacrificial layer, would affect the length of the nozzle extension that remained but would have no bearing on the nozzle feature's final width. The variability seen in the alignment was on the order of $\pm 50\mu\text{m}$, which fell well within the length of the nozzle extension.

6.5 Milling Throughput Capabilities

Milling throughput capabilities were tested over the course of a 5-day, 40-hour workweek. During this throughput experiment, alignment of hot embossed features was performed with the use of the positive-relief alignment features that were milled directly into the sacrificial layer before post-embossing milling was performed. The hot embossed thermoplastic material was secured to the sacrificial layer with the use of a double-sided tape (Scotch Brand, St. Paul, MN, USA), which provided enough of an adhering force to allow for milling to occur. Once the embossed thermoplastic material was secured onto the sacrificial layer, the endmill was zeroed in the x-, y- and z-direction. The z-direction needed to be re-zeroed with every endmill change during the milling process. In order to provide a consistency from one zeroing to the next, the same x and y

coordinates were used every time the endmill was re-zeroed. There were 5 separate steps of the post-embossing milling program, each with their own specific purpose.

Overall, with the time required to change endmills from one step to the next, the entire milling program took a total of 30.6 minutes on average, with a mode value of 30 minutes. There was an average of ~10-12 minutes required to remove a milled microfluidic device from the milling machine and subsequently secure another embossed thermoplastic material onto the sacrificial layer. Over a 5-day period, 51 milling procedures were run and a total of 51 thermoplastic microfluidic devices were fabricated. Table 6-1 provides the results of the 5-day throughput experiment, including hot embossing and milling times:

Monday							
Device #	Epoxy #	Begin HE	End HE	Δ HE (min)	Begin Mill	End Mill	Δ Mill (min)
1	1	9:00 AM	9:34 AM	34	9:48 AM	10:15 AM	27
2	1	9:37 AM	10:11 AM	34	10:28 AM	10:58 AM	30
3	1	10:15 AM	10:51 AM	36	11:12 AM	11:39 AM	27
4	1	10:55 AM	11:32 AM	37	11:49 AM	12:19 PM	30
5	1	11:36 AM	12:13 PM	37	12:28 PM	12:54 PM	26
6	1	12:18 PM	12:56 PM	38	1:03 PM	1:32 PM	29
7	1	1:06 PM	1:36 PM	30	1:54 PM	2:26 PM	30
8	1	1:39 PM	2:15 PM	36	2:36 PM	3:06 PM	30
9	1	2:19 PM	2:59 PM	40	3:16 PM	3:48 PM	32
10	1	3:03 PM	3:37 PM	34	3:56 PM	4:19 PM	23
11	1	3:43 PM	4:17 PM	34	4:30 PM	4:56 PM	36

Tuesday							
Device #	Epoxy #	Begin HE	End HE	Δ HE (min)	Begin Mill	End Mill	Δ Mill (min)
1	1	9:09 AM	9:47 AM	38	10:22 AM	11:03 AM	41
2	1	9:56 AM	10:32 AM	36	11:10 AM	11:36 AM	26
3	2	10:36 AM	11:15 AM	39	11:42 AM	12:09 PM	27
4	2	11:19 AM	11:58 AM	39	12:17 PM	12:46 PM	29
5	1	12:01 PM	12:41 PM	40	12:53 PM	1:24 PM	31
6	1	12:43 PM	1:18 PM	35	1:38 PM	2:08 PM	30
7	1	1:21 PM	2:04 PM	43	2:20 PM	2:52 PM	32
8	1	2:08 PM	2:41 PM	33	3:00 PM	3:27 PM	27
9	1	2:44 PM	3:22 PM	38	3:34 PM	4:09 PM	35
10	1	3:24 PM	3:59 PM	35	4:15 PM	4:39 PM	24

Wednesday							
Device #	Epoxy #	Begin HE	End HE	Δ HE (min)	Begin Mill	End Mill	Δ Mill (min)
1	2	9:00 AM	9:30 AM	30	9:30 AM	10:00 AM	30
2	2	9:35 AM	9:55 AM	20	10:10 AM	10:46 AM	36
3	2	10:00 AM	10:39 AM	39	10:54 AM	11:40 AM	46
4	2	10:42 AM	11:17 AM	35	11:58 AM	12:28 PM	30
5	2	11:20 AM	11:58 AM	38	12:34 PM	1:03 PM	29
6	2	12:02 PM	12:42 PM	40	1:08 PM	1:39 PM	31
7	2	12:45 PM	1:26 PM	41	2:50 PM	3:18 PM	28
8	2	1:29 PM	2:18 PM	49	3:25 PM	3:52 PM	27
9	2	2:20 PM	3:16 PM	56	3:59 PM	4:27 PM	28
10	2	3:19 PM	3:59 PM	40	4:32 PM	5:00 PM	28

Thursday							
Device #	Epoxy #	Begin HE	End HE	Δ HE (min)	Begin Mill	End Mill	Δ Mill (min)
1	2	9:00 AM	9:35 AM	35	9:36 AM	10:06 AM	30
2	2	9:38 AM	10:03 AM	25	10:12 AM	10:52 AM	30
3	2	10:05 AM	10:45 AM	40	11:00 AM	11:40 AM	40
4	2	10:47 AM	11:15 AM	28	11:58 AM	12:38 PM	30
5	2	11:20 AM	11:54 PM	34	12:44 PM	1:14 PM	30
6	2	12:00 PM	12:36 PM	36	1:20 PM	1:58 PM	38
7	2	12:40 PM	1:14 PM	34	2:20 PM	3:18 PM	38
8	2	1:20 PM	1:52 PM	32	3:22 PM	3:49 PM	27
9	2	2:00 PM	2:36 PM	36	3:59 PM	4:30 PM	31
10	2	2:40 PM	3:15 PM	35	4:36 PM	5:06 PM	30

Friday							
Device #	Epoxy #	Begin HE	End HE	Δ HE (min)	Begin Mill	End Mill	Δ Mill (min)
1	3	9:20 AM	9:59 AM	39	10:05 AM	10:34 AM	29
2	3	10:00 AM	10:36 AM	36	10:46 AM	11:16 AM	30
3	3	10:39 AM	11:11 AM	32	11:24 AM	11:55 AM	31
4	3	11:13 AM	11:57 AM	44	12:10 PM	12:37 PM	27
5	3	12:00 PM	12:35 PM	35	12:45 PM	1:08 PM	23
6	3	12:39 PM	1:15 PM	36	1:12 PM	1:44 PM	32
7	3	1:30 PM	2:06 PM	36	2:10 PM	2:44 PM	34
8	3	2:08 PM	2:40 PM	32	2:50 PM	3:20 PM	30
9	3	2:45 PM	3:10 PM	25	3:24 PM	4:01 PM	37
10	3	3:15 PM	3:50 PM	35	4:10 PM	4:39 PM	29

Table 6-1 Times associated with the beginning and ending of each hot emboss and milling procedure performed throughout the week-long throughput test, as well as the time per each hot emboss and milling procedure.

With the particular milling procedure that was used for this particular microfluidic design, a total of 10 devices could be embossed and milled over an 8-hour workday. This allows for 51 devices to be produced in a week. However, this number could be increased even further with microfluidic designs that require simpler post-embossing milling procedures and the incorporation of multiple microfluidic designs on a single hot embossing mold.

It should also be noted that a quality assurance check was performed on the 51 devices that were fabricated over the course of the 5-day workweek. Out of the 51 devices, 16 did not pass the quality control check and 35 devices did. This showed a success rate of 69%. However, this percentage should be looked at more closely. During the earlier part of the throughput experiment, modifications were being made to the milling process in order to mill the perimeter as close to the theoretical location as possible without milling

directly into the nozzle region of the device. During this early parameter selection period a number of devices were negatively affected as a result. Another issue that was corrected for was with one of the milled alignment features being too wide and not allowing the hot embossed alignment marks to comfortably fit in place. Once this issue was noticed and corrected the embossed alignment features snapped into place in a noticeably more complementary fashion. During the latter half of the throughput experiment, once all milling-related issues were accounted for, the quality control check showed a success rate of 100%. Table 6-2 below provides the number of successful devices produced per day:

Number of Successful Devices Produced Each Day				
Monday	Tuesday	Wednesday	Thursday	Friday
3/11	4/10	7/10	10/10	10/10

Table 6-2 Number of devices produced each day that successfully passed the quality assurance check.

Chapter 7

Conclusion and Future Work

7.1 Conclusion

This chapter is aimed to provide a summary of all work that has been previously discussed as well as potential areas of future work. The entire fabrication process has been broken down into its several components and each area has been studied to provide future researchers and manufacturers an understanding of the requirements necessary to produce high quality thermoplastic microfluidic devices at a medium volume throughput for the purposes of prototyping during research and development.

The first step in the process was the fabrication of a wafer master mold through photolithography processes. Two separate mask aligner systems were studied for their potential to UV expose SU-8 photoresist and align multiple layer features in a precise fashion. The EVG 620 mask aligner provided the potential to align SU-8 features accurately through the use of objective lenses and an alignment stage with an accompanied graphical user interface. Positive draft angles were obtained for SU-8 features through backside photolithography on a Pyrex wafer substrate. These draft angles were tuned to the values seen with injecting molding fabrication processes.

Positive draft angles were required for ease of demolding during hot embossing down stream.

The second step in the fabrication process was the conversion of the wafer master mold into a hot embossing mold made from aluminum-filled epoxy. This was performed through fabrication of a PDMS negative-relief feature mold through soft lithography and subsequent pouring of aluminum-filled epoxy over the PDMS features. Improvements were made to the epoxy mold fabrication process through the development of an epoxy mold fabrication jig, which ensured that uniformly thick epoxy molds with consistent dimensions could be produced from one epoxy mold fabrication to the next. Bubbles trapped within the bulk of the epoxy material was also eliminated through the introduction of an additional centrifugation step prior to the pouring of epoxy over the PDMS negative-relief feature mold. Additional features were incorporated into the epoxy mold after it was hardened through micromilling techniques. This allowed microfluidic designs to incorporate ramps from one feature height to another, which is not attainable through photolithography with SU-8 negative photoresist.

The third step of the fabrication process was the hot embossing of a thermoplastic material with the previously fabricated hot embossing epoxy mold. Hot embossing was performed on the thermoplastics PMMA and COP. Hot embossing was tested on two separate hot embossing machines, which were the Carver Press and the EVG 520HE. A characterization of embossing quality was performed for both thermoplastic materials on both hot embossing machines by testing different embossing parameters including

temperature, applied force and dwell time. Cross-sectional image analysis was performed and a fidelity of feature transfer was attained between the epoxy mold and the embossed thermoplastic cross-sectional features. Ease of demolding was looked into and it was found that a combination of positive draft angle features with surface coating, using the Weicon releasing agent, provided the greatest ease of demolding between the embossed thermoplastic and epoxy mold. Epoxy mold deformation was also studied by applying hot embossing conditions at the upper limit of those used for thermoplastic device fabrication and analyzing changes seen in the epoxy mold dimensions. No epoxy mold deformation was noticed under embossing conditions of 170°C and 6000 lbf. Hot embossing was performed using a silicon wafer with SU-8 features as a hot embossing mold. This was studied as a comparison between silicon wafer hot embossing molds and aluminum-filled epoxy hot embossing molds. Given the time and complexity associated with the fabrication of wafer master molds within tight tolerances, epoxy hot embossing molds were viewed as a better option. Epoxy hot embossing molds can also be produced from a single silicon wafer, which assured consisted feature dimensions from one hot embossing mold to the next while also preserving the wafer master mold. Hot embossing throughput was also studied, noting an average hot embossing time of 30 minutes for the Carver Press and 45 minutes for the EVG 520HE.

The last step in the process was the milling of the embossed thermoplastic microfluidic device perimeter. A method for improving the accuracy of alignment between milling coordinates and hot embossed features was studied. This required the incorporation of alignment marks into the hot embossing epoxy mold, which directly transferred into the

thermoplastic material. These negative-relief feature channels could be used to mount directly onto the milling machine where a milling alignment jig was developed for quick accurate alignment. Positive-relief features on the milling alignment jig were fitted into the negative-relief feature alignment marks on the embossed thermoplastic and this provided immediately alignment between milling coordinate and embossed feature coordinates. In order to help preserve the embossed feature channel dimensions, during the post-emboss milled step, tolerances were built directly into the microfluidic design. This ensured that areas of particular interest in the microfluidic design had their features preserved. Milling throughput capabilities was also studied to identify how many milling runs could be performed in a day. The milling of the first device design studied was performed over 30 minutes per device. This was the most complex post-emboss milling code employed and all other milling times would scale according to the complexity of the associated G-code. The largest time associated with milling was the alignment between milling coordinates and hot embossed feature coordinates, which was addressed through the development of the milling alignment jig.

7.2 Summary

A study was performed on the throughput capabilities of thermoplastic microfluidic device fabrication. Multiple improvements were made throughout the process. These included:

1. Positive draft angles on SU-8 features through backside lithography with a Pyrex wafer
2. Optimization of hot embossing epoxy mold fabrication process
3. Characterization of hot embossing parameters for PMMA and COP feature transfer fidelity on the Carver Press and EVG 520HE hot embossing machines
4. Precise milling of additional features post-hot embossing with the use of a milling alignment jig
5. Volume throughput analysis of a multi-layer microfluidic device prototype through hot embossing and milling techniques

With these improvements and a detailed focus on the fabrication process from start to finish, rapid prototyping of thermoplastic microfluidic devices can be achieved for complex, multi-feature designs. Rapid prototyping will help to provide companies interested in mass-producing microfluidic technology with a means to test their devices in an accurate fashion during the iterative design stage of research and development. With the ability to produce at least 50 microfluidic devices in a week, there is the potential to have quick turnaround time from the device design to the testing of its functions. This is a necessary advancement to consider in its applicability. This rapid prototyping of thermoplastic microfluidic devices is extendable to a number of designs. To date, this process has been applied to three separate designs for research groups working in Bio-Rad Laboratories.

7.3 Future work

The work presented has provided a methodology for rapid prototyping of thermoplastic microfluidic devices, which can be extended further to include future areas of research and improvement. These areas of future work include:

1. Looking into the potential for applying epoxy mold fabrication to produce parts specifically for injection molding fabrication of microfluidic devices
2. Extending a characterization of hot embossing parameters to include different thermoplastic materials for a more complete understanding of conditions required for high fidelity transfer for a wider array of materials
3. Use the methodologies described previously to produce a streamlined fabrication process for prototyped modular, reconfigurable microfluidic devices
4. Design and implementation of a more consistent and repeatable wafer master mold fabrication process, particularly when spinning layers of SU-8 photoresist to a specific feature height within a tight tolerance
5. Precise alignment and bonding of two separately hot embossed thermoplastic devices with distinct features to produce a more complex microfluidic design

References

- [1] E. W. K. Young and C. A. Simmons, “Macro- and microscale fluid flow systems for endothelial cell biology.,” *Lab Chip*, vol. 10, no. 2, pp. 143–60, Jan. 2010.
- [2] L. L. Bischel, E. W. K. Young, B. R. Mader, and D. J. Beebe, “Biomaterials Tubeless micro fluidic angiogenesis assay with three-dimensional endothelial-lined microvessels,” vol. 34, 2013.
- [3] P. Neuži, S. Giselbrecht, K. Länge, T. J. Huang, and A. Manz, “Revisiting lab-on-a-chip technology for drug discovery,” *Nat. Rev. Drug Discov.*, vol. 11, no. 8, pp. 620–632, 2012.
- [4] E. W. K. Young, E. Berthier, D. J. Guckenberger, E. Sackmann, C. Lamers, I. Meyvantsson, A. Huttenlocher, and D. J. Beebe, “Rapid prototyping of arrayed microfluidic systems in polystyrene for cell-based assays,” *Anal. Chem.*, vol. 83, no. 4, pp. 1408–1417, 2011.
- [5] S. M. Langelier, E. Livak-Dahl, A. J. Manzo, B. N. Johnson, N. G. Walter, and M. a Burns, “Flexible casting of modular self-aligning microfluidic assembly blocks.,” *Lab Chip*, vol. 11, no. 9, pp. 1679–1687, 2011.
- [6] D. C. Duffy, J. C. McDonald, O. J. A. Schueller, and G. M. Whitesides, “Rapid Prototyping of Microfluidic Systems in Poly(dimethylsiloxane),” *Anal. Chem.*, vol. 70, no. 23, pp. 4974–4984, Dec. 1998.
- [7] K. Chung, Y. Kim, J. S. Kanodia, E. Gong, S. Y. Shvartsman, and H. Lu, “A microfluidic array for large-scale ordering and orientation of embryos.,” *Nat. Methods*, vol. 8, no. 2, pp. 171–6, Feb. 2011.
- [8] J. L. Tan, J. Tien, D. M. Pirone, D. S. Gray, K. Bhadriraju, and C. S. Chen, “Cells lying on a bed of microneedles: an approach to isolate mechanical force.,” *Proc. Natl. Acad. Sci. U. S. A.*, vol. 100, no. 4, pp. 1484–9, Feb. 2003.
- [9] M. Murrell, R. Kamm, and P. Matsudaira, “Substrate viscosity enhances correlation in epithelial sheet movement.,” *Biophys. J.*, vol. 101, no. 2, pp. 297–306, Jul. 2011.
- [10] C. Moraes, J.-H. Chen, Y. Sun, and C. A. Simmons, “Microfabricated arrays for high-throughput screening of cellular response to cyclic substrate deformation.,” *Lab Chip*, vol. 10, no. 2, pp. 227–34, Jan. 2010.

- [11] G. Mehta, J. Lee, W. Cha, Y.-C. Tung, J. J. Linderman, and S. Takayama, “Hard top soft bottom microfluidic devices for cell culture and chemical analysis.,” *Anal. Chem.*, vol. 81, no. 10, pp. 3714–22, May 2009.
- [12] J. Friend and L. Yeo, “Fabrication of microfluidic devices using polydimethylsiloxane,” *Biomicrofluidics*, vol. 4, no. 2, pp. 1–5, 2010.
- [13] J. M. K. NG, I. GITLIN, A. D. STROOCK, and G. M. WHITESIDES, “Components for integrated poly(dimethylsiloxane) microfluidic systems,” *Electrophoresis*, vol. 23, no. 20, pp. 3461–3473.
- [14] J. Wu, W. Cao, W. Wen, D. C. Chang, and P. Sheng, “Polydimethylsiloxane microfluidic chip with integrated microheater and thermal sensor.,” *Biomicrofluidics*, vol. 3, no. 1, p. 12005, Jan. 2009.
- [15] S. A. Vanapalli, M. H. G. Duits, and F. Mugele, “Microfluidics as a functional tool for cell mechanics.,” *Biomicrofluidics*, vol. 3, no. 1, p. 12006, Jan. 2009.
- [16] D. W. Trahan and P. S. Doyle, “Simulation of electrophoretic stretching of DNA in a microcontraction using an obstacle array for conformational preconditioning.,” *Biomicrofluidics*, vol. 3, no. 1, p. 12803, Jan. 2009.
- [17] D. Luo, S. R. Pullela, M. Marquez, and Z. Cheng, “Cell encapsules with tunable transport and mechanical properties.,” *Biomicrofluidics*, vol. 1, no. 3, p. 34102, Jan. 2007.
- [18] W. Y. Ng, Y. C. Lam, and I. Rodríguez, “Experimental verification of Faradaic charging in ac electrokinetics.,” *Biomicrofluidics*, vol. 3, no. 2, p. 22405, Jan. 2009.
- [19] N. Lewpiriyawong, C. Yang, and Y. C. Lam, “Dielectrophoretic manipulation of particles in a modified microfluidic H filter with multi-insulating blocks.,” *Biomicrofluidics*, vol. 2, no. 3, p. 34105, Jan. 2008.
- [20] L. Liu, W. Cao, J. Wu, W. Wen, D. C. Chang, and P. Sheng, “Design and integration of an all-in-one biomicrofluidic chip.,” *Biomicrofluidics*, vol. 2, no. 3, p. 34103, Jan. 2008.
- [21] W. Ebina, A. C. Rowat, and D. A. Weitz, “Electrodes on a budget: Micropatterned electrode fabrication by wet chemical deposition.,” *Biomicrofluidics*, vol. 3, no. 3, p. 34104, Jan. 2009.
- [22] Y. Srivastava, M. Marquez, and T. Thorsen, “Microfluidic electrospinning of biphasic nanofibers with Janus morphology.,” *Biomicrofluidics*, vol. 3, no. 1, p. 12801, Jan. 2009.

- [23] X. Gong and W. Wen, “Polydimethylsiloxane-based conducting composites and their applications in microfluidic chip fabrication.,” *Biomicrofluidics*, vol. 3, no. 1, p. 12007, Jan. 2009.
- [24] S. K. Das, S. Chung, I. Zervantonakis, J. Atnafu, and R. D. Kamm, “A microfluidic platform for studying the effects of small temperature gradients in an incubator environment.,” *Biomicrofluidics*, vol. 2, no. 3, p. 34106, Jan. 2008.
- [25] A. Martel, M. Burghammer, R. Davies, E. Dicola, P. Panine, J.-B. Salmon, and C. Riekel, “A microfluidic cell for studying the formation of regenerated silk by synchrotron radiation small- and wide-angle X-ray scattering.,” *Biomicrofluidics*, vol. 2, no. 2, p. 24104, Jan. 2008.
- [26] N. Koo, M. Bender, U. Plachetka, A. Fuchs, T. Wahlbrink, J. Bolten, and H. Kurz, “Improved mold fabrication for the definition of high quality nanopatterns by Soft UV-Nanoimprint lithography using diluted PDMS material,” *Microelectron. Eng.*, vol. 84, no. 5–8, pp. 904–908, May 2007.
- [27] Y. Xia and G. M. Whitesides, “SOFT LITHOGRAPHY,” *Annu. Rev. Mater. Sci.*, vol. 28, no. 1, pp. 153–184, Aug. 1998.
- [28] E. Berthier, E. W. K. Young, and D. Beebe, “Engineers are from PDMS-land, Biologists are from Polystyrenia,” *Lab Chip*, vol. 12, no. 7, p. 1224, 2012.
- [29] J. S. Kuo and D. T. Chiu, “Disposable microfluidic substrates: transitioning from the research laboratory into the clinic.,” *Lab Chip*, vol. 11, no. 16, pp. 2656–65, Aug. 2011.
- [30] V. N. Goral, Y.-C. Hsieh, O. N. Petzold, R. A. Faris, and P. K. Yuen, “Hot embossing of plastic microfluidic devices using poly(dimethylsiloxane) molds,” *J. Micromechanics Microengineering*, vol. 21, no. 1, p. 017002, Jan. 2011.
- [31] D. J. Guckenberger, T. de Groot, A. M.-D. Wan, D. Beebe, and E. Young, “Micromilling: A method for ultra-rapid prototyping of plastic microfluidic devices,” *Lab Chip*, 2015.
- [32] a. Mathur, S. S. Roy, M. Tweedie, S. Mukhopadhyay, S. K. Mitra, and J. a. McLaughlin, “Characterisation of PMMA microfluidic channels and devices fabricated by hot embossing and sealed by direct bonding,” *Curr. Appl. Phys.*, vol. 9, no. 6, pp. 1199–1202, 2009.
- [33] J. Narasimhan and I. Papautsky, “Polymer embossing tools for rapid prototyping of plastic microfluidic devices,” *J. Micromechanics Microengineering*, vol. 14, no. 1, pp. 96–103, 2003.

- [34] H. Klank, J. P. Kutter, and O. Geschke, “CO(2)-laser micromachining and back-end processing for rapid production of PMMA-based microfluidic systems.,” *Lab Chip*, vol. 2, no. 4, pp. 242–6, Nov. 2002.
- [35] M. B. Wabuyele, S. M. Ford, W. Stryjewski, J. Barrow, and S. A. Soper, “Single molecule detection of double-stranded DNA in poly(methylmethacrylate) and polycarbonate microfluidic devices.,” *Electrophoresis*, vol. 22, no. 18, pp. 3939–48, Oct. 2001.
- [36] K. Lee and D. A. Dornfeld, “Micro-burr formation and minimization through process control,” *Precis. Eng.*, vol. 29, no. 2, pp. 246–252, Apr. 2005.
- [37] J. Steigert, S. Haeberle, T. Brenner, C. Müller, C. P. Steinert, P. Koltay, N. Gottschlich, H. Reinecke, J. Rühe, R. Zengerle, and J. Ducrée, “Rapid prototyping of microfluidic chips in COC,” *J. Micromechanics Microengineering*, vol. 17, no. 2, pp. 333–341, 2007.
- [38] J. S. Jeon, S. Chung, R. D. Kamm, and J. L. Charest, “Hot embossing for fabrication of a microfluidic 3D cell culture platform.,” *Biomed. Microdevices*, vol. 13, no. 2, pp. 325–33, Apr. 2011.
- [39] C. W. Tsao and D. L. DeVoe, “Bonding of thermoplastic polymer microfluidics,” *Microfluid. Nanofluidics*, vol. 6, no. 1, pp. 1–16, 2009.
- [40] P. W. Leech, “Hot embossing of cyclic olefin copolymers,” *J. Micromechanics Microengineering*, vol. 19, no. 5, p. 055008, May 2009.
- [41] K. R. Hawkins and P. Yager, “Nonlinear decrease of background fluorescence in polymer thin-films - a survey of materials and how they can complicate fluorescence detection in microTAS.,” *Lab Chip*, vol. 3, no. 4, pp. 248–52, Nov. 2003.
- [42] A. Piruska, I. Nikcevic, S. H. Lee, C. Ahn, W. R. Heineman, P. A. Limbach, and C. J. Seliskar, “The autofluorescence of plastic materials and chips measured under laser irradiation.,” *Lab Chip*, vol. 5, no. 12, pp. 1348–54, Dec. 2005.
- [43] G. A. Diaz-Quijada, R. Peytavi, A. Nantel, E. Roy, M. G. Bergeron, M. M. Dumoulin, and T. Veres, “Surface modification of thermoplastics--towards the plastic biochip for high throughput screening devices.,” *Lab Chip*, vol. 7, no. 7, pp. 856–62, Jul. 2007.
- [44] T. Gervais, J. El-Ali, A. Günther, and K. F. Jensen, “Flow-induced deformation of shallow microfluidic channels.,” *Lab Chip*, vol. 6, no. 4, pp. 500–7, Apr. 2006.

- [45] J. Y. Park, S. J. Yoo, E.-J. Lee, D. H. Lee, J. Y. Kim, and S.-H. Lee, “Increased poly(dimethylsiloxane) stiffness improves viability and morphology of mouse fibroblast cells,” *BioChip J.*, vol. 4, no. 3, pp. 230–236, Sep. 2010.
- [46] Y. S. Heo, L. M. Cabrera, J. W. Song, N. Futai, Y.-C. Tung, G. D. Smith, and S. Takayama, “Characterization and resolution of evaporation-mediated osmolality shifts that constrain microfluidic cell culture in poly(dimethylsiloxane) devices.,” *Anal. Chem.*, vol. 79, no. 3, pp. 1126–34, Feb. 2007.
- [47] Y. Zhang, M. Ishida, Y. Kazoe, Y. Sato, and N. Miki, “Water-vapor permeability control of PDMS by the dispersion of collagen powder,” *IEEJ Trans. Electr. Electron. Eng.*, vol. 4, no. 3, pp. 442–449, May 2009.
- [48] W. D. Niles and P. J. Coassini, “Cyclic olefin polymers: innovative materials for high-density multiwell plates.,” *Assay Drug Dev. Technol.*, vol. 6, no. 4, pp. 577–90, Aug. 2008.
- [49] H. Shiku, T. Saito, C.-C. Wu, T. Yasukawa, M. Yokoo, H. Abe, T. Matsue, and H. Yamada, “Oxygen Permeability of Surface-modified Poly(dimethylsiloxane) Characterized by Scanning Electrochemical Microscopy,” *Chem. Lett.*, vol. 35, no. 2, pp. 234–235, Jan. 2006.
- [50] S. G. Charati and S. A. Stern, “Diffusion of Gases in Silicone Polymers: Molecular Dynamics Simulations,” *Macromolecules*, vol. 31, no. 16, pp. 5529–5535, Aug. 1998.
- [51] M. W. Toepke and D. J. Beebe, “PDMS absorption of small molecules and consequences in microfluidic applications.,” *Lab Chip*, vol. 6, no. 12, pp. 1484–6, Dec. 2006.
- [52] K. J. Regehr, M. Domenech, J. T. Koepsel, K. C. Carver, S. J. Ellison-Zelski, W. L. Murphy, L. A. Schuler, E. T. Alarid, and D. J. Beebe, “Biological implications of polydimethylsiloxane-based microfluidic cell culture.,” *Lab Chip*, vol. 9, no. 15, pp. 2132–9, Aug. 2009.
- [53] J. N. Lee, C. Park, and G. M. Whitesides, “Solvent compatibility of poly(dimethylsiloxane)-based microfluidic devices.,” *Anal. Chem.*, vol. 75, no. 23, pp. 6544–54, Dec. 2003.
- [54] D. T. Eddington, J. P. Puccinelli, and D. J. Beebe, “Thermal aging and reduced hydrophobic recovery of polydimethylsiloxane,” *Sensors Actuators B Chem.*, vol. 114, no. 1, pp. 170–172, Mar. 2006.
- [55] H. Becker, “It’s the economy...,” *Lab Chip*, vol. 9, no. 19, pp. 2759–62, Oct. 2009.

- [56] J. M. Shaw, J. D. Gelorme, N. C. LaBianca, W. E. Conley, and S. J. Holmes, “Negative photoresists for optical lithography,” *IBM J. Res. Dev.*, vol. 41, no. 1.2, pp. 81–94, 1997.
- [57] a Del Campo and C. Greiner, “SU-8: a photoresist for high-aspect-ratio and 3D submicron lithography,” *J. Micromechanics Microengineering*, vol. 17, no. 6, pp. R81–R95, 2007.
- [58] G. C. Lisenky, D. J. Campbell, K. J. Beckman, C. E. Calderon, P. W. Doolan, and A. B. Ellis, “Replication and Compression of Surface Structures with Polydimethylsiloxane Elastomer,” *J. Chem. Educ.*, vol. 76, no. 4, p. 537, Apr. 1999.
- [59] J. D. Mackenzie, Q. Huang, and T. Iwamoto, “Mechanical properties of ormosils,” *J. Sol-Gel Sci. Technol.*, vol. 7, no. 3, pp. 151–161, 1996.
- [60] Y. J. Jung, S. Kar, S. Talapatra, C. Soldano, G. Viswanathan, X. Li, Z. Yao, F. S. Ou, A. Avadhanula, R. Vajtai, S. Curran, O. Nalamasu, and P. M. Ajayan, “Aligned carbon nanotube-polymer hybrid architectures for diverse flexible electronic applications.,” *Nano Lett.*, vol. 6, no. 3, pp. 413–8, Mar. 2006.
- [61] L. Chen, P. Degenaar, and D. D. C. Bradley, “Polymer Transfer Printing: Application to Layer Coating, Pattern Definition, and Diode Dark Current Blocking,” *Adv. Mater.*, vol. 20, no. 9, pp. 1679–1683, May 2008.
- [62] H. Becker and U. Heim, “Hot embossing as a method for the fabrication of polymer high aspect ratio structures,” *Sensors Actuators A Phys.*, vol. 83, no. 1–3, pp. 130–135, May 2000.
- [63] R. K. Jena, C. Y. Yue, Y. C. Lam, P. S. Tang, and a. Gupta, “Comparison of different molds (epoxy, polymer and silicon) for microfabrication by hot embossing technique,” *Sensors Actuators, B Chem.*, vol. 163, no. 1, pp. 233–241, 2012.
- [64] D. Nilsson, S. Jensen, and A. Menon, “Fabrication of silicon molds for polymer optics,” *J. Micromechanics Microengineering*, vol. 13, no. 4, pp. S57–S61, Jul. 2003.
- [65] G. S. Fiorini, G. D. M. Jeffries, D. S. W. Lim, C. L. Kuyper, and D. T. Chiu, “Fabrication of thermoset polyester microfluidic devices and embossing masters using rapid prototyped polydimethylsiloxane molds.,” *Lab Chip*, vol. 3, no. 3, pp. 158–63, Aug. 2003.
- [66] H. Mizuno, O. Sugihara, T. Kaino, N. Okamoto, and M. Hosino, “Low-loss polymeric optical waveguides with large cores fabricated by hot embossing,” *Opt. Lett.*, vol. 28, no. 23, p. 2378, Dec. 2003.

- [67] S. Belligundu, “Study on two-stage hot embossing microreplication: silicon to polymer to polymer,” *J. Micro/Nanolithography, MEMS, MOEMS*, vol. 5, no. 2, p. 021103, Apr. 2006.
- [68] L. Martynova, L. E. Locascio, M. Gaitan, G. W. Kramer, R. G. Christensen, and W. A. MacCrehan, “Fabrication of Plastic Microfluid Channels by Imprinting Methods,” *Anal. Chem.*, vol. 69, no. 23, pp. 4783–4789, Dec. 1997.
- [69] L. Brown, T. Koerner, J. H. Horton, and R. D. Oleschuk, “Fabrication and characterization of poly(methylmethacrylate) microfluidic devices bonded using surface modifications and solvents.,” *Lab Chip*, vol. 6, no. 1, pp. 66–73, Jan. 2006.
- [70] R. Woodbury, “History of the Milling Machine: A Study in Technical Development,” 1960.
- [71] F.-C. Huang, Y.-F. Chen, and G.-B. Lee, “CE chips fabricated by injection molding and polyethylene/thermoplastic elastomer film packaging methods.,” *Electrophoresis*, vol. 28, no. 7, pp. 1130–7, Apr. 2007.
- [72] M. A. Roberts, J. S. Rossier, P. Bercier, and H. Girault, “UV Laser Machined Polymer Substrates for the Development of Microdiagnostic Systems.,” *Anal. Chem.*, vol. 69, no. 11, pp. 2035–42, Jun. 1997.
- [73] C.-W. Tsao, J. Liu, and D. L. DeVoe, “Droplet formation from hydrodynamically coupled capillaries for parallel microfluidic contact spotting,” *J. Micromechanics Microengineering*, vol. 18, no. 2, p. 025013, Feb. 2008.
- [74] C. H. Ahn, J.-W. Choi, G. Beauchage, J. Nevin, J.-B. Lee, A. Puntambekar, and R. J. Y. Lee, “Disposable Smart Lab on a Chip for Point-of-Care Clinical Diagnostics,” *Proc. IEEE*, vol. 92, no. 1, pp. 154–173, Jan. 2004.
- [75] A. Bhattacharyya and C. M. Klapperich, “Thermoplastic microfluidic device for on-chip purification of nucleic acids for disposable diagnostics.,” *Anal. Chem.*, vol. 78, no. 3, pp. 788–92, Feb. 2006.
- [76] L. Rieger, M. Grumann, J. Steigert, S. Lutz, C. P. Steinert, C. Mueller, J. Viertel, O. Prucker, J. Rühe, R. Zengerle, and J. Ducrée, “Single-step centrifugal hematocrit determination on a 10-\$ processing device.,” *Biomed. Microdevices*, vol. 9, no. 6, pp. 795–9, Dec. 2007.
- [77] C. K. Fredrickson, Z. Xia, C. Das, R. Ferguson, F. T. Tavares, and Z. H. Fan, “Effects of Fabrication Process Parameters on the Properties of Cyclic Olefin Copolymer Microfluidic Devices,” *J. Microelectromechanical Syst.*, vol. 15, no. 5, pp. 1060–1068, Oct. 2006.

- [78] C.-W. Tsao and D. L. DeVoe, “Bonding of thermoplastic polymer microfluidics,” *Microfluid. Nanofluidics*, vol. 6, no. 1, pp. 1–16, Nov. 2008.
- [79] B. D. Gates, Q. Xu, M. Stewart, D. Ryan, C. G. Willson, and G. M. Whitesides, “New approaches to nanofabrication: molding, printing, and other techniques.,” *Chem. Rev.*, vol. 105, no. 4, pp. 1171–96, Apr. 2005.
- [80] B. D. Gates, Q. Xu, J. C. Love, D. B. Wolfe, and G. M. Whitesides, “UNCONVENTIONAL NANOFABRICATION,” *Annu. Rev. Mater. Res.*, vol. 34, no. 1, pp. 339–372, Aug. 2004.
- [81] G. M. Wallraff and W. D. Hinsberg, “Lithographic Imaging Techniques for the Formation of Nanoscopic Features,” *Chem. Rev.*, vol. 99, no. 7, pp. 1801–1822, Jul. 1999.
- [82] M. Rothschild, “Projection optical lithography,” *Mater. Today*, vol. 8, no. 2, pp. 18–24, Feb. 2005.
- [83] T. A. Brunner, “Why optical lithography will live forever,” *J. Vac. Sci. Technol. B Microelectron. Nanom. Struct.*, vol. 21, no. 6, p. 2632, Dec. 2003.
- [84] T. Ito and S. Okazaki, “Pushing the limits of lithography,” *Nature*, vol. 406, no. 6799, pp. 1027–31, Aug. 2000.
- [85] C. Grant Willson and B. C. Trinque, “The Evolution of Materials for the Photolithographic Process,” *J. Photopolym. Sci. Technol.*, vol. 16, no. 4, pp. 621–627, 2003.
- [86] M. Rothschild, T. M. Bloomstein, R. R. Kunz, V. Liberman, M. Switkes, S. T. Palmacci, J. H. C. Sedlacek, D. Hardy, and A. Grenville, “Liquid immersion lithography: Why, how, and when?,” *J. Vac. Sci. Technol. B Microelectron. Nanom. Struct.*, vol. 22, no. 6, p. 2877, Dec. 2004.
- [87] D. Gil, T. A. Brunner, C. Fonseca, N. Seong, B. Streefkerk, C. Wagner, and M. Stavenga, “Immersion lithography: New opportunities for semiconductor manufacturing,” *J. Vac. Sci. Technol. B Microelectron. Nanom. Struct.*, vol. 22, no. 6, p. 3431, Dec. 2004.
- [88] K. KUWABARA, “Fluorescence measurements of nanopillars fabricated by high-aspect-ratio nanoprint technology,” *Microelectron. Eng.*, vol. 73–74, pp. 752–756, Jun. 2004.
- [89] E. Delamarche, D. Juncker, and H. Schmid, “Microfluidics for processing surfaces and miniaturizing biological assays,” *Adv. Mater.*, 2005.

- [90] M. A. Burns, “An Integrated Nanoliter DNA Analysis Device,” *Science* (80-.), vol. 282, no. 5388, pp. 484–487, Oct. 1998.
- [91] P. F. Wagler, U. Tangen, T. Maeke, H. P. Mathis, and J. S. McCaskill, “Microfabrication of a BioModule composed of microfluidics and digitally controlled microelectrodes for processing biomolecules,” *Smart Mater. Struct.*, vol. 12, no. 5, pp. 757–762, Oct. 2003.
- [92] T. Thorsen, S. J. Maerkl, and S. R. Quake, “Microfluidic large-scale integration.,” *Science*, vol. 298, no. 5593, pp. 580–4, Oct. 2002.
- [93] F. ROMANATO, “X-ray lithography for 3D microfluidic applications,” *Microelectron. Eng.*, vol. 73–74, pp. 870–875, Jun. 2004.
- [94] F. Pérennès, B. Marmiroli, M. Matteucci, M. Tormen, L. Vaccari, and E. Di Fabrizio, “Sharp beveled tip hollow microneedle arrays fabricated by LIGA and 3D soft lithography with polyvinyl alcohol,” *J. Micromechanics Microengineering*, vol. 16, no. 3, pp. 473–479, Mar. 2006.
- [95] R. A. Brown, M. Wiseman, C.-B. Chuo, U. Cheema, and S. N. Nazhat, “Ultrarapid Engineering of Biomimetic Materials and Tissues: Fabrication of Nano- and Microstructures by Plastic Compression,” *Adv. Funct. Mater.*, vol. 15, no. 11, pp. 1762–1770, Nov. 2005.
- [96] V. K. Popov, A. V. Evseev, A. L. Ivanov, V. V. Roginski, A. I. Volozhin, and S. M. Howdle, “Laser stereolithography and supercritical fluid processing for custom-designed implant fabrication,” *J. Mater. Sci. Mater. Med.*, vol. 15, no. 2, pp. 123–128, Feb. 2004.
- [97] Y. Liu, S. Sun, S. Singha, M. R. Cho, and R. J. Gordon, “3D femtosecond laser patterning of collagen for directed cell attachment.,” *Biomaterials*, vol. 26, no. 22, pp. 4597–605, Aug. 2005.
- [98] H. Kusakabe, T. Sakamaki, K. Nihei, Y. Oyama, S. Yanagimoto, M. Ichimiya, J. Kimura, and Y. Toyama, “Osseointegration of a hydroxyapatite-coated multilayered mesh stem.,” *Biomaterials*, vol. 25, no. 15, pp. 2957–69, Jul. 2004.
- [99] M. E. Hoque, D. W. Hutmacher, W. Feng, S. Li, M.-H. Huang, M. Vert, and Y. S. Wong, “Fabrication using a rapid prototyping system and in vitro characterization of PEG-PCL-PLA scaffolds for tissue engineering,” *J. Biomater. Sci. Polym. Ed.*, vol. 16, no. 12, pp. 1595–1610, Jan. 2005.
- [100] M. Martina, G. Subramanyam, J. C. Weaver, D. W. Hutmacher, D. E. Morse, and S. Valiyaveettil, “Developing macroporous bicontinuous materials as scaffolds for tissue engineering.,” *Biomaterials*, vol. 26, no. 28, pp. 5609–16, Oct. 2005.

- [101] A. C. Jones, A. Sakellariou, A. Limaye, C. H. Arns, T. J. Senden, T. Sawkins, M. A. Knackstedt, D. Rohner, D. W. Hutmacher, A. Brandwood, and B. K. Milthorpe, “Investigation of microstructural features in regenerating bone using micro computed tomography,” *J. Mater. Sci. Mater. Med.*, vol. 15, no. 4, pp. 529–532, Apr. 2004.
- [102] D. W. Hutmacher, “Scaffold design and fabrication technologies for engineering tissues — state of the art and future perspectives,” *J. Biomater. Sci. Polym. Ed.*, vol. 12, no. 1, pp. 107–124, Jan. 2001.
- [103] J. C. Palmaz, A. Benson, and E. A. Sprague, “Influence of Surface Topography on Endothelialization of Intravascular Metallic Material,” *J. Vasc. Interv. Radiol.*, vol. 10, no. 4, pp. 439–444, Apr. 1999.
- [104] A. K. Geim, S. V Dubonos, I. V Grigorieva, K. S. Novoselov, A. A. Zhukov, and S. Y. Shapoval, “Microfabricated adhesive mimicking gecko foot-hair.,” *Nat. Mater.*, vol. 2, no. 7, pp. 461–3, Jul. 2003.
- [105] M. Jin, X. Feng, L. Feng, T. Sun, J. Zhai, T. Li, and L. Jiang, “Superhydrophobic Aligned Polystyrene Nanotube Films with High Adhesive Force,” *Adv. Mater.*, vol. 17, no. 16, pp. 1977–1981, Aug. 2005.
- [106] M. Sitti and R. S. Fearing, “Synthetic gecko foot-hair micro/nano-structures as dry adhesives,” *J. Adhes. Sci. Technol.*, vol. 17, no. 8, pp. 1055–1073, Jan. 2003.
- [107] B. Yurdumakan, N. R. Ravikar, P. M. Ajayan, and A. Dhinojwala, “Synthetic gecko foot-hairs from multiwalled carbon nanotubes.,” *Chem. Commun. (Camb)*., no. 30, pp. 3799–801, Aug. 2005.
- [108] A. Folch and M. Toner, “Microengineering of cellular interactions.,” *Annu. Rev. Biomed. Eng.*, vol. 2, pp. 227–56, Jan. 2000.
- [109] D. J. Beebe, G. A. Mensing, and G. M. Walker, “Physics and applications of microfluidics in biology.,” *Annu. Rev. Biomed. Eng.*, vol. 4, pp. 261–86, Jan. 2002.
- [110] K. Ohno, K. Tachikawa, and A. Manz, “Microfluidics: applications for analytical purposes in chemistry and biochemistry.,” *Electrophoresis*, vol. 29, no. 22, pp. 4443–53, Nov. 2008.
- [111] C. Moraes, K. Wyss, E. Brisson, B. A. Keith, Y. Sun, and C. A. Simmons, “An Undergraduate Lab (on-a-Chip): Probing Single Cell Mechanics on a Microfluidic Platform,” *Cell. Mol. Bioeng.*, vol. 3, no. 3, pp. 319–330, May 2010.
- [112] E. W. K. Young and C. a Simmons, “Macro- and microscale fluid flow systems for endothelial cell biology.,” *Lab Chip*, vol. 10, no. 2, pp. 143–160, 2010.

- [113] C. W. T. Yang, E. Ouellet, and E. T. Lagally, “Using inexpensive Jell-O chips for hands-on microfluidics education.,” *Anal. Chem.*, vol. 82, no. 13, pp. 5408–14, Jul. 2010.
- [114] D. E. Discher, P. Janmey, and Y.-L. Wang, “Tissue cells feel and respond to the stiffness of their substrate.,” *Science*, vol. 310, no. 5751, pp. 1139–43, Nov. 2005.
- [115] E. Verneuil, A. Buguin, and P. Silberzan, “Permeation-induced flows: Consequences for silicone-based microfluidics,” *Europhys. Lett.*, vol. 68, no. 3, pp. 412–418, Nov. 2004.
- [116] A. L. Paguirigan and D. J. Beebe, “Microfluidics meet cell biology: bridging the gap by validation and application of microscale techniques for cell biological assays.,” *Bioessays*, vol. 30, no. 9, pp. 811–21, Sep. 2008.
- [117] A. L. Paguirigan and D. J. Beebe, “From the cellular perspective: exploring differences in the cellular baseline in macroscale and microfluidic cultures.,” *Integr. Biol. (Camb)*., vol. 1, no. 2, pp. 182–95, Feb. 2009.
- [118] E. W. K. Young, C. Pak, B. S. Kahl, D. T. Yang, N. S. Callander, S. Miyamoto, and D. J. Beebe, “Microscale functional cytomics for studying hematologic cancers,” *Blood*, vol. 119, no. 10, 2012.
- [119] S. Bersini, J. S. Jeon, G. Dubini, C. Arrigoni, S. Chung, J. L. Charest, M. Moretti, and R. D. Kamm, “Biomaterials A micro fluidic 3D in vitro model for specific study of breast cancer metastasis to bone,” vol. 35, pp. 2454–2461, 2014.
- [120] H. Becker and C. Gärtner, “Polymer microfabrication technologies for microfluidic systems.,” *Anal. Bioanal. Chem.*, vol. 390, no. 1, pp. 89–111, Jan. 2008.
- [121] S. Lan, H.-J. Lee, E. Kim, J. Ni, S.-H. Lee, X. Lai, J.-H. Song, N. K. Lee, and M. G. Lee, “A parameter study on the micro hot-embossing process of glassy polymer for pattern replication,” *Microelectron. Eng.*, vol. 86, no. 12, pp. 2369–2374, Dec. 2009.
- [122] Y.-J. Juang, L. J. Lee, and K. W. Koelling, “Hot embossing in microfabrication. Part I: Experimental,” *Polym. Eng. Sci.*, vol. 42, no. 3, pp. 539–550, Mar. 2002.
- [123] M. T. Gale, “Replication techniques for diffractive optical elements,” *Microelectron. Eng.*, vol. 34, no. 3–4, pp. 321–339, Dec. 1997.
- [124] R. M. McCormick, R. J. Nelson, M. G. Alonso-Amigo, D. J. Benvegnu, and H. H. Hooper, “Microchannel Electrophoretic Separations of DNA in Injection-Molded Plastic Substrates,” *Anal. Chem.*, vol. 69, no. 14, pp. 2626–2630, Jul. 1997.

- [125] D. A. Mair, E. Geiger, A. P. Pisano, J. M. J. Fréchet, and F. Svec, “Injection molded microfluidic chips featuring integrated interconnects.,” *Lab Chip*, vol. 6, no. 10, pp. 1346–54, Oct. 2006.
- [126] Y. Bang, K. Lee, and S. Oh, “5-axis micro milling machine for machining micro parts,” *Int. J. Adv. Manuf. Technol.*, vol. 25, no. 9–10, pp. 888–894, Feb. 2004.